MICROCOPY RESOLUTION TEST CHART

IRIAI STANDARDS 1963 A

AD-A193 638

INVESTIGATION OF THE HIGHER-ORDER ELEMENTS IN THE SAMSON2 CODE

Steven S. Miller
Harold C. Sorensen

Washington State University
Pullman, WA 99163

April 1988

Final Report

DTIC
ELECTE
MAY 1 8 1988
E

AIR FORCE WEAPONS LABORATORY
Air Force Systems Command
Kirtland Air Force Base, NM 87117-6008

88   1.   022

This thesis was prepared by Washington State University, Pullman, Washington, under Contract F29601-85-K-0050, Job Order 8809131A with the Air Force Weapons Laboratory Kirtland Air Force Base, New Mexico. Douglas R. Seemann (NTES) was the Laboratory Project Officer-in-Charge.

When Government drawings, specifications, or other data are used for any purpose other than in connection with a definitely Government-related procurement, the United States Government incurs no responsibility or any obligation whatsoever. The fact that the Government may have formulated or in any way supplied the said drawings, specifications, or other data, is not to be regarded by implication, or otherwise in any manner construed, as licensing the holder, or any other person or corporation; or as conveying any rights or permission to manufacture, use, or sell any patented invention that may in any way be related thereto.
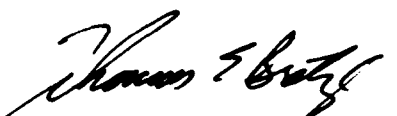
This report has been authored by a contractor of the United States Government. Accordingly, the United States Government retains a nonexclusive, royalty-free license to publish or reproduce the material contained herein, or allow others to do so, for the United States Government purposes.
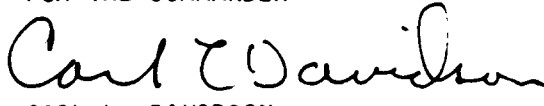
This report has been reviewed by the Public Affairs Office and is releasable to the National Technical Information Service (NTIS). At NTIS, it will be available to the general public, including foreign nationals.

If your address has changed, if you wish to be removed from our mailing list, or if your organization no longer employs the addressee, please notify AFWL/NTES, Kirtland AFB, NM 87117-6008 to help us maintain a current mailing list.

This thesis has been reviewed and is approved for publication.

DOUGLAS R. SEEMANN
Project Officer

FOR THE COMMANDER

THOMAS E. BRETZ, JR.   CARL L. DAVIDSON
Lt Col, USAF   Col, USAF
Chief, Applications Branch   Chief, Civil Engineering
                                       Research Division

_____

DO NOT RETURN COPIES OF THIS REPORT UNLESS CONTRACTUAL OBLIGATIONS OR NOTICE ON A SPECIFIC DOCUMENT REQUIRES THAT IT BE RETURNED.

REPORT DOCUMENTATION PAGE

1a REPORT SECURITY CLASSIFICATION		1b RESTRICTIVE MARKINGS			
Unclassified					

2a SECURITY CLASSIFICATION AUTHORITY	3 DISTRIBUTION/AVAILABILITY OF REPORT
2b DECLASSIFICATION/DOWNGRADING SCHEDULE	Approved for public release; distribution unlimited.

4 PERFORMING ORGANIZATION REPORT NUMBER(S)	5 MONITORING ORGANIZATION REPORT NUMBER(S)
	AFWL-TR-86-85

6a. NAME OF PERFORMING ORGANIZATION	6b. OFFICE SYMBOL (If applicable)	7a NAME OF MONITORING ORGANIZATION
Washington State University		Air Force Weapons Laboratory

6c. ADDRESS (City, State, and ZIP Code)	7b ADDRESS (City, State, and ZIP Code)
Pullman, WA 99163	Kirtland Air Force Base, NM 87117-6008

8a. NAME OF FUNDING/SPONSORING ORGANIZATION	8b OFFICE SYMBOL (If applicable)	9 PROCUREMENT INSTRUMENT IDENTIFICATION NUMBER
		F29601-85-K-0050

8c. ADDRESS (City, State, and ZIP Code)	10 SOURCE OF FUNDING NUMBERS			
	PROGRAM ELEMENT NO	PROJECT NO	TASK NO	WORK UNIT ACCESSION NO
	62601F	8809	13	1A

11 TITLE (Include Security Classification)

INVESTIGATION OF THE HIGHER-ORDER ELEMENTS IN THE SAMSON2 CODE

12. PERSONAL AUTHOR(S)
Miller, Steven Scott and Sorensen Harold C.

13a. TYPE OF REPORT	13b. TIME COVERED	14 DATE OF REPORT (Year, Month, Day)	15 PAGE COUNT
Final	FROM Apr 85 TO Jul 86	1988, April	198

16 SUPPLEMENTARY NOTATION

Thesis

17	COSATI CODES		18 SUBJECT TERMS (Continue on reverse if necessary and identify by block number)
FIELD	GROUP	SUB-GROUP	Finite Elements Continuum Analysis
12	01		High Order Elements
20	11		Dynamic Analysis

19 ABSTRACT (Continue on reverse if necessary and identify by block number)

The objective of this research effort was to determine whether the current finite element formulation in the SAMSON2 code for the eight-node quadrilateral higher-order isoparametric continuum element produces consistent and reliable results. Some effort was also performed toward investigating the finite element formulations for the five-node and the six-node triangular isoparametric continuum elements.

Four tasks were executed in this research effort. The first task was a study of some of the previous work which had been performed. The second task involved comparisons between program results and analytical solutions for various problems. The third task was the verification and correction where necessary of the finite element formulation for the eight-node quadrilateral continuum element. The fourth task was a study of the effects on the problem results which were caused by the corrected finite element formulation.

20. DISTRIBUTION/AVAILABILITY OF ABSTRACT	21 ABSTRACT SECURITY CLASSIFICATION
☒ UNCLASSIFIED/UNLIMITED ☐ SAME AS RPT ☐ DTIC USERS	Unclassified

22a. NAME OF RESPONSIBLE INDIVIDUAL	22b TELEPHONE (Include Area Code)	22c OFFICE SYMBOL
Douglas Seemann	(505) 846-6473	NTES

DD FORM 1473, 84 MAR
83 APR edition may be used until exhausted.
All other editions are obsolete.

SECURITY CLASSIFICATION OF THIS PAGE

UNCLASSIFIED

19. ABSTRACT (Continued)

The results from this investigation showed that the current finite element formulation for the eight-node quadrilateral continuum element produces accurate results for problems which are analyzed using plane continuum elements. However, corrections to the finite element formulation for the analyses of axisymmetric continua were necessary to obtain accurate results using the eight node quadrilateral element. These corrections to the SAMSON2 code were performed based on the results obtained in the verification of the finite element formulation.

ACKNOWLEDGMENTS

I would like to take the opportunity to thank the entire faculty and staff in the Department of Civil and Environmental Engineering for their support and guidance during my academic tenure at Washington State University.

I would like to personally thank Carrie Lee Babcock for her invaluable effort in the typing of this report.

I am also indebted to Dr. Timothy J. Ross and Doug Seemann of the Air Force Weapons Laboratory for the opportunity to work on Department of Defense related research.

A very special thanks goes to my wife, Nancy, and our two sons, Travis and Brandon, for their patience and love. I am also very thankful to my parents, Mr. and Mrs. William L. Miller, for all of their assistance, love and support throughout my years in college.

Finally, I would like to thank the following people for their invaluable friendship and support: B. Mickelsen, M. Warman, B. Bigelis, P Bucich, S. Omberg, C. Weber, M. Johnson, B. Hollenbeck, K. Kimball, B. Schamberger, and B Falk.

Accession For	
NTIS GRA&I	X
DTIC TAB	☐
Unannounced	☐
Justification	
By	
Distribution/	
Availability Codes	
Dist	Avail and/or Special
A-1	

QUALITY INSPECTED 4

INVESTIGATION OF THE HIGHER-ORDER ELEMENTS

IN THE SAMSON2 CODE

Abstract

by Steven Scott Miller, M.S.
Washington State University
August 1986

Chair: Harold C. Sorensen

The objective of this research effort was to determine if the current finite element formulation in the SAMSON2 code for the eight-node quadrilateral higher-order isoparametric continuum element produces consistent and reliable results. Some effort was also performed toward investigating the finite element formulations for the five-node and the six-node triangular isoparametric continuum elements.

Four tasks were executed in this research effort. The first task was a study of some of the previous work which had been performed. The second task involved comparisons between program results and analytical solutions for various problems. The third task was the verification and correction where necessary of the finite element formulation for the eight-node quadrilateral continuum element. The fourth task was a study of the effects on the problem results which were caused by the corrected finite element formulation.

The results from this investigation showed that the current finite element formulation for the eight-node quadrilateral continuum element produces accurate results for problems which are analyzed using plane continuum elements. However, corrections to the finite element formulation for the analyses of axisymmetric continua were necessary in order for accurate results to

be obtained using the eight-node quadrilateral element. These corrections to the SAMSON2 code were performed based in the results obtained in the verification of the finite element formulation.

TABLE OF CONTENTS

LIST OF TABLES

LIST OF FIGURES

LIST OF SYMBOLS

A = cross-sectional area

B = bulk modulus

$[B]$ = strain-displacement matrix

$[\bar{B}]$ = strain-displacement matrix used in SAMSON2 in order to determine velocity strains

$[C]$ = viscous damping matrix

C_1 = mass proportional damping factor

C_2 = stiffness proportional damping factor

c^E = elastic stress-strain matrix

c^{EP} = elastic-plastic stress-strain matrix

E = modulus of elasticity

E_T = plastic modulus

F = yield function

$\{F_{int}\}$ = internal nodal force vector

$\{F_{ext}\}$ = external nodal force vector

G = shearing modulus

I = moment of inertia

$|J|$ = determinant of the Jacobian matrix

$[K]$ = structural stiffness matrix

K_L = bulk modulus for loading segment of hydrostat curve

K_U = bulk modulus for unloading/reloading segment of hydrostat curve

L = beam length

M = moment

$[M]$ = total diagonal lumped mass matrix

N_I = shape function for node I

P = concentrated load

P_o = constant value for uniformly distributed load

[R] = velocity strain transformation matrix

S_{ii} = deviatoric normal stresses (i=1,2,3)

U = internal strain energy

{U} = nodal displacement vector

V = volume

V_n = normal velocity component

V_t = tangential velocity component

V_x = x-component of velocity

V_y = y-component of velocity

W = external work

WIM = linear impulse

X = global x-axis

Y = global y-axis

$Y_n(t)$ = amplitude of vibration for mode n at time t

a = Gauss-Legendre abscissae coefficient

a_n = constant values used in modal analyses

c = wave speed

d = x-distance from y-axis to a quadrature point

{d} = global velocity strain vector

{$\hat{d}$} = corotational velocity strain vector

Δe = strain energy increment

f_x = x-component of external nodal force

f_y = y-component of external nodal force

h_i = Gauss-Legendre weight coefficient

iorder = order of integration

$\bar{m}$ = constant value for mass per unit length

n = mode of vibration

$\bar{r}$ = distance from y-axis to geometric center of an element

t = time

u = displacement

$\dot{u}$ = velocity

$\ddot{u}$ = acceleration

u_x = x-component of displacement

u_y = y-component of displacement

w(t) = time varying uniformly distributed load

x = global x-coordinate

$\hat{x}$ = corotational x-coordinate

y = global y-coordinate

$\hat{y}$ = corotational y-coordinate

y_{max} = maximum y-displacement

Δ = increment of time (t), stress (σ), and strain (ε)

Σ = summation

$\phi_n(x)$ = vibration shape for mode n at any x

γ = shearing strain

ε = normal strain

η = local y-coordinate for an element

Θ = angle of rotation

μ = fraction of critical element damping

ν = Poisson's ratio

ξ = local x-coordinate for an element

π = 3.1416 . . .

ρ = mass density

σ = normal stress

σ_{yld} = yield stress

τ = shearing stress

ω = frequency (also rotational velocity)

ω_{max} = maximum frequency of the system

CHAPTER 1

Introduction

The content of this report gives a detailed description of the research which was performed during the investigation of the higher-order isoparametric continuum finite elements (five-node triangle, six-node triangle, and eight-node quadrilateral) which are available for use in the SAMSON2 code (1). SAMSON2 is a dynamic nonlinear two-dimensional finite element computer code which was developed at the Illinois Institute of Technology Research Institute (IITRI) for the Air Force Weapons Laboratory (AFWL) located at Kirtland AFB in Albuquerque, New Mexico. SAMSON2 is used to solve structure-media interface (SMI) problems and problems which involve large displacements, large strains and nonlinear material behaviors.

In analyses performed previously at the AFWL, it was found that the solutions obtained by using the higher-order elements (HOE) were anomalous. It was concluded that these anomalous results were caused by inconsistencies in the HOE formulations. Hence, use of the finite element library of elements for SAMSON2 by the AFWL is limited. Therefore, the overall objective of this research was to rectify this situation by modifying and correcting as necessary the HOE formulations so that consistent and reliable results can be obtained. In addition, by using the HOE, it was believed that solutions may be performed more efficiently with improved accuracy and fewer elements compared to solutions with the four-node quadrilateral continuum element now in use by the AFWL.

Three tasks were undertaken in order to attain the desired objective of this research. The first task was to study previous work performed with the use of the HOE. The reason for this study was to acquire background information as to where possible problems may exist in the HOE formulations. The second task was to perform finite element analyses on various problems using the HOE available in the SAMSON2 code. The solutions of these problems were studied and compared with analytical solutions in order to determine if the correct solutions were obtained. The complexities and the types of the problems which were selected were varied in order to fully test the HOE algorithms. The third task was to investigate the developments of the HOE algorithms in the code. These formulations were checked for validity and, if errors were identified, corrections for these errors were postulated. The eight-node quadrilateral formulation was the only one investigated thoroughly since the eight-node quadrilateral is the most important HOE to the AFWL for analysis purposes. The five- and six-node triangular elements are essentially used only for transitions from eight-node quadrilaterals to four-node quadrilaterals and were therefore considered less important for this study.

After the completion of these three tasks, the results were compiled and are discussed in this report. In addition, modifications to the HOE formulation are suggested and detailed along with conclusions based on these results.

CHAPTER 2

Previous Investigations Associated With the Higher-Order Elements

The only continuum element currently being used by the AFWL is the four-node quadrilateral (4NQ) because it is known to produce correct solutions and because AFWL personnel are somewhat concerned about the accuracy of the solutions produced by the HOE. Due to this concern, a few investigations pertaining to the HOE have been undertaken.

The content of this chapter provides a discussion of two of the prior examinations of the HOE that were reported to the author. These investigations were studied in order to gain some insight into possible problems associated with the HOE. Furthermore, the information obtained from the studies was to be used as a starting point for the current investigation.

The majority of the previous efforts toward investigating the HOE has been performed by Dr. Howard L. Schreyer (2) at the New Mexico Engineering Research Institute (NMERI) in Albuquerque, New Mexico. Based on experiences involving the five-node and six-node triangular (5NT, 6NT) continuum elements and the eight-node quadrilateral (8NQ) continuum element, Schreyer concluded that use of these elements has yielded anomalous results. In addition, the matrix that relates stress to strain (the B-matrix) and the internal force vector have been investigated at NMERI and at the AFWL and have been accepted as being correct. Based on this information, Schreyer's first approach in his investigation was to analyze the one-dimensional wave propagation problem shown in Appendix A (Case A1) of the SAMSON2 Users Manual (3)

using the 8NQ element available in the SAMSON2 code. By performing this analysis he found that at the second time step in the solution the right-side nodes of the first element did not move as predicted. Instead he found the corner nodes moved to the left (in the opposite direction of the applied force) while the midside node moved to the right. He also found this displacement pattern did not correct with time. Based on these findings he concluded that the shape functions installed in SAMSON2 for the 8NQ may not be appropriate and that strains might be produced by rigid body motions. He then checked the 8NQ shape functions for rigid body displacement and rotation and found no strains were produced. After this check and with the results from the one-dimensional wave propagation problem, he concluded there was a different reason for the anomaly and began reviewing the internal force computations and a modified system of shape functions. This last review was never completed.

The only other reported work was conducted by Rod Galloway, an employee at the AFWL. Doug Seemann, the AFWL project representative for the current investigation of the HOE, stated that Rod had inspected the HOE formulation in SAMSON2 and found no obvious errors. Unfortunately, Rod's work was not documented.

Doug Seemann also expressed some possible reasons why the HOE formulation was not functioning properly based on his review of Schreyer's work (4). He stated that the element in question might have been unstable due to the fact that the finite element discretization and problem input were poorly defined. He also believed that approximations used in the element formulation might be causing an instability. If the

problem were instability, he suggested three possible solutions: (1) a more accurate formulation (assuming approximations are causing the error), (2) more rigid specifications on how to use the elements and (3) a better scheme for determining a stable time step.

CHAPTER 3

Finite Element Analyses

For this study, various problems were selected, modeled and analyzed using the higher-order finite elements in the SAMSON2 computer code (1). Most of the problems chosen had known analytical solutions so that the results generated by SAMSON2 could be examined and evaluated for errors.

There were two purposes for analyzing these problems. First, the capabilities of the HOE were to be thoroughly explored. Second, these analyses were to be used to discover possible errors in the HOE formulation used in the SAMSON2 code. These two goals were obtained by varying the complexities and the types of problems which were analyzed.

The 8NQ continuum element was given the main emphasis in the analyses with only minimal use of the 5NT and 6NT continuum elements. The 4NQ continuum element was also used for comparison purposes, especially for problems without analytical solutions.

The problem configuration, loading, and material parameters are provided in the succeeding sections along with a description of each test problem. Pertinent results are also provided. Examples of input data are provided in Appendix A for each problem.

3.1 One-Dimensional Wave Propagation

A uniform bar subjected to a dynamic axial load was chosen to test the solution involving one-dimensional wave propagation which was obtained with the use of the 8NQ. The bar problem was selected for

analysis because Dr. Schreyer (2) had used it in his previous investigation of the higher-order elements, and, therefore, the results and observations from his work could be verified. The one-dimensional problem was also used in Appendix A of the SAMSON2 Users Manual (3) to test the 4NQ.

The geometric configuration of the uniform bar can be seen in Figure 3.1 along with some of the input parameters and the load used in the analyses. The load which was used was a displacement function applied to the left boundary of the bar. The nodes on the left and right boundaries of the bar were fixed in the vertical (y) direction and free in the horizontal (x) direction. The remainder of the input used for the analyses is given in Appendix A. This input is identical to that in Reference 3 for the 4NQ. The input required for the 8NQ for this problem is slightly different than the input for the 4NQ. The input for the 8NQ solution required an order of integration which was chosen as 2.0 for this analysis. The bar problem was analyzed dynamically (undamped) using an elastic plane strain material model.

The discretizations used in the analyses of the one-dimensional wave problem were 16-4NQ elements with 27 nodes and 16-8NQ with 69 nodes both divided into 2 rows of 8 elements. The 4NQ discretization was the same as Case A1 mentioned previously. Hence, the same number of 8NQ elements were used since two rows of elements were desired with each element having an aspect ratio (ratio of length of element to height) of 1.0. The same discretization was used for each ana'.sis since the relative improvement in the results by increasing or decreasing the number of elements was not important in this study.
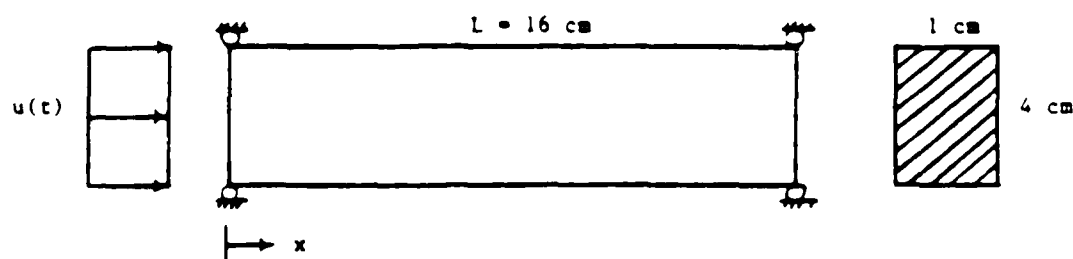
a) Geometric Configuration

Δt = 0.25 sec   (time step)

E   = 1.0 dyne/cm^2 (modulus of elasticity)

ρ = 1.0 dyne-sec^2/cm^4 (mass density)

ν = 0.0   (Poisson's ratio)

μ = 0.0   (damping ratio)

b) Input Parameters
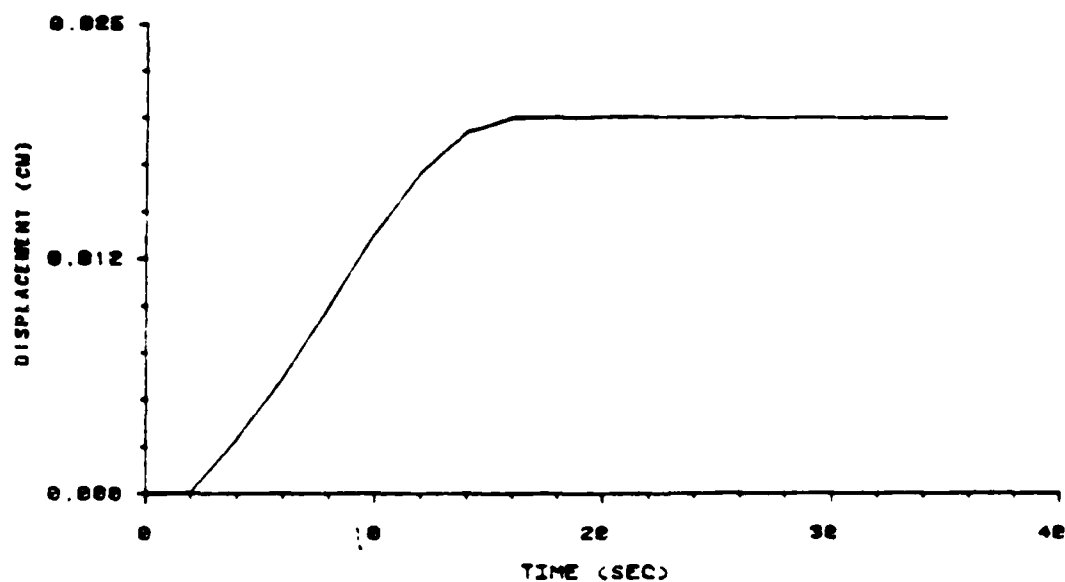
c) Applied Load

Figure 3.1   One-Dimensional Wave Propagation Problem

The results generated by SAMSON2 for this wave propagation problem were compared with the results of the corresponding analytical solution which can be found in either Appendix A of the SAMSON2 Users Manual (with $\omega = \frac{\pi c}{L}$) or Clough and Penzien (5). The first observation made when comparing the 8NQ solution with the analytical solution was that Schreyer's statements were only partially true. The right-side corner nodes of the first element did displace to the left (negative sense) which is opposite to the applied force. But, contrary to what Schreyer observed, these nodal displacements did change to the predicted direction (in the direction of the applied force) in time (15 time steps). A similar displacement pattern also occurred for other nodes. The magnitudes of the initial negative displacements had minimal effects on the final results as can be seen in Figure 3.2. It has been concluded that these initial negative displacements were caused by numerical dispersion and were inherent in the 8NQ shape functions and element formulation.

Additional results can be seen in Figures 3.3-3.7. The results for the 4NQ and the analytical solution are identical to those shown in Appendix A of the SAMSON2 Users Manual. The 8NQ results compare with the analytical solution quite well, except for the oscillatory numerical dispersion present. Only one displacement graph is given which is representative of all the other displacement graphs. All displacement graphs showed similar degrees of correlation between the 8NQ and the analytical solution results. The displacement and stress graphs have the best agreement between the 8NO solution and the analytical solution, while the velocity graphs displayed a greater amount of dispersion.
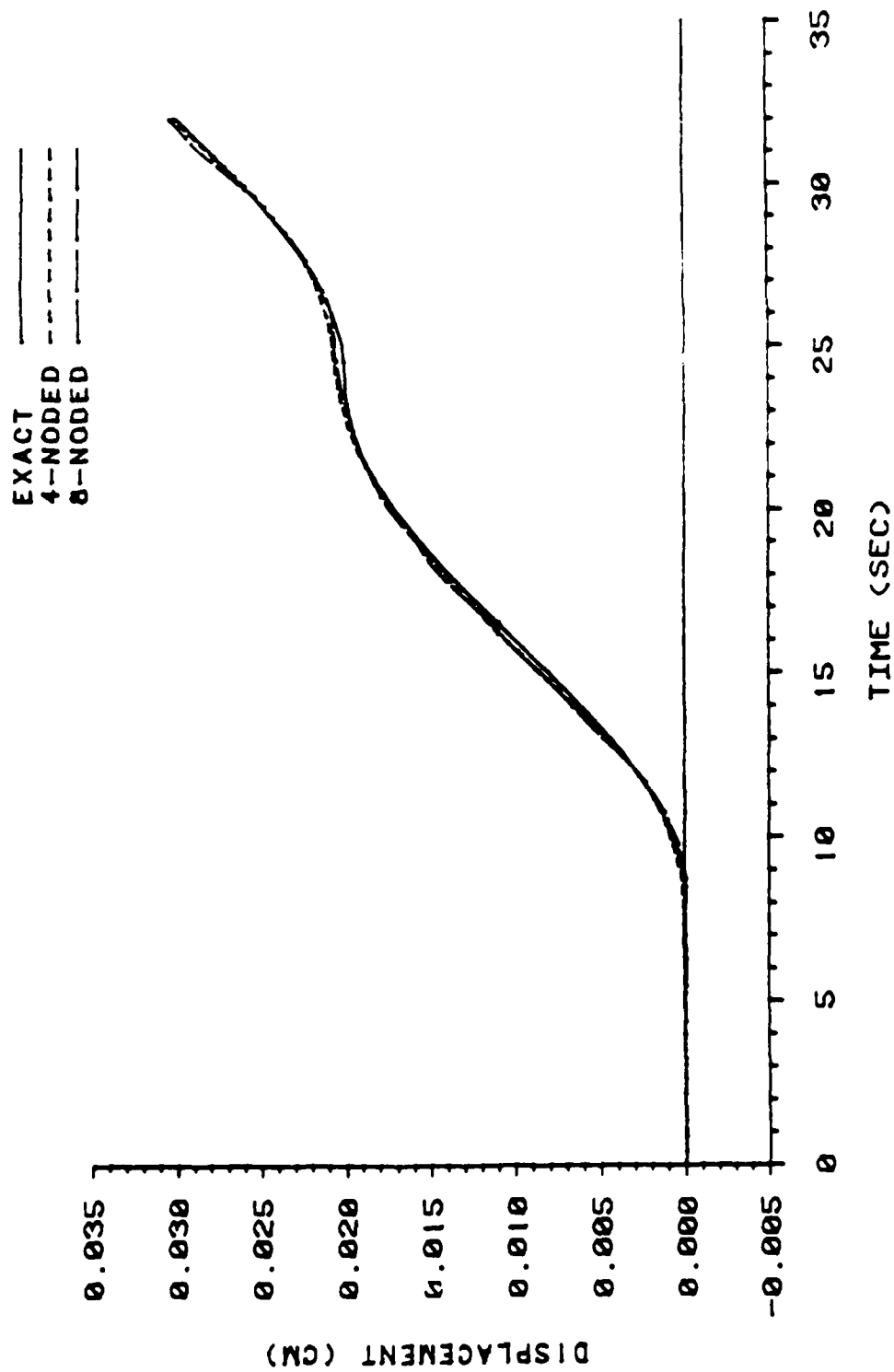
Figure 3.2   One-Dimensional Wave Propagation Problem: Displacement vs. Time at X = 8.0 cm.
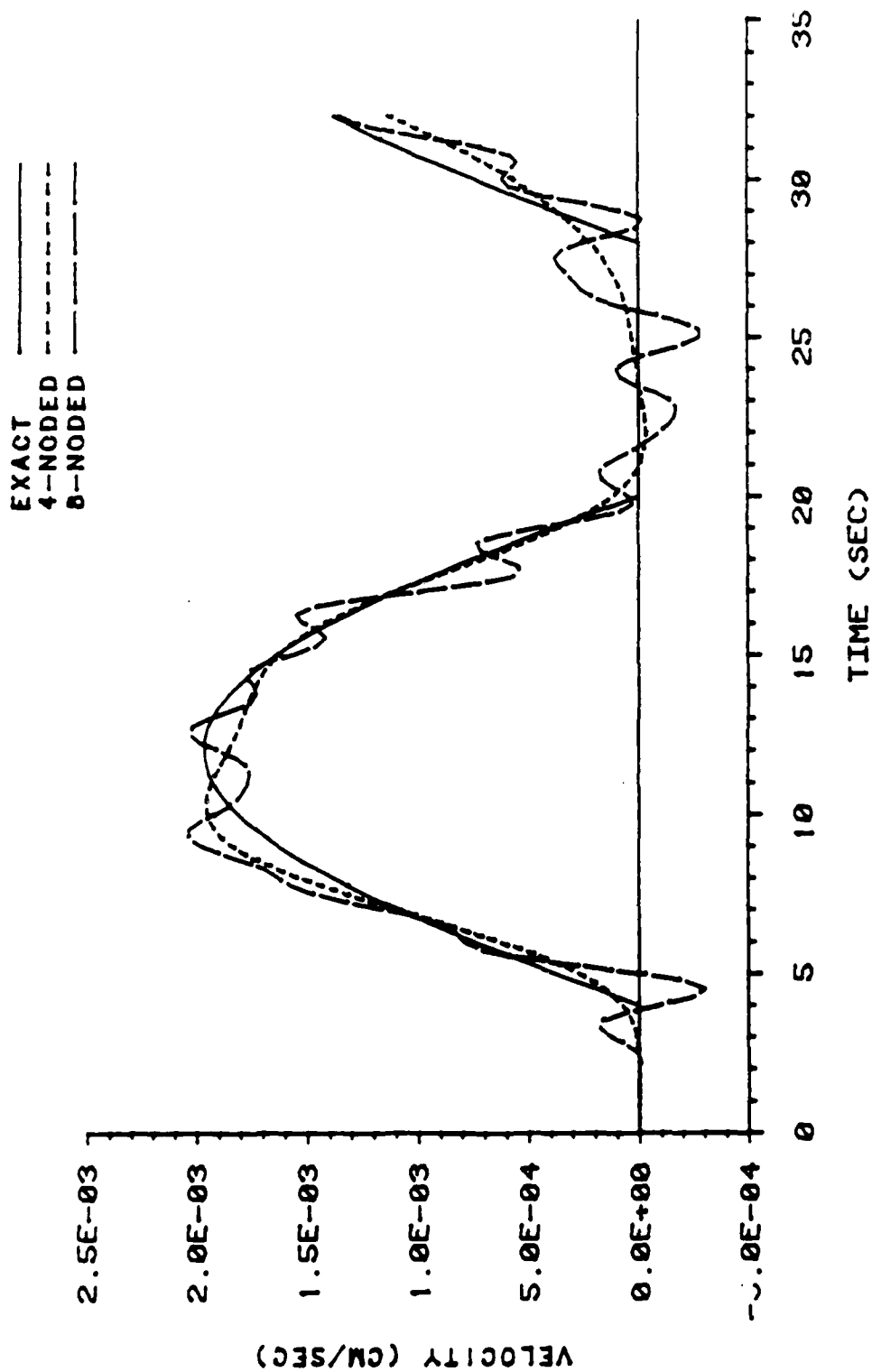
Figure 3.3   One-Dimensional Wave Propagation Problem: Velocity vs. Time at X = 4.0 cm.

11
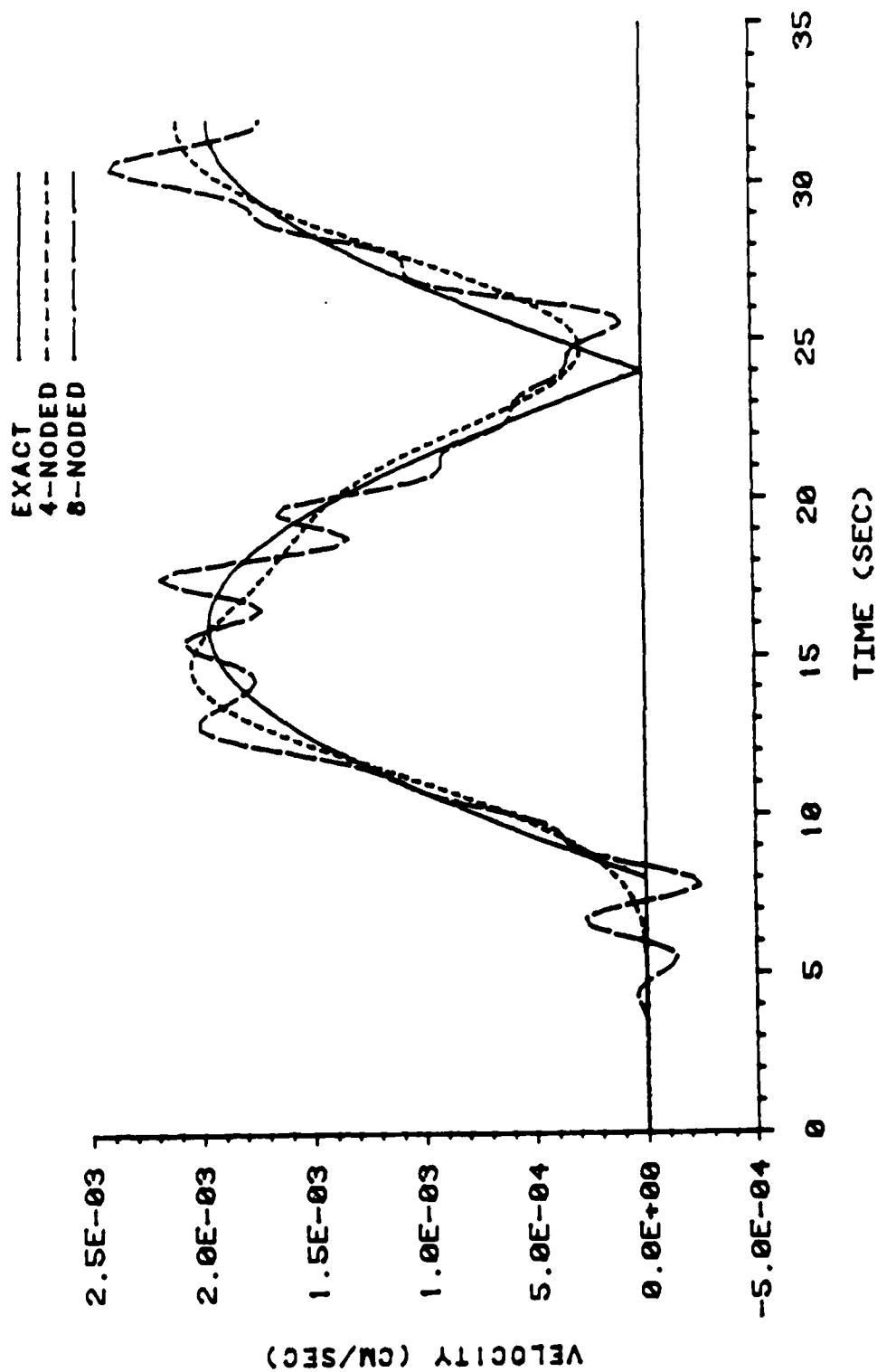
Figure 3.4   One-Dimensional Wave Propagation Problem: Velocity vs. Time at X = 8.0 cm.
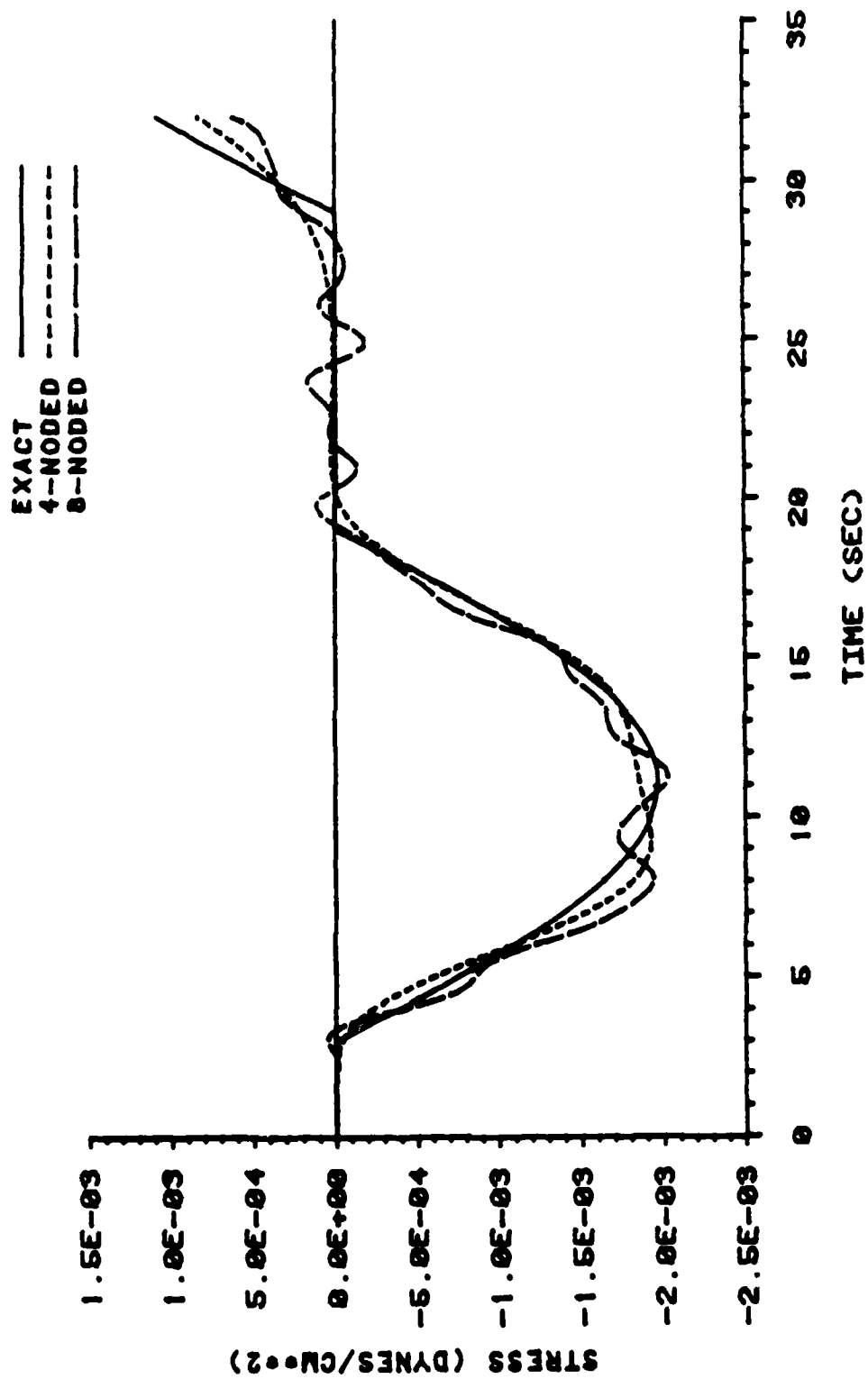
Figure 3.5   One-Dimensional Wave Propagation Problem: Stress vs. Time at X = 3.0 cm.
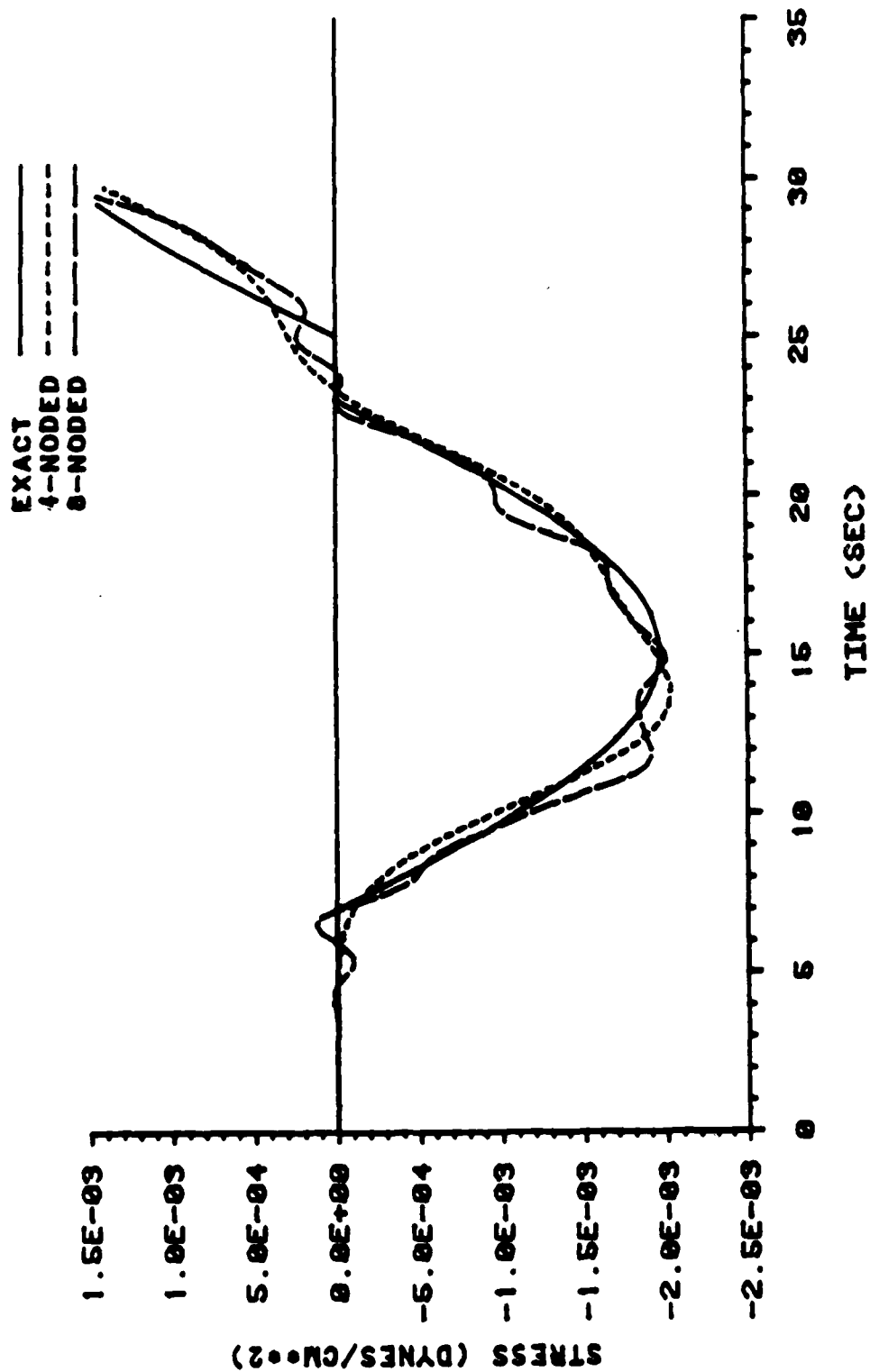
Figure 3.6   One-Dimensional Wave Propagation Problem: Stress vs. Time at X = 7.0 cm.

14
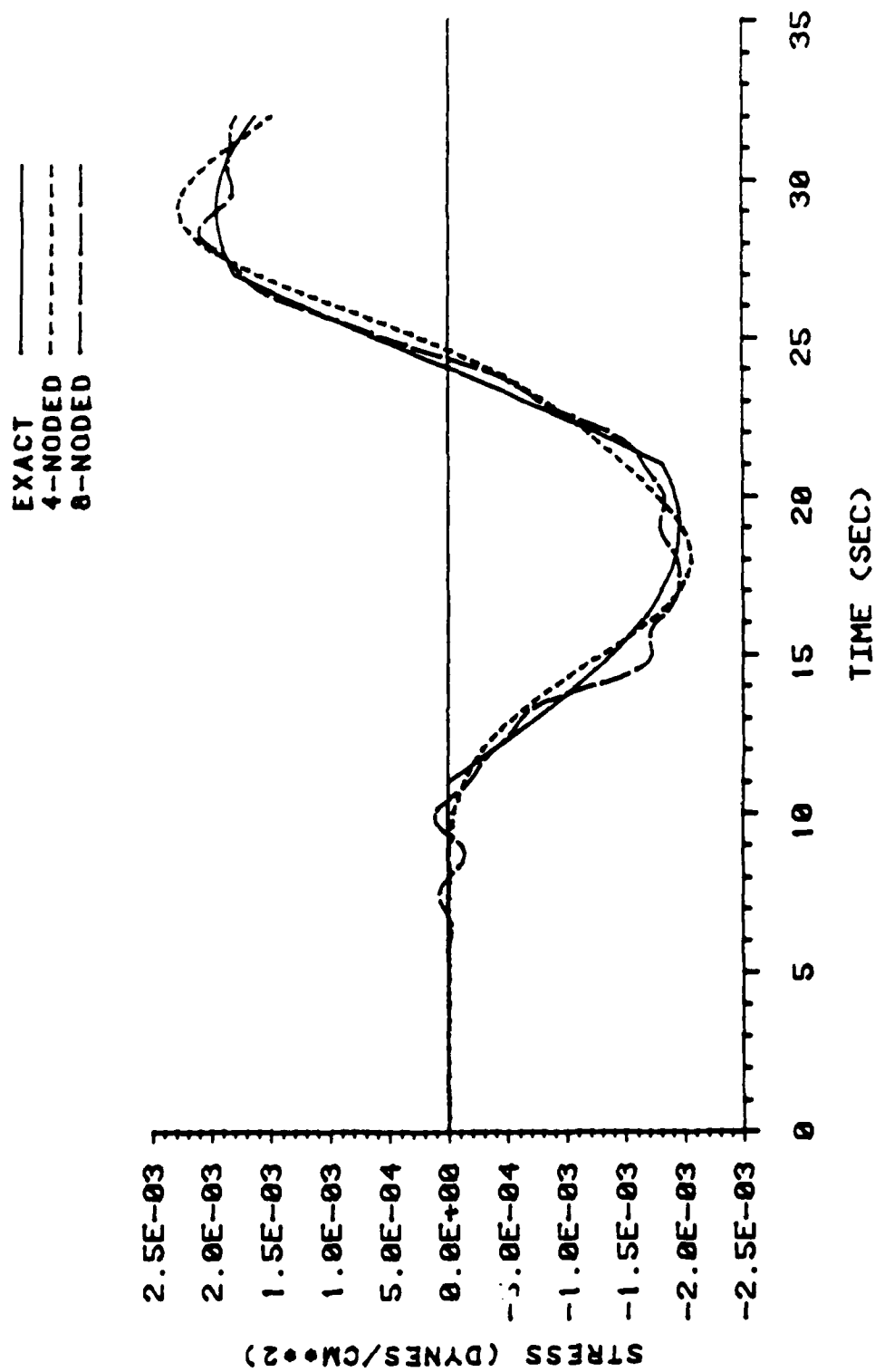
Figure 3.7   One-Dimensional Wave Propagation Problem: Stress vs. Time at X = 11.0 cm.

One conclusion, based on the results generated by SAMSON2, was that the 8NQ element is satisfactory for use in the one-dimensional wave propagation problem for which a dynamic elastic solution was performed. The only discrepancies in any of the results which should be noted existed in the values for the deflections, velocities, and stresses in the y-direction at points where the 4NQ solution and the 8NQ were compared. However, the magnitudes of these discrepancies were insignificant.

Some other conclusions that were obtained include: 1) the formulation for the 8NQ has some inherent problems, and 2) the solution obtained with the 4NQ was more efficient than that obtained with the 8NQ. The CPU time for the 4NQ solution was 7.20 secs. compared to 24.33 secs. for the 8NQ.

3.2 Cantilever Beam

A problem involving a cantilever beam was solved in order to verify the formulation for the 4NQ which appears in both the SAMSON2 Users Manual and the STEALTH and SAMSON2 Verifications Manual (6). Hence, this beam problem is used to test the performance of the 5NT, 6NT, and 8NQ elements in flexure when analyzed both statically and dynamically.

The geometric configuration of the cantilever beam can be seen in Figure 3.8 along with a sample of the pertinent input data and loads used in the analyses. The nodes on the left boundary were fixed in both the x- and y-directions. The maximum stable time step for the 8NQ discretization was obtained by trial and error (based on successive unsuccessful computer executions) until a satisfactory solution was
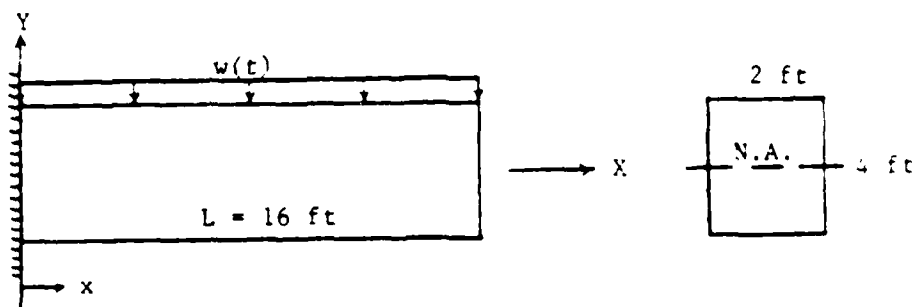
a) Geometric Configuration

Δt	=	3.4E-5 sec	(time step)
E	=	4176.0×10^6 psf	(modulus of elasticity)
ρ	=	16.0 lb-sec^2/ft^4	(mass density)
ν	=	0.0	(Poisson's ratio)
μ	=	0.0	(damping ratio)
C_1	=	1000	(mass proportional damping)

b) Input Parameters
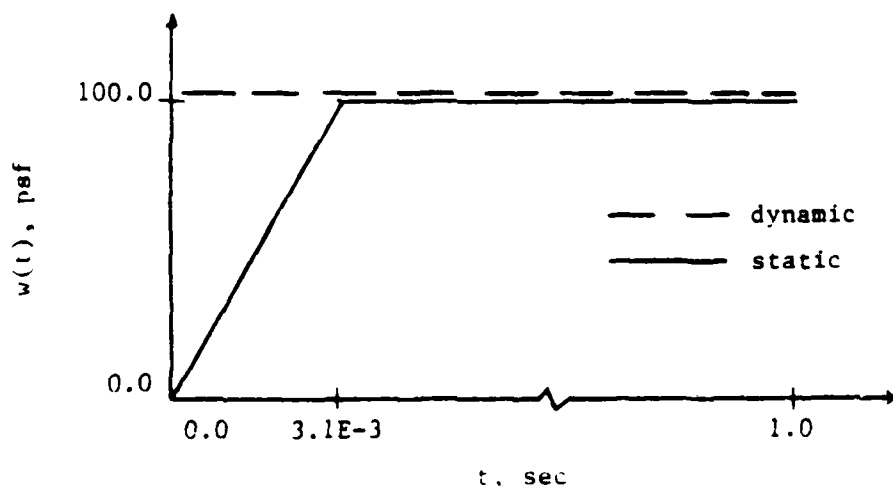
c) Applied Load

Figure 3.8   Cantilever Beam Problem.

obtained. Once chosen, the same time step was used for all of the analyses. Mass proportional damping (C_1) was used to obtain the static solutions by dynamic relaxation techniques (3). The beam was subjected to a static and a dynamic uniformly distributed pressure load. A short rise time was used for the static analyses in order to reduce the time required for convergence to the solution. The material law for a state of biaxial elastic-plastic plane stress was used in the analyses with Poisson's ratio equal to 0.0. An order of integration of 2.0 was chosen for the 5NT, 6NT, and 8NQ. Examples of the remainder of the input data used for the static analyses are contained in Appendix A. Only two changes were made to this input data in order to execute the dynamic analyses. The first change was the removal of the mass proportional damping factor from the input. The second change was to eliminate the short rise time in the static loading curve in order to make it an instantaneous dynamic load.

The finite element discretizations used for the analyses of the cantilever beam are shown in Figure 3.9a, b, c and d. The 4NQ grid was based on the example problems in the SAMSON2 Users Manual. The element dimensions were selected to be 1 ft x 1 ft in order to maintain an aspect ratio equal to one as recommended in Reference 6. The 8NQ discretization was selected such that one 8NQ element replaced four 4NQ elements. This ratio of one 8NQ to four 4NQs was chosen so that the same number of stress and strain calculations for the two discretization would be performed. Hence, the efficiencies of the two solution schemes could be compared. The aspect ratio for the 8NQ was also 1.0. The discretizations for both the 5NT and 6NT contained 32 elements.

a) 4NQ Elements

b) ⌐NQ Elements

Figure 3.9   Cantilever Beam Problem: Finite Element Discretizations.

c) 5NT Elements
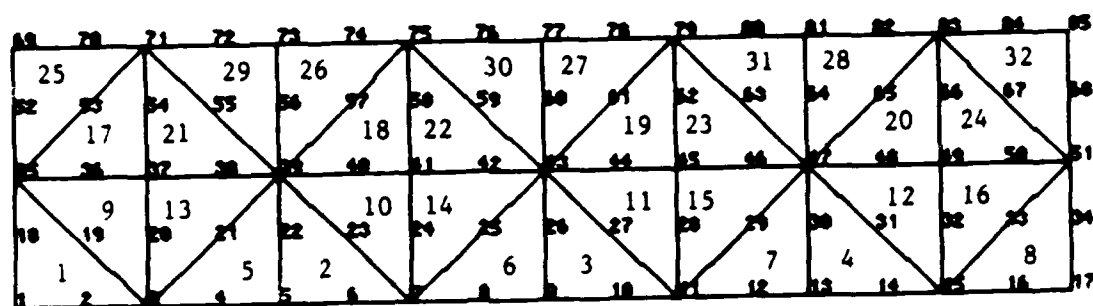
d) 6NT Elements

Figure 3.9   Cantilever Beam Problem: Finite Element Discretizations
             (Continued).

Therefore, the number of 5NT and 6NT elements used in the analyses was twice the number of 8NQ elements and one-half the number of 4NQ elements. Fewer triangular elements (5NT and 6NT) were selected compared to the number of 4NQ because the order of integration was greater for the 5NT and 6NT than for the 4NQ. Once selected, the discretizations used in the analyses were never changed.

The results of the static analyses for each of the four element discretizations were compared to the corresponding analytical solutions. These solutions were obtained with the use of basic principles of mechanics (7). The maximum y-displacements (y_{max}) obtained from the computer analyses were compared to the theoretical value computed from the following equation:

$$y_{max} = -\frac{wL^4}{8EI} - \frac{3wL^2}{2EA} \tag{3.1}$$

where,

w = 200.0 lb/ft

L = 16.0 ft

E = 4176.0 x 10^6 psf

I = 10.667 ft^4

A = 8.0 ft^2

therefore,

y_{max} = -0.3908 x 10^{-4} ft .

This value for the maximum displacement was computed at $x = L$ and included shear deformation effects. Table 3.1 shows the comparison between the results generated by SAMSON2 for the maximum y-displacement and the value computed using the analytical solution.

Table 3.1   Comparison Between the Results Generated by SAMSON2 for the Maximum Y-Displacement and the Corresponding Analytical Solution.

Element Type	SAMSON2 y_{max} (ft $\times 10^{-4}$)	Analytical Solution y_{max} (ft $\times 10^{-4}$)	Percent Difference Based On Analytical Solution
4NQ	-0.4067 (Node 51)	-0.3908	4.07%
8NQ	-0.3861 (Node 43)	-0.3908	1.20%
5NT	-0.3535 (Node 35)	-0.3908	9.54%
6NT	-0.3858 (Node 51)	-0.3908	1.28%

The results for the 4NQ, 8NQ, and 6NT elements as seen from Table 3.1 differed only slightly when compared to the value obtained from the analytical solution. The 5NT element results were not acceptable as they varied from the analytical solution by more than 10%. A comparison between the analytical and SAMSON2 solutions for normal stresses (σ_x) was also performed. The normal stress values used for comparison were computed analytically using the following equation:

$$\sigma_x = \frac{My}{I_x} = \frac{(100x^2 - 3200x + 25,600)y}{I_x} \tag{3.2}$$

where,

M = moment in the beam at any distance x (measured from the left end of beam) $0.0 \leq x \leq 16.0$,

y = distance from the neutral axis (N.A.) of the beam $-2.0 \leq y \leq 2.0$, and

I_x = moment of inertia of the cross-sectional area of the beam with respect to the x-axis.

Table 3.2 shows some of the comparisons made between the computed normal
stresses from Equation 3.2 to those computed using SAMSON2. As before,
the results for the 4NQ, 8NQ, and 6NT elements compared well, but
results for the 5NT did not. Normal stresses for other elements in the
meshes were compared, but are not shown here. Similar observations for
the stresses in these other elements were made with regard to the four
different element discretization solutions.

The results from the dynamic analyses were also compared to the
corresponding analytical solution and are shown in Figures 3.10 to 3.17
and Tables 3.3 and 3.4. The analytical solution for the displacement
response at the free end of the cantilever beam was generated using
Equations 3.3, 3.4, and 3.5 (8). These equations are for the elementary
case and do not include shear distortion and rotary inertia or
axial-force effects. These three quantities were omitted to simplify
the solution.

$$V(x,t) = \sum_{n=1}^{\infty} \phi_n(x) \, Y_n(t) \tag{3.3}$$

where,

$V(x,t) =$ displacement response at any x for any time t,

$\phi_n(x) =$ vibration shape at any x for mode n, and

$Y_n(t) =$ amplitude of vibration for mode n at any time t.

$$\phi_n(x) = (\cosh a_n x - \cos a_n x) - C_n(\sinh a_n x - \sin a_n x) \tag{3.4}$$

where,

$$C_n = \frac{\cos a_n L + \cosh a_n L}{\sin a_n L + \sinh a_n L},$$

Table 3.2 A Comparison Between the SAMSON2 Results and the Values Obtained by Use of Equation 3.2 for Normal Stresses (σ_x).

Element Type	Element Number	Stress Location Within The Element x-coordinate (ft)	y-coordinate (ft)	SAMSON2 σ_x (psf)	Analytical Solution σ_x (psf)	Percent Difference Based on Analytical Solution
4NQ	1	0.5	-1.5[a]	-3604[b]	-3379	6.7%
4NQ	8	7.5	-1.5	-1077	-1016	6.0%
8NQ	1 (int. pt. #1)[c]	0.4226	-1.577	-3601	-3588	0.4%
8NQ	4 (int. pt. #3)	7.577	-1.577	-1049	-1049	0.0%
5NT	1 (int. pt. #3)	0.1501	-1.44	-2857	-3391	15.8%
5NT	4 (int. pt. #2)	7.69	-1.6429	-1132	-1064	6.4%
6NT	1 (int. pt. #3)	0.1501	-1.44	-3415	-3391	0.7%
6NT	6 (int. pt. #2)	7.69	-1.6429	-1078	-1064	1.3%

[a]Negative y-coordinate indicates below the neutral axis.

[b]Negative represents a compressive stress.

[c]Integration point within the element where the stress value was computed.

x = distance from fixed end, and

a_1 = 1.875/L , a_2 = 4.694/L , and a_3 = 7.855/L.

$$Y_n(t) = \frac{P_0}{\bar{m}} \left(\frac{I_n}{\omega_n^2}\right)(1 - \cos \omega_n t) \tag{3.5}$$

where,

P_0 = constant value for the uniformly distributed load (lb/ft),

$\bar{m}$ = constant value for mass per unit length (lb-sec^2/ft^2),

$$I_n = \frac{\int_0^L \phi_n(x)dx}{\int_0^L \phi_n^2(x)dx} \; ; \; I_1 = 0.7830 \, , \; I_2 = 0.4340 \, , \; I_3 = 0.2589,$$

$$\omega_n^2 = \frac{a_n^4 EI}{\bar{m}} = \text{frequency of vibration for mode n;}$$

ω_1 = 256.18 , ω_2 = 1605.59 , ω_3 = 4,496.16, and

t = time in sec.

The first three modes of vibration (n=1,2,3) were used to predict the displacement responses of the cantilever beam as shown in Figures 3.10 and 3.11. As shown in these figures, the analyses using the 4NQ, 8NQ, and 6NT elements all overestimate the results from the analytical solution. In addition, the response of these elements has a longer period of vibration relative to that of the exact solution. The opposite is true of the 5NT element response, i.e., the 5NT solution underestimates displacements and has a shorter period of vibration. The 4NQ and the exact solution correspond to what is presented in Reference 3. A numerical comparison of the average peak values for the displacements for each curve in each figure can be seen in Table 3.3
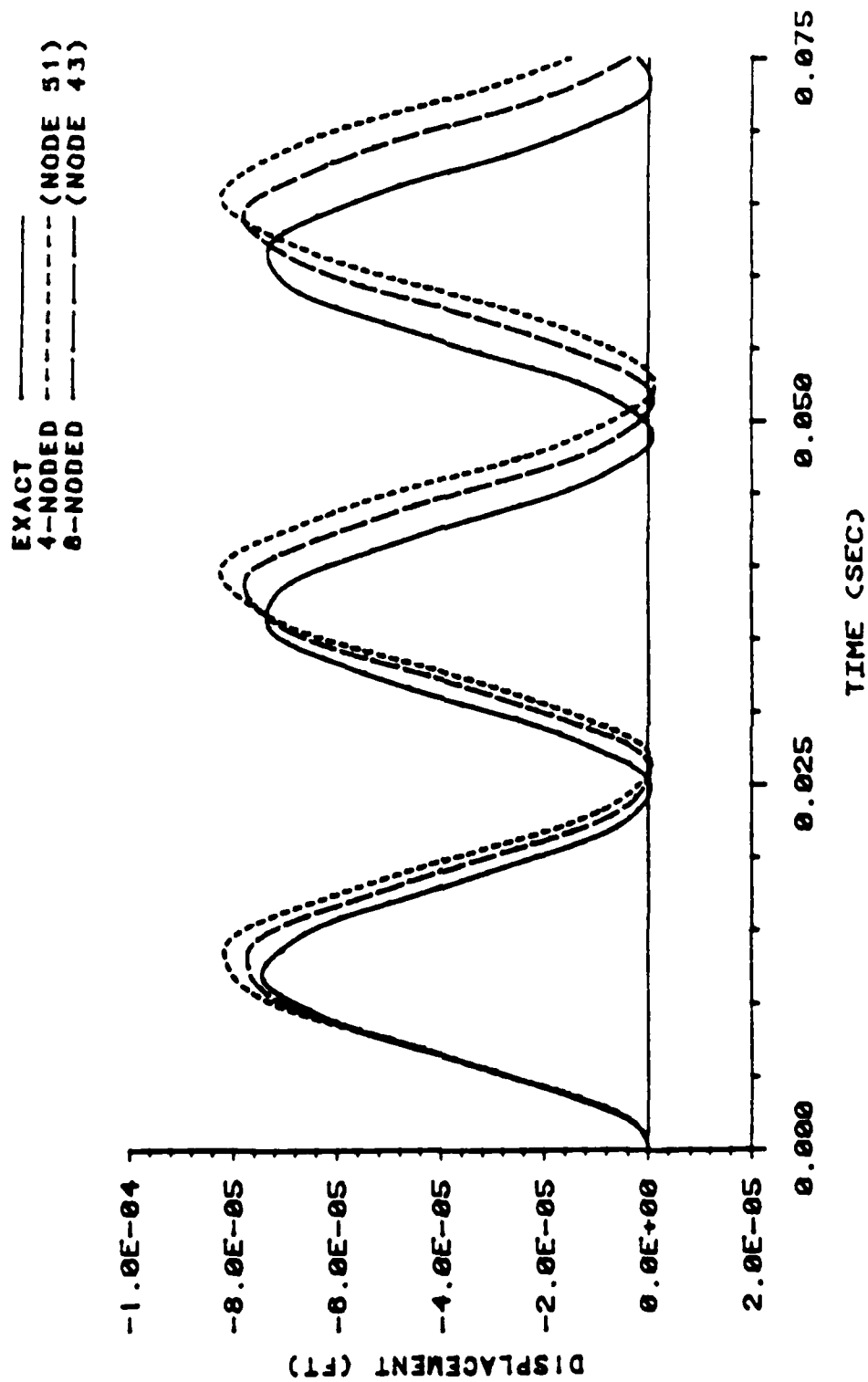
Figure 3.10   Cantilever Beam Problem: Maximum Displacement vs. Time (Undamped Response).
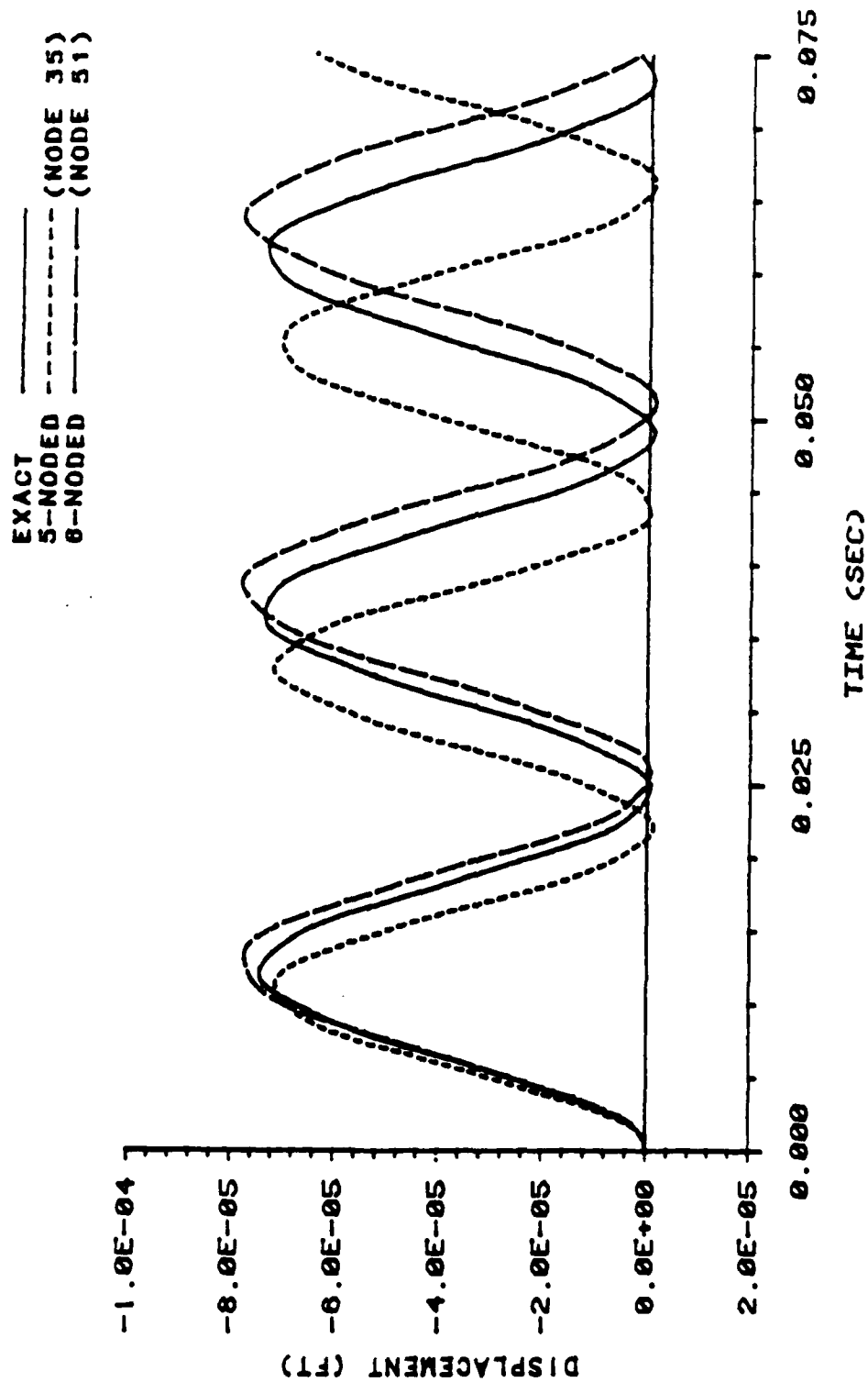
Figure 3.11   Cantilever Beam Problem: Maximum Displacement vs. Time (Undamped Response).

Table 3.3   Comparison of Average Values of Peak Displacement and
              Average Periods of Oscillation for the Curves Shown in
              Figures 3.10 and 3.11.

Solution Type	Average Value of Peak Displacement (ft x 10^{-4})	1 Percent Difference Based on Analytical Solution	2 Percent Difference When Compared to 2 Times Static Displacement (0.7816 x 10^{-4})	3 Average Period of Oscillation (sec)
Analytical	-0.7403	---	---	0.0248
4NQ	-0.8238	11.3%	5.4%	0.0259
8NQ	-0.7793	5.3%	0.3%	0.0255
5NT	-0.7134	3.6%	8.7%	0.0219
6NT	-0.7810	5.5%	0.1%	0.0254

along with the average periods of oscillation. In this table, the first comparison was made between the average peak value for the exact curve and each of the other four curves. These results were different than those obtained from the static analyses in that the 5NT element solution exhibited the best correlation to the analytical solution. It was concluded that this good correlation resulted from neglecting shear distortion in the analytical solution. Another comparison was performed between a dynamic displacement response value equal to two times the static displacement and the average peak values from each of the other four curves. The conclusions from this comparison were similar to those from the static solution, and, hence, the results from the 4NQ, 8NQ, and 6NT element solutions are acceptable. The periods of vibration for these three element types were also in good agreement with those of the

exact solution. The 5NT element solution had the largest discrepancies in columns 2 and 3 of Table 3.3, but the solution was acceptable based on column 1 in which shear distortion was neglected. The dynamic normal stress (σ_x) responses generated for the four element types were also studied. The following equation was used to compute the stress response values that were used to compare with the output from the analyses using the four different element types:

$$\sigma_x(x,t) = Ey \sum_{n=1}^{\infty} \Phi_n''(x) \, Y_n(t) \qquad (3.6)$$

where,

$$\Phi_n''(x) = a_n^2 \left[(\cosh a_n x + \cos a_n x) - C_n(\sinh a_n x + \sin a_n x) \right].$$

Curves showing the variation in the maximum stress and the stress at midspan (same locations and elements as in the static analyses) for each element type are given in Figures 3.12 to 3.17. The results are similar to those from the static analyses and the displacement response comparisons. The 4NQ, 8NQ, and 6NT element solutions agree well with the exact solution, but the 5NT solution does not agree with the analytical solution as well. Table 3.4 shows the comparison between the peak stress values for each element type relative to the exact solution. The 6NT and 8NQ higher-order elements agree with the exact solution the best. The 4NQ element solution is acceptable, but the 5NT element gives the worst correlation to the exact solution.
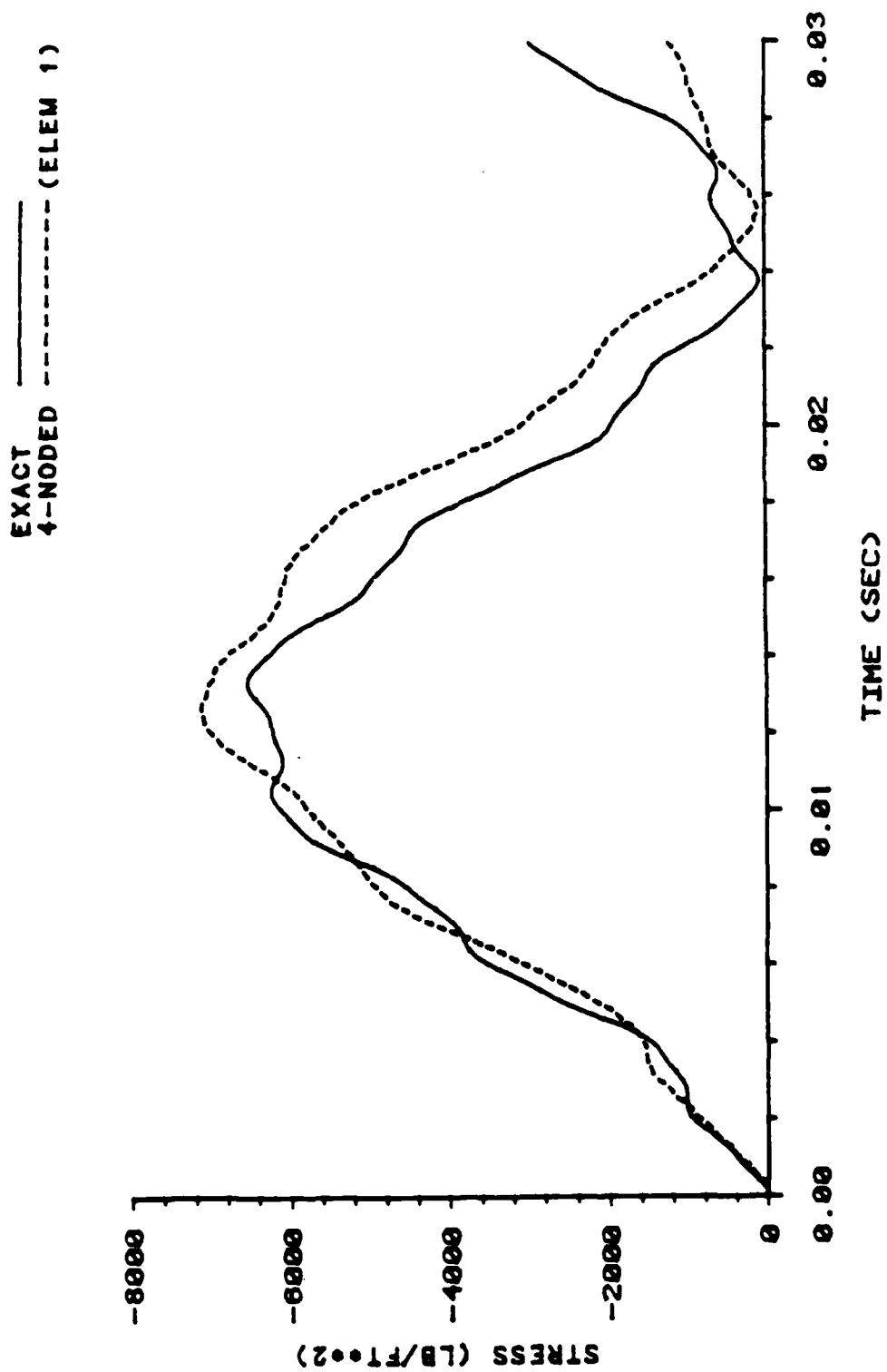
Figure 3.12   Cantilever Beam Problem: Maximum Stress vs. Time (Undamped Response).
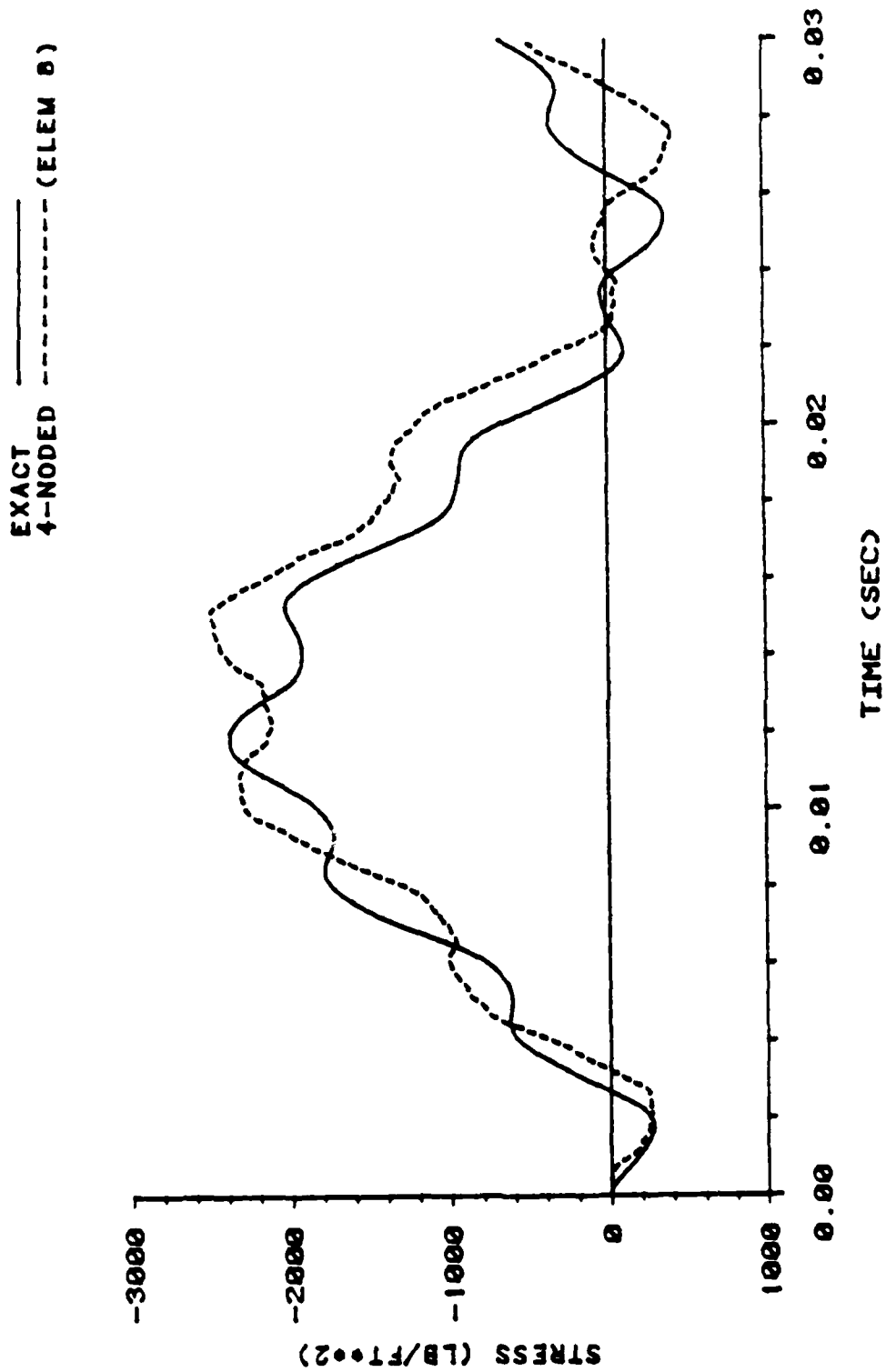
Figure 3.13   Cantilever Beam Problem: Stress vs. Time (Undamped Response).
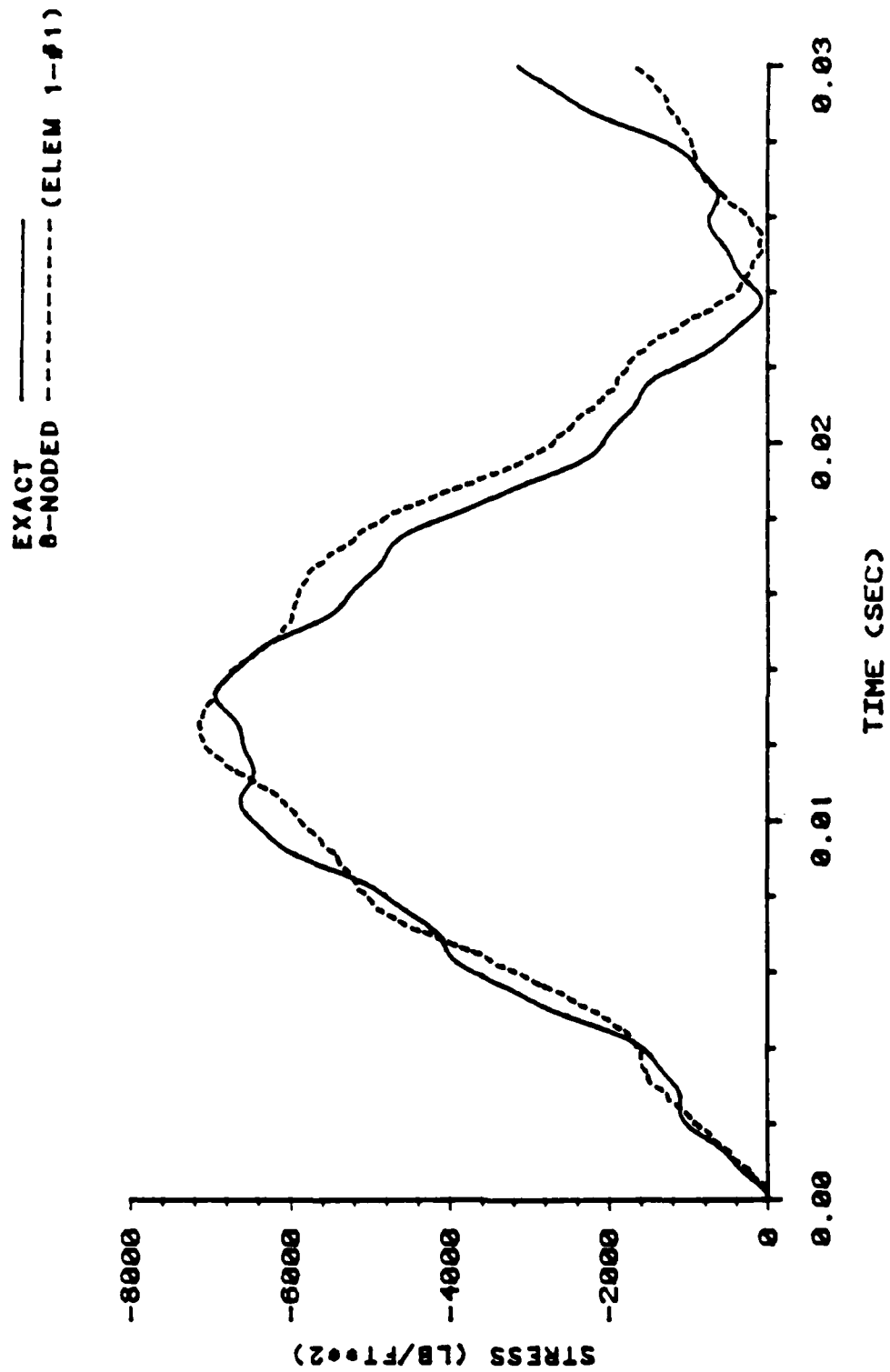
Figure 3.14 Cantilever Beam Problem: Maximum Stress vs. Time (Undamped Response).
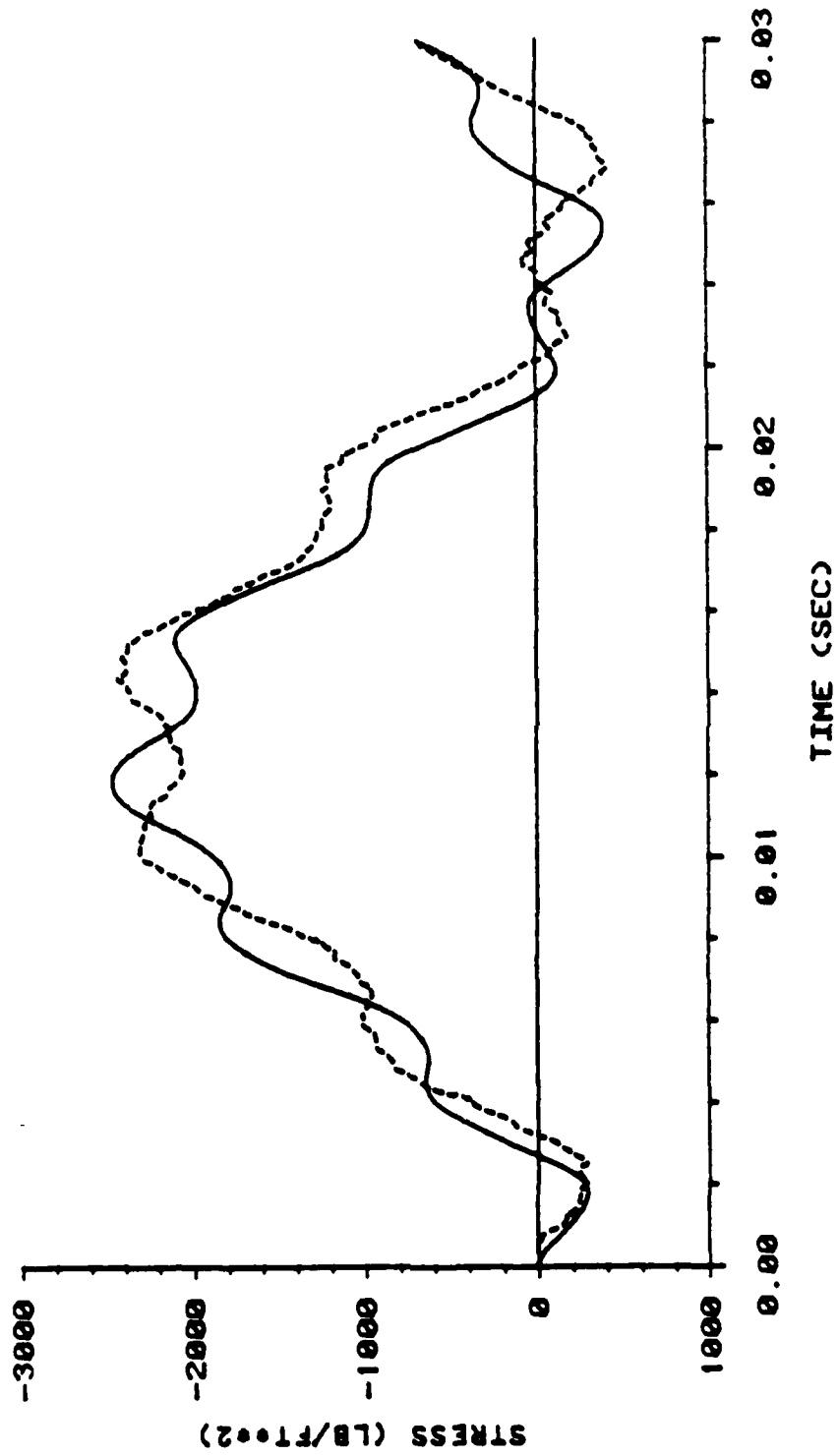
Figure 3.15   Cantilever Beam Problem: Stress vs. Time (Undamped Response).
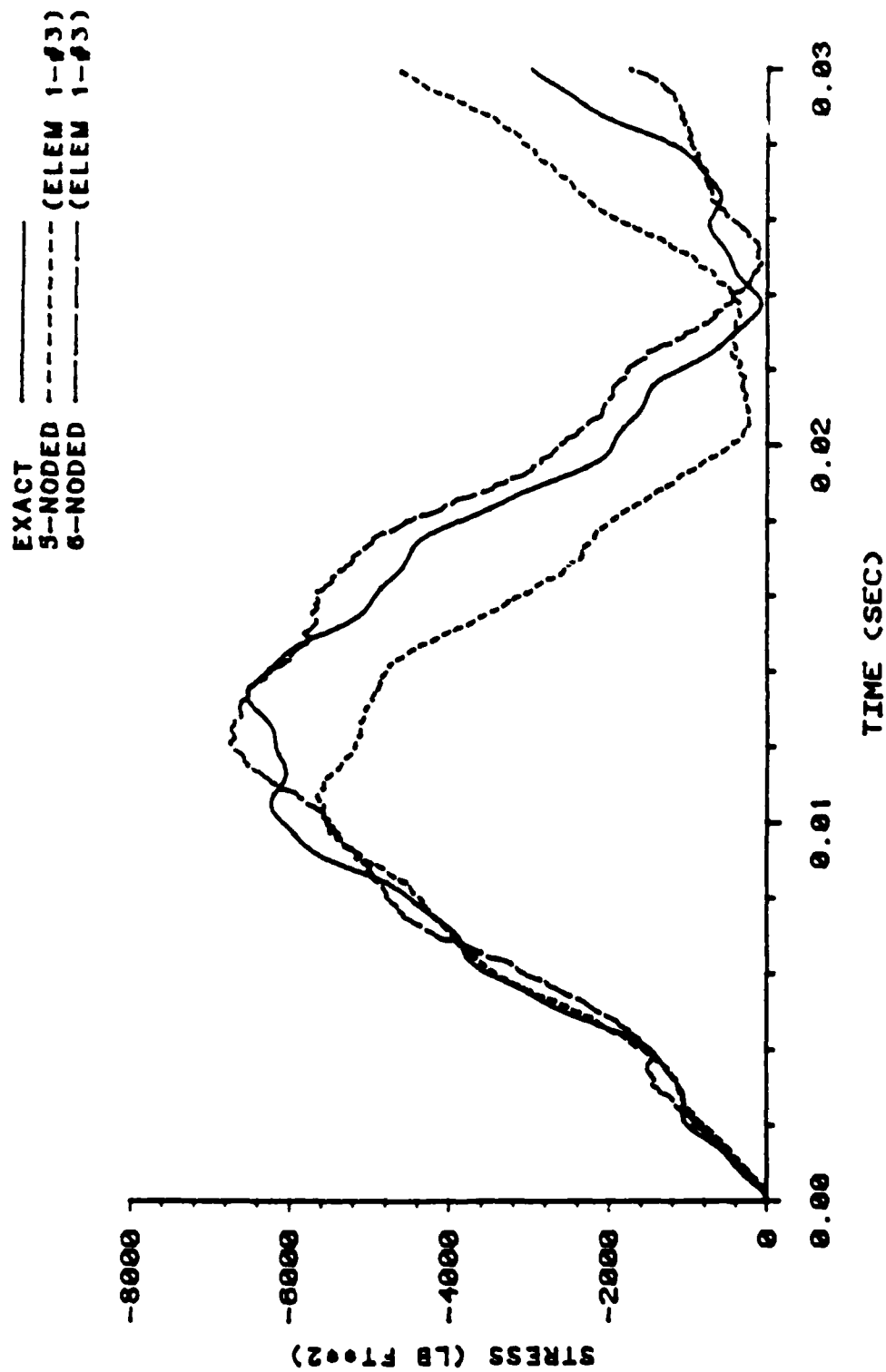
Figure 3.16   Cantilever Beam Problem: Maximum Stress vs. Time (Undamped Response).
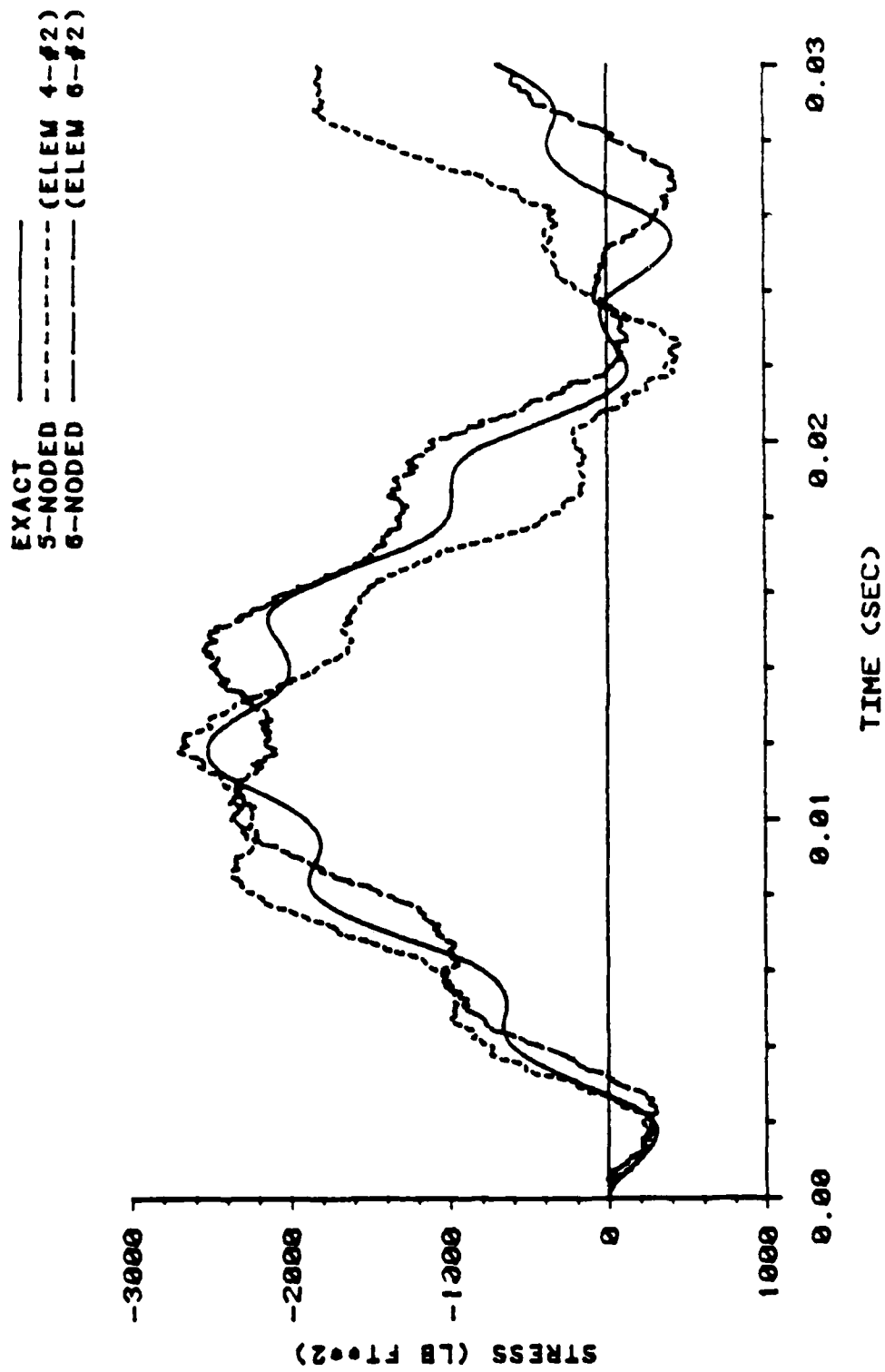
Figure 3.17   Cantilever Beam Problem: Stress vs. Time (Undamped Response).

35

Table 3.4   Comparison of Peak Values for the Curves in Figures 3.12 to 3.17.

Element Type	Element Number	Stress Location Within The Element x-coordinate (ft)	y-coordinate (ft)	Peak Stress from SAMSON2 (psf)	Peak Stress Analytical Solution (psf)	Percent Difference Based on Analytical Solution
4NQ	1	0.5	-1.5	-7126	-6556	8.7%
4NQ	8	7.5	-1.5	-2505	-2387	4.9%
8NQ	1 (int. pt. #1)	0.4226	-1.577	-7156	-6954	2.9%
8NQ	4 (int. pt. #3)	7.577	-1.577	-2447	-2474	1.1%
5NT	1 (int. pt. #3)	0.1501	-1.44	-5670	-6547	13.4%
5NT	4 (int. pt. #2)	7.69	-1.6429	-2711	-2524	7.4%
6NT	1 (int. pt. #3)	0.1501	-1.44	-6769	-6547	3.4%
6NT	6 (int. pt. #2)	7.69	-1.6429	-2560	-2524	1.4%

The execution times (CPU times) were recorded for each analysis of the cantilever beam in addition to the results presented previously. These CPU times were used to determine the relative efficiencies of the solutions using the four element types. Table 3.5 shows a representative sample of the CPU times obtained from the analyses. As shown, the 4NQ element solution was two to three times more efficient than the three HOE solutions. These significant increases in CPU time for the HOE solutions as compared to the 4NQ solution were attributed to the following: (1) more terms are included for each calculation involving the shape functions for the HOE due to the increased number of nodes per element, (2) more subroutines are used in the HOE solution schemes, and (3) the 5NT and 6NT element solutions involve twice as many stress calculations as the 4NQ element solution. It should be noted that these three conditions more than offset the time saved by the reduction in the number of the nodes resulting from the use of the HOE. Based on the third condition, if the same number of stress calculations were performed, an increase in CPU time of between 50 and 75 percent would be expected for the 5NT and 6NT element solutions when compared to the 4NQ solution.

Some general conclusions which are based on the results presented in the previous paragraphs, are as follows. The 6NT and 8NQ higher-order elements and the 4NQ element give correct solutions for both static and dynamic analyses for a problem involving flexural response with an elastic plane stress material law. Solutions involving these two HOE showed more accurate results with fewer nodes and elements than the 4NQ element solutions, but were much less efficient (more

Table 3.5   CPU Time Comparisons for the Four Element Types Used in the Analyses of the Cantilever Beam.

Element Type	CPU Time (secs)	Percent Difference Based on 4NQ Solution
4NQ	105.0	---
8NQ	224.1	113.4%
5NT	317.0	201.9%
6NT	339.8	223.6%

expensive). The decrease in the accuracy of the 4NQ element solution is due to the under-integration inherent in the formulation of this element as it exists in the SAMSON2 code (3). The 5NT element results varied greatly with respect to results from the other three elements for both the static and dynamic cases, except for the maximum dynamic displacement which compared well to results from an analytical solution which neglects the effects of shear deformation. These poor results were believed to be due to the fact that the 5NT element is not an entirely linear strain triangle because it only has two quadratic displacement sides. This fact could cause the 5NT element to behave in a manner similar to a constant strain triangle in that a soft response might occur which could only be corrected by increasing the number of elements used in the analysis (3). Another possible cause of the poor results exhibited by the 5NT element was the position of the midside nodes in the 5NT elements. For the analyses which were performed, the midside nodes were positioned on the hypotenuse and on one side of the triangle. A different discretization was devised with the two midside nodes being

on the two sides of the triangle and not on the hypotenuse. A solution using this different discretization involving the nodes on the two sides was attempted, but no output was obtained because of an incompatibility (zero area was computed by the program) between the input and the corresponding formulation of the 5NT element which could not be resolved. A final note on the 5NQ element is that this element did produce some acceptable results when compared to the analytical solution. Therefore, it might be possible to make use of this element for the transition from an 8NQ element to a 4NQ element as it was intended.

3.3 Soil-Structure Interaction

Based on the results for the HOE solutions from the previous two sections, especially the results for the 8NQ element, a more complex problem was chosen in order to further check the performance of the 8NQ element. A problem involving soil-structure interaction, the type of problem for which SAMSON2 was designed, was chosen. For this problem, no analytical solution is available and all of the 8NQ results were compared to those obtained by using the 4NQ. Although this comparison may not appear to be very practical, it gave a qualitative measure of the performance of the 8NQ element for this problem. The 4NQ has been shown by personnel at the AFWL to be reliable and accurate for similar soil-structure interaction problems when compared to actual test data.

The configuration of the soil-structure problem is shown in Figure 3.18a, b and c along with some input data and the primary load
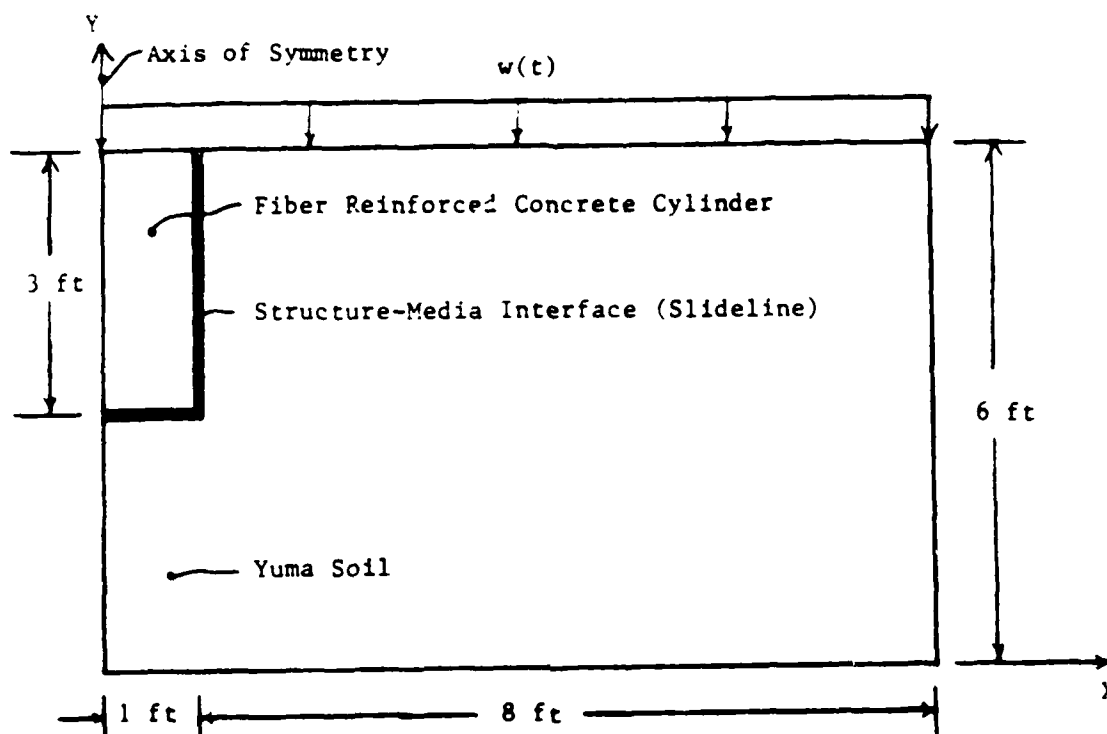
a) Problem Configuration

Δt = 1.0E-6 sec (time step)

ρ_c = .2516E-3 lb-sec^2/in^4 (mass density of concrete)

ρ_s = .173E-3 lb-sec^2/in^4 (mass density of soil)

E_c = .42E7 psi (modulus of elasticity of concrete)

E_s = .158E7 psi (modulus of elasticity of soil)

ν_c = 0.24 (Poisson's ratio for concrete)

ν_s = 0.38 (Poisson's ratio for soil)

μ = 0.01 (damping ratio)

b) Input Parameters

Figure 3.18   Soil-Structure Interaction Problem.

t ms	w(t) psi
0.0	0
0.2	50,000
0.4	25,000
1.2	15,000
3.0	7,000
6.0	3,000
10.2	2,200
20.2	1,000
40.2	500
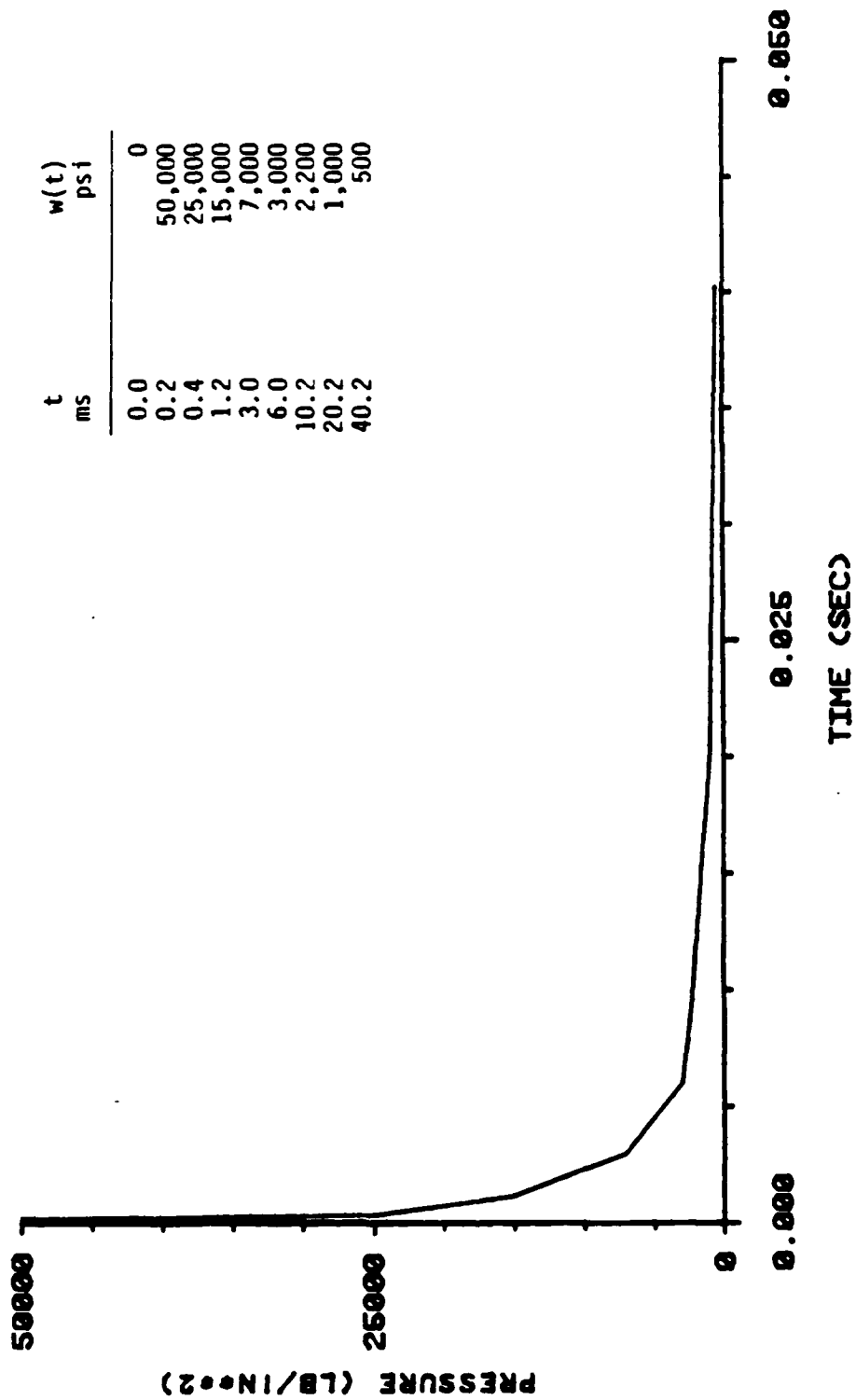
c) Applied Load

Figure 3.18   Soil-Structure Interaction Problem (Continued).

(nuclear airblast) used in the analyses. This problem is a scaled version of one which was analyzed and experimentally tested by the AFWL. The structure is a fiber reinforced concrete cylinder surrounded by Yuma soil separated by a structure-media interface. The input data pertaining to the two materials were obtained from AFWL material models. Additional input data are contained in Appendix A. Also, the slideline data are from the AFWL bilinear failure surface model for Yuma soil and fiber reinforced concrete. An integration order of 2.0 was used in the 8NQ analyses. The load curve was obtained from an actual test performed by the AFWL and was estimated for use in the analyses with the use of the NMERI Speicher/Brode Nuclear Airblast Curve algorithm based on a peak pressure of 50 ksi and a yield of 225 kt.

In the analysis of the soil-structure problem, the nodes on the bottom boundary of the soil field were not allowed to displace in the y-direction, while those on the right boundary could not displace in the x-direction. The lower right corner node was fixed in both the x- and y-directions. The problem was analyzed dynamically using an axisymmetric material law developed by the AFWL. The law is called the AFWL "engineering" model and was primarily designed to model soil behavior. It is defined by a piecewise linear hydrostat (a plot of hydrostatic pressure vs. volumetric strain) for which the critical identifying points are given as part of the input data (3). Strain softening and dilation cannot be modeled by the AFWL "engineering" law. Therefore, the hydrostat curve must be monotonically increasing (strain hardening) (6). It is important to note that the soil-structure problem should be analyzed in three dimensions in order to obtain the most

accurate results. However, SAMSON2 is a two-dimensional code, and, therefore, this problem was analyzed axisymmetrically with SAMSON2.

The soil-structure interaction problem was discretized separately into 4NQ and 8NQ elements for the analyses. The initial finite element mesh for the 4NQ consisted of 216 - 6 in. x 6 in. elements (204 soil elements, 12 concrete elements) and the initial mesh for the 8NQ consisted of 54 - 12 in. x 12 in. elements (51 soil elements, 3 concrete elements). These meshes contained relatively large elements (a coarse discretization) in order to keep the CPU times as short as possible, especially for the 8NQ solutions, and because only qualitative results were desired for comparison purposes. The 8NQ discretization was chosen such that one 8NQ element replaced four 4NQ elements. Therefore, a CPU time comparison could be made as was done for the cantilever beam problem.

A qualitative comparison was performed between the two solutions. In making this comparison, the principal values considered were the displacements and accelerations in the y-direction for all the nodes in the concrete cylinder as well as for a representative number of nodes in the soil. Also, the stresses in the y-direction (σ_y) were considered important for all elements in the concrete and for a typical number of soil elements. The values for these three output parameters were studied, both qualitatively with regard to their variation in response with time and numerically.

The comparisons for the initial (coarse) meshes rendered very few acceptable results. In general, the results obtained from the 8NQ element solution using the initial coarse mesh in the concrete

(Figure 3.19b) exhibited a significant amount of variation. For instance, the upper right node in the structural mesh (node 202) had a y-displacement value three times that of the other two adjacent nodes (nodes 200 and 201) at the end of the tenth time step (the first time step for which output was obtained). This variation was thought to be due to one of three conditions: (1) the mesh which was used was too coarse, (2) instability existed in the solution, or (3) the slideline calculations for the 8NQ element were in error. The 4NQ element solution, in contrast to the 8NQ solution, had very consistent results. In fact, the top three nodes in the coarse 4NQ finite element mesh of the concrete cylinder (nodes 242, 249, and 256 in Figure 3.19a) had equal values for both the y-displacements and y-accelerations at the end of the tenth time step. The stresses for the 4NQ solution were also consistent, while those for the 8NQ were erratic due to the unequal y-displacements and y-accelerations of the upper nodes. A comparison of the values for the y-displacements, y-accelerations, and stresses in the y-direction (σ_y) was performed at the end of the tenth time step. The y-displacement and y-acceleration values for nodes 242 and 249 in the 4NQ mesh were twice those of nodes 200 and 201 in the 8NQ mesh, while the values for node 256 in the 4NQ mesh were significantly less than those for node 202 in the 8NQ mesh. A comparison of stresses between the top element in the 8NQ mesh (element 54) and the top four elements in the 4NQ mesh (elements 209, 210, 215 and 216) showed an acceptable correlation for only one stress value. The stress at the upper right integration point of element 54 was within 12% of the stress in element 216. The normal stress (σ_x) also compared well at this location. The

45

52

53

54

b) 8NQ Elements

216	215	214	213	212	211
210	209	208	207	206	205
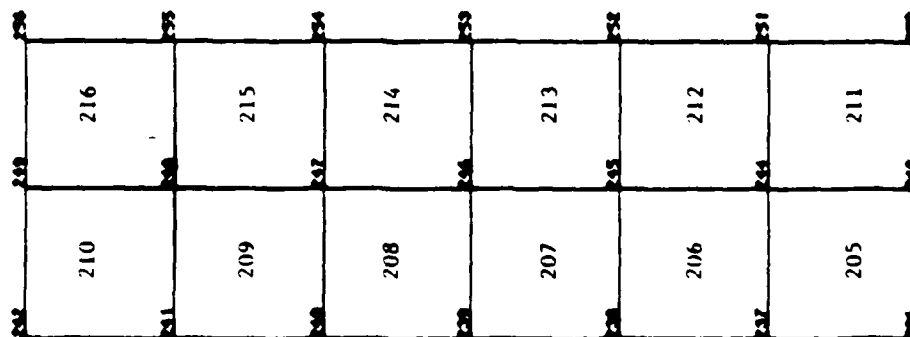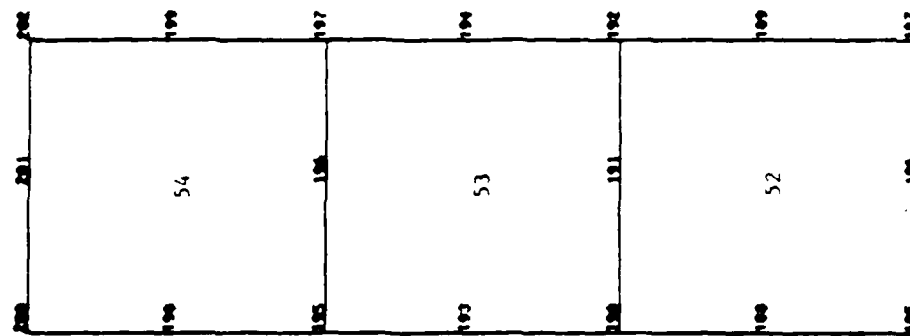
a) 4NQ Elements

Figure 3.19   Soil-Structure Interaction Problem: Initial (Coarse) 4NQ and 8NQ Discretizations of the Concrete Cylinder.

shearing stresses in the 8NQ solution at the tenth time step were significantly higher than those from the 4NQ solution. These large differences in the shearing stresses as well as for the other stresses resulted from the large numerical discrepancies in the y-displacements at the top of the 8NQ mesh. The other nodes in the 8NQ mesh behaved much the same as the top row of nodes, but exhibited one additional trend which was previously discovered in the one-dimensional wave propagation problem. Many of the nodes located below the second row of nodes in the 8NQ mesh (nodes 198 and 199) displaced upward (positive direction) which is opposite to the direction of the applied blast load, while the corresponding nodes in the 4NQ all displaced downward (negative direction).

The 8NQ solution was corrected with time as in the wave propagation problem, but only to a certain extent. Most of the nodes in the structure did reverse directions by the end of 400 time steps. The y-displacement values for nodes 200, 201 and 202 did tend toward the same value, but the y-displacement for node 202 was still greater. The y-displacements for the nodes on the right vertical boundary (slideline nodes 202, 199, 197, 194, 102, 189, and 187) were, in most instances, greater than the y-displacements for the corresponding nodes to the left of the slideline. Stress values (σ_y) at similar levels within the structural mesh were approximately equal (consistent at these levels) at certain times during the solution, but this consistency was not observed on a regular basis. Oscillations (wave propagations) were apparent throughout the solution as was shown in the plots of y-accelerations, stresses in the y-direction (σ_y), and y-displacements in the SAMSON2

output. Results from the soil elements were consistent for the entire time of solution.

Quantitative comparisons of results between the 4NQ solution (solution remained consistent with the nodes being almost equal for each individual row, but those on the slideline displaced slightly more than the others) and the 8NQ solution were performed at every tenth time step in addition to a qualitative overall comparison. Some numerical comparisons showed acceptable results, while the majority of the results compared poorly. The y-displacements for the top two rows of nodes in the soil were within 8% of each other at t = .2E-3 (200 time steps), but deviated by up to 37% at t = .4E-3 (400 time steps), respectively. The best soil stress correlations differed by 17%. Stresses in the concrete cylinder, particularly σ_y, matched well at certain times, but varied with the propagations of the waves through the structures. Therefore, this correlation of stresses might have been by coincidence more than anything else. The large shear stress discrepancies discovered at the tenth time step were significantly reduced with time. Qualitatively, both solutions displayed the wave propagation phenomenon throughout the structure, but the 8NQ solution was trailing that of the 4NQ as if the wave speeds in the two were quite different. The plots of the y-displacements in the SAMSON2 output for the 4NQ solution showed the wave propagation interaction more than those for the 8NQ solution. In general, the nodal displacements for the corresponding rows are qualitatively similar such that the displacements are larger for nodes closer to the slideline. The values for the nodal y-displacements from the 4NQ solution are greater than those from the 8NQ solution, except in

the top row, even though at certain times there was good agreement between corresponding values.

Many variations in the solutions were attempted in order to improve the results stated in the previous paragraphs for the initial 4NQ and 8NQ coarse discretizations. The variations to the input were as follows:

(1) energy error output was requested for the two solutions to determine if unstable conditions were present,

(2) the slave nodes were reordered in the slideline in an attempt to eliminate the erratic behavior present in the 8NQ solution,

(3) reduced loadings were applied to reduce the possibility of instabilities occurring in the solution,

(4) finer mesh discretizations of the concrete cylinder were used in the 4NQ and 8NQ solutions, and

(5) the order of integration was increased to 3.0 for the 8NQ solution.

The results from requesting the energy error output are shown in Figures 3.20 and 3.21. These figures, if assumed reliable based on the findings of Berglund and Rudeen in Reference 6, show that both solutions are unstable because the energy error exceeds 1% (1, 9). In Reference 6, it was pointed out that the energy terms calculated in SAMSON2 are either in error or incomplete and need to be corrected. In the current study, assuming the results from the Figures 3.20 and 3.21 to be reliable, the possibility of excessive distortion was investigated in order to determine if the 8NQ formulation was still valid (11). No
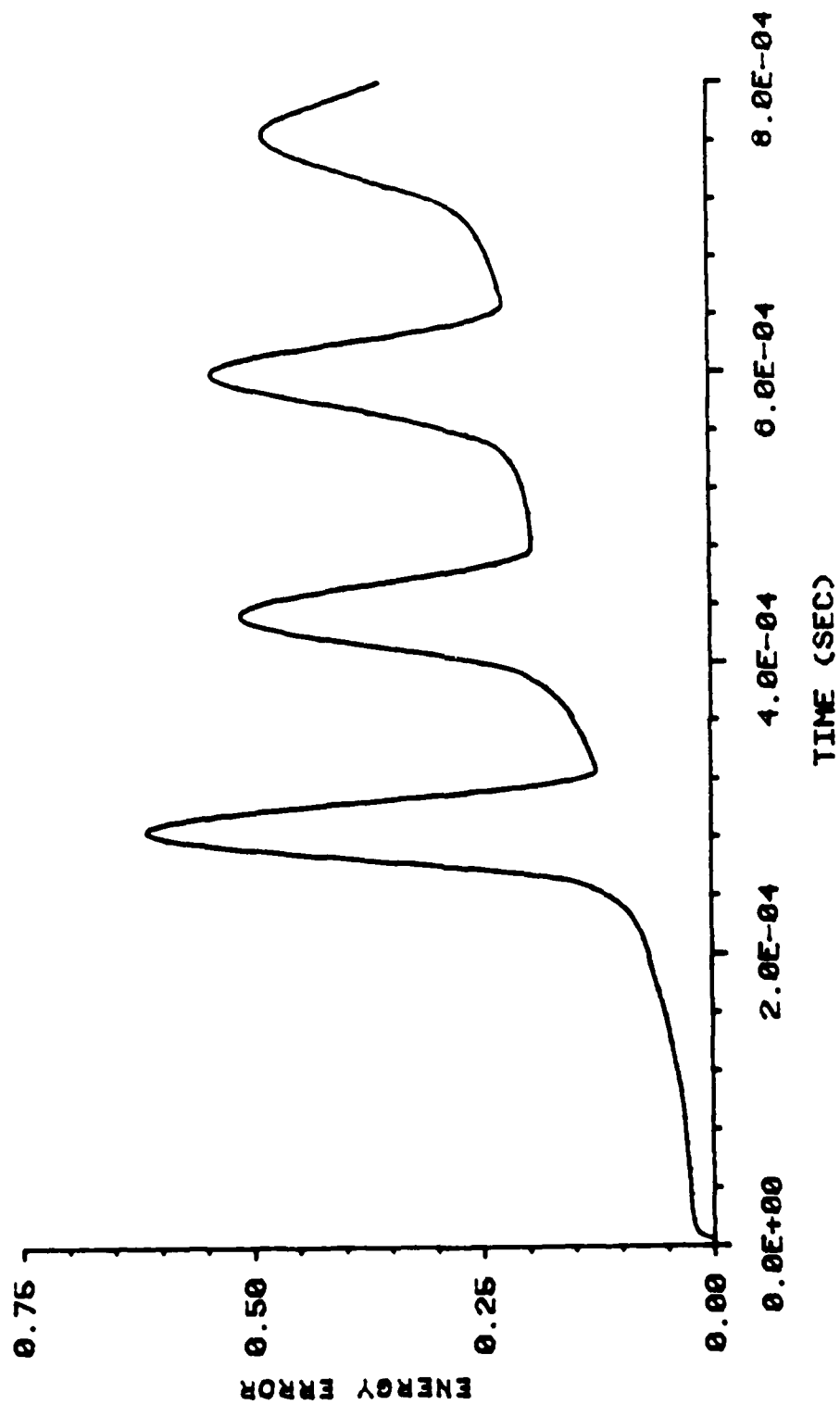
Figure 3.20   Soil-Structure Interaction Problem: Energy Error vs. Time for the 4NQ Element Discretization.

49
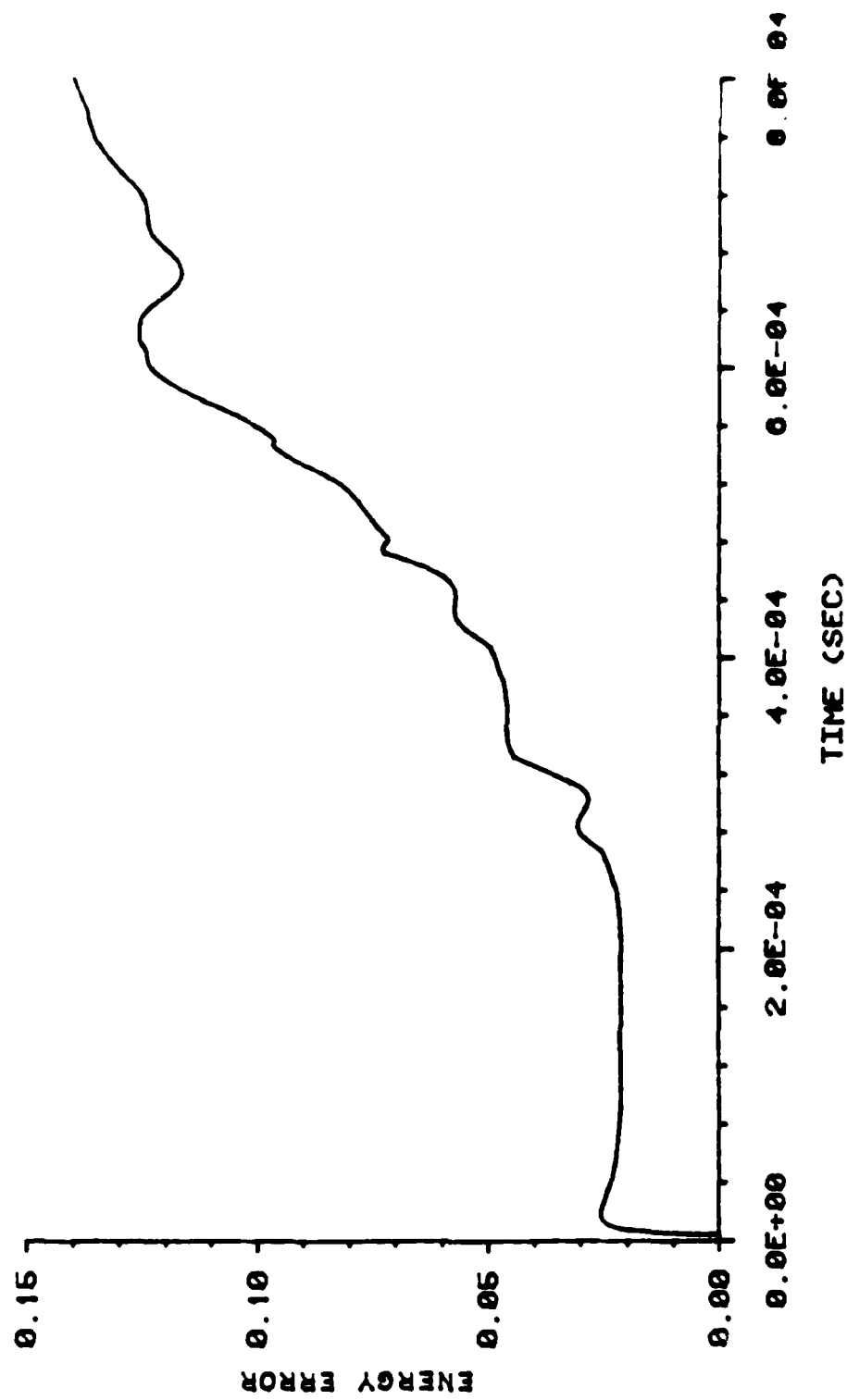
Figure 3.21 Soil-Structure Interaction Problem: Energy Error vs. Time for the 8MJ Element Discretization.

apparent excessive distortion was located during the current study. Upon investigating the possibility of excessive distortion, a study of time step sizes versus changes in the solutions was performed. The time step size was halved, and then halved again. No apparent changes occurred in either of these two solutions. Therefore, the solutions were considered to be stable, especially since Figures 3.20 and 3.21 show the 4NQ solution to be more unstable than that for the 8NQ for the same time step size. It was found in the execution of the cantilever beam problem that the stable time step for the 8NQ solution was less than that which could have been used in the 4NQ solution. An additional note to this information is that the curves for each of the energy components (kinetic, internal, and external work) displayed the same patterns.

The second variation in the input that was performed in an attempt to improve the 8NQ results when compared to those obtained for the 4NQ, was a change to the order of the slideline nodes. This change was performed due to a phone conversation with personnel of the AFWL (4). The actual change was just a reversal of the order of the input for the slave nodes. Instead of inputting the nodes from top to bottom, they were input from bottom to top so that the first slave node was adjacent to the last master node on the slideline. The result of this change was very minor and affected mostly the lower nodes of the structural meshes. No relative improvement in results was obtained.

The third variation was the application of a reduced load in order to lessen the chance of instabilities occurring as well as to make the solution perform more elastically with little or no plastic flow. The

first load variation was the blast load reduced by a factor of 500 (peak pressure of 100 psi in place of 50,000 psi). The results obtained for the initial structural meshes with this applied load were no better than those for the originally applied airblast load. The same trends in the nodal displacements existed in these solutions as in the previous ones. Another solution was executed with the 100 psi load reduced to a peak value of 1 psi and twice the run time used in each of the previous solutions. The solution time was doubled in order to determine if the 8NQ solution would converge further. The results from the solution using the 1 psi load and the double run time compared well with those obtained with the use of the 100 psi load, such that at time $t = .4E-3$ (the total run time for the 100 psi solution) all results differed by a factor of 100 which was the same ratio between the two applied loads. These results showed that the two solutions which were obtained with the use of the reduced loads were both stable and in the elastic range as was desired in these analyses. The remainder of the results (from $t = .4E-3$ to $.8E-3$) for the 1 psi peak load revealed the following:

(1) The nodes on the slideline in the two solutions no longer had the largest values for the y-displacement, but instead the displacements got larger in proceeding toward the left side of the structural mesh along a row. This behavior was opposite to that found for previous solutions. The slideline nodes acted as if they had reached a limiting state. This new displacement pattern was found throughout the entire 4NQ mesh and in the top two-thirds of the 8NQ mesh.

(2) Some better comparisons were obtained between the two solutions for values of nodal displacements and elemental stresses. But, as before, these good results were only obtained for particular locations and not throughout the structural meshes.

(3) The 8NQ results were much more consistent and reacted more like the 4NQ solution. All y-displacements for the 8NQ structural mesh (coarse) were downward after 680 time steps (t = .68E-3).

The fourth variation undertaken to further improve the results between the 4NQ and 8NQ solutions was new discretizations of the structural meshes using more nodes and elements. These new discretizations were done in order to determine if the element sizes in the two initial structural meshes caused the discrepancies in the results shown previously. The first new discretization involved an increase in the number of nodes and elements in the 8NQ structural mesh (the finer mesh in Figure 3.22b). An analysis using this finer mesh and the 1.0 psi peak load was executed. The outcome from this analysis was much more consistent (displacements [stresses] within the structure were approximately equal at similar levels in the mesh) compared to prior analyses. Qualitatively, this solution exhibited the same trends when compared to the 4NQ solution for the 1.0 psi load performed previously. When these two solutions were compared numerically at the same time step, the values for the y-displacements for the 8NQ solution were an average of 20% less than those for the 4NQ solution (stress values were correspondingly less also). Table 3.6 shows values for the
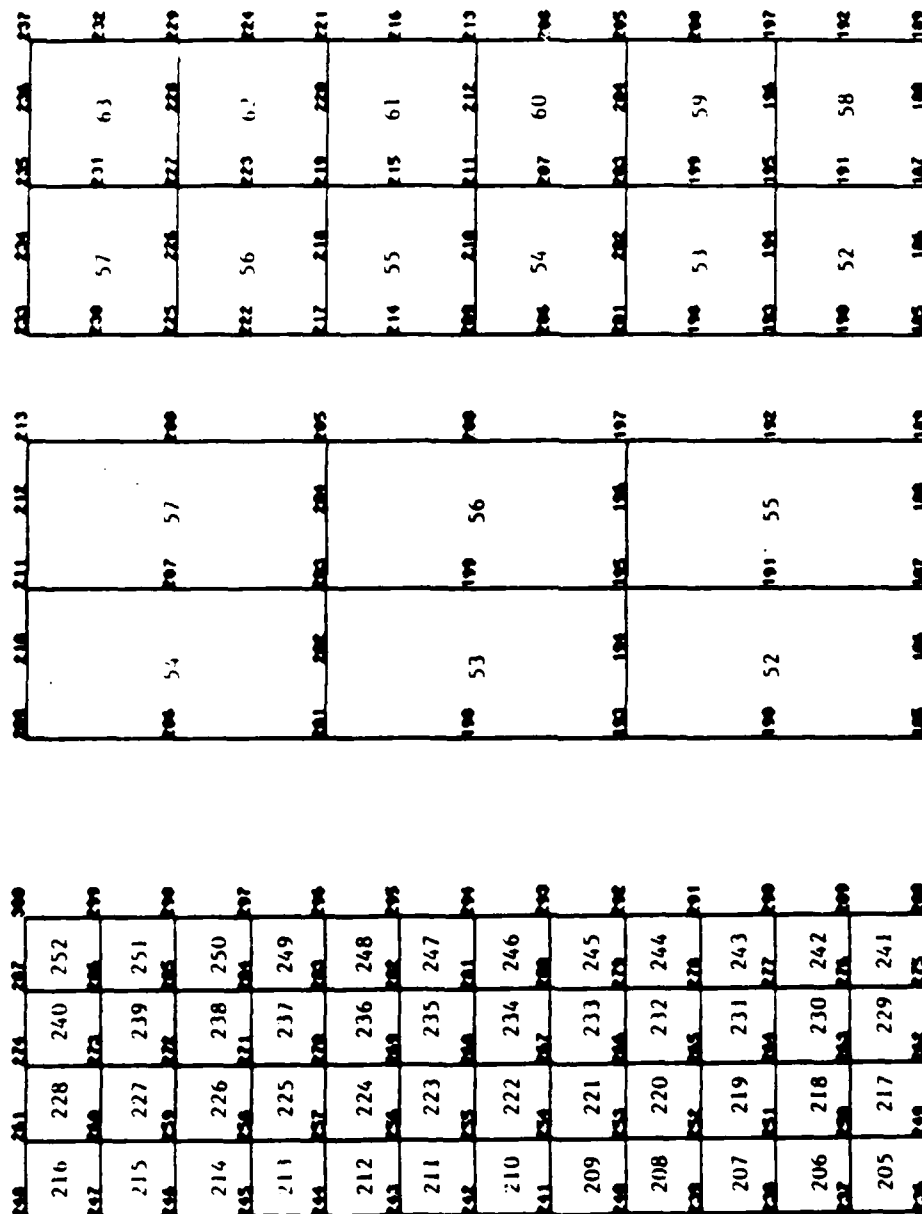
a) 4NQ Element Discretizations

b) 8NQ Element Discretizations

Figure 3.22   Soil-Structure Interaction Problem: Finer 4NQ and 8NQ Discretizations of the Concrete Cylinder.

Table 3.6   Comparison of Y-Displacements Between the 8NQ Solution (Finer Mesh) and the 4NQ Solution for a 1.0 psi Peak Load.

Original Node Location		8NQ Y-Displacement $t=.8 \times 10^{-3}$ sec	4NQ Y-Displacement $t=.8 \times 10^{-3}$ sec	Percent Difference Compared to 4NQ at $t=.8 \times 10^{-3}$ sec
x-coordinate (in)	y-coordinate (in)	(in x 10^{-4})	(in x 10^{-4})	
0.0	72.0	-.1927	-.2112	8.8%
3.0	72.0	-.1851	---	---
6.0	72.0	-.1749	-.2009	12.9%
9.0	72.0	-.1633	---	---
12.0	72.0	-.1678	-.1972	14.9%
0.0	66.0	-.1774	-.2073	14.4%
6.0	66.0	-.1699	-.1961	13.4%
12.0	66.0	-.1587	-.1912	17.0%
0.0	60.0	-.1618	-.1996	18.9%
3.0	60.0	-.1626	---	---
6.0	60.0	-.1593	-.1878	15.2%
9.0	60.0	-.1550	---	---
12.0	60.0	-.1463	-.1831	20.1%
0.0	54.0	-.1498	-.1949	23.1%
6.0	54.0	-.1421	-.1785	20.4%
12.0	54.0	-.1304	-.1710	23.7%
0.0	48.0	-.1343	-.1898	29.2%
3.0	48.0	-.1264	---	---
6.0	48.0	-.1218	-.1711	28.8%
9.0	48.0	-.1183	---	---
12.0	48.0	-.1161	-.1612	28.0%
0.0	42.0	-.0944	-.1788	47.2%
6.0	42.0	-.1095	-.1639	33.2%
12.0	42.0	-.1162	-.1563	25.7%

y-displacements obtained from the two solutions at time $t = .8 \times 10^{-3}$ sec (the last time step). A comparison of the two sets of values from the two solutions resulted in a percent difference ranging between 9% and 47% (average was approximately 20%). The reason for this significant difference between the two solutions for such a small loading was not readily apparent to the author at that point in time.

However, the reason was determined later in this investigation. Further refinements were made to both the 4NQ and 8NQ structural meshes (the finer 4NQ mesh and the finest 8NQ mesh in Figure 3.22). These meshes were then used in the analyses. The results from these new analyses still produced a 20% difference between the two solutions. The two finest meshes were then subjected to the initially applied blast load (50 ksi peak pressure) to determine if a 20% difference between the two solutions would still occur. The comparison of the results from these two executions yielded a 15% difference between the same values of y-displacement. It should be noted that the stress values could not be compared at similar time steps due to the differences in the wave speeds in the two solutions. One further observation involving only the 8NQ solution was that the results were much more consistent compared to previous analyses using the blast loading.

The fifth variation used in the analyses of the 8NQ solution was an increase in the order of integration from 2.0 to 3.0. The integration order for the 8NQ was increased in an effort to further reduce the differences in values between the 4NQ and 8NQ element solutions. The results occurring from this change showed no relative improvement in the comparison between the two solutions.

Three conclusions and one related recommendation were made based on the results of the analyses for the soil-structure interaction problem using the 8NQ element. The first conclusion was that the 8NQ solutions (those obtained using the two refined meshes in Figure 3.22b) produced consistent results for the different analyses of a soil-structure interaction problem involving an applied blast load and analyzed

axisymmetrically using the AFWL "engineering" model. The results from these solutions have not, as yet, been shown to be reliable. In fact, these solutions were significantly different (15-20%) when compared to those obtained with the use of the 4NQ element. These differences must be interpreted carefully however, because the true reliability of the 8NQ solution has not been verified since no analytical solutions or test data were available for comparison. The second conclusion was that the energy formulation was in error. The third conclusion was that the 8NQ element solutions were definitely obtained less efficiently than analyses obtained using the 4NQ element. The 8NQ element solutions required on the average 75% more execution time than those solutions using the 4NQ elements. The reasons for this CPU time difference were explained in the discussion for the cantilever beam. The one recommendation was that the 8NQ element should be used by personnel at the AFWL in an analysis of a soil-structure interaction problem for which test data are available. The comparison between the test data and this 8NQ element solution would give a measure of the reliability of the 8NQ solution. However, if the 8NQ is still found to be unreliable it may be due to one of the following: (1) an error in the 8NQ axisymmetric formulation, (2) an incorrect interaction between the slideline and 8NQ formulations, or (3) an incorrect definition of plastic flow in the 8NQ formulation. It should be noted that the version of SAMSON2 used in the analyses in this study does not include any updates in the slideline routines which have been formulated by the AFWL in the last couple years.

3.4 Additional Analyses

Two more problems were analyzed using the 8NQ higher-order element (a 4NQ analysis was also performed for each) for which analytical solutions exist. The first problem was a static analysis (dynamic relaxation) of a fixed-end beam. This beam had the same dimensions and discretization as the cantilever beam discussed earlier in this investigation and was subjected to a concentrated load at the center of the beam. The beam was analyzed using a biaxial elastic-perfectly plastic plane stress (Poisson's ratio = 0.0) material law. This problem was chosen for analysis in order to further determine the reliability of a 8NQ solution after plastic flow had been initiated. The second problem was an axisymmetric analysis involving one-dimensional wave propagation. The orientation of the geometric configuration for the previous one-dimensional wave-propagation problem was rotated 90° for use in the current axisymmetric analysis. The same element discretizations (nodes renumbered) and material law were used for this axisymmetric analysis. The same displacement function versus time was applied to the lower nodes for this axisymmetric configuration. The boundary conditions were changed to fixed in the x-direction and free in the y-direction. This problem was selected in order to further test the reliability of a dynamic axisymmetric 8NQ solution. The input data used in the analyses of these two problems are in Appendix A.

The results from the 8NQ element analysis of the fixed-end beam compared very well, both elastically and plastically, to the analytical solutions. The maximum y-displacement and normal stress values obtained from the elastic 8NQ solution differed by 0.5% and 1.5%, respectively,

when compared to values obtained from calculations involving Equations 3.7 and 3.8.

$$y_{max} = \frac{PL^3}{192EI_x} + \frac{1.2\ PL}{4GA} \tag{3.7}$$

where,

P = peak value of the applied concentrated load (lbs),

L = length of the beam (ft),

E = modulus of elasticity for the beam (psf),

I_x = moment of inertia about the x-axis (ft^4),

G = shearing modulus (psf), and

A = cross-sectional area of the beam (ft^2).

$$\sigma_x = \frac{M_x y}{I_x} = (\frac{4Px}{8} - \frac{PL}{8})\ \frac{y}{I_x} \tag{3.8}$$

where,

M_x = moment at any distance $x < \frac{L}{2}$ from the left side of the beam (ft-lb),

x = distance to the right of the left side of the beam (ft), and

y = distance above (+) or below (-) the neutral axis of the beam (ft).

Other values for other locations within the beam also compared well.

The elastic-perfectly plastic 8NQ solution was not compared directly to analytical solution values, but instead was compared qualitatively to corresponding theoretical concepts and to the 4NQ solution through observation of the stress patterns in the 8NQ solutions after the yield point value had been reached. The 4NQ and 8NQ solutions

both exhibited local yielding for elements in their respective meshes after the yield point value had been exceeded. The stress (σ_x) distributions for particular cross-sections of the beam were plotted both before and after yielding and the results were compatible with mechanics of materials principles (7, 11). The distributions for the elastic cross-sections varied linearly, while those for the elastic-perfectly plastic solutions were constant for the top and bottom portions of the beam with connecting linear variations. Another observation made from the results was that redistribution in elemental stresses occurred as a result of local yielding. The elements nearest to the fixed-ends and nearest to the center of the beam had very small increases in stress values after the initial elastic load was increased, while the other elements had much larger stress increases. This difference between the relative increases in stress values between the different elements was compatible with plasticity theory. Two other observations were made: (1) the y-displacements for the nodes at the center of the beam for both the 4NQ and 8NQ solutions were much larger after yielding had occurred as opposed to the elastic displacements, and (2) the output values (displacements and stresses) were larger in the 8NQ solution compared to those of the 4NQ due to the fact that the 8NQ solution predicts higher elastic stress values because of the difference in the order of integration between the 4NQ and 8NQ elements.

The results for the axisymmetric analysis of a wave propagation problem were compared numerically and qualitatively to the previous solutions (Section 3.1). Output values obtained from the current 4NQ solution (displacements, velocities, and stresses in the y-direction)

were identical to the corresponding values from the previous 4NQ analysis of the one-dimensional wave propagation problem (displacements, velocities, and stresses in the y-direction). However, similar values obtained from the current axisymmetric 8NQ solution did not compare well with those from either the current axisymmetric 4NQ solution or the previous one-dimensional solution. Figures 3.23, 3.24, and 3.25 show representative examples of the deviations between the 4NQ and 8NQ axisymmetric solutions. Similar deviations occurred between the two solutions for other nodal y-displacement and y-velocity values as well as for other elemental stress (σ_y) values. In comparing Figures 3.23-3.25 to similar figures in Section 3.1, it was apparent that the 8NQ solution lagged the 4NQ solution in the axisymmetrical analyses, particularly in the displacement and stress plots. The results from comparing these two axisymmetric solutions numerically at the same time step were that the 8NQ values were around 15% less than those from the 4NQ solution.

Two conclusions were made based on these results. The first conclusion was that the 8NQ performed properly when used in a static elastic-perfectly plastic plane stress solution. Strain hardening was not attempted since the elastic-perfectly plastic solution results were so good. The second conclusion was that an error appears to be present in the 8NQ axisymmetric formulation. This conclusion was made on the basis of results obtained from the current wave propagation analyses and the axisymmetric analyses of the soil-structure interaction problem.
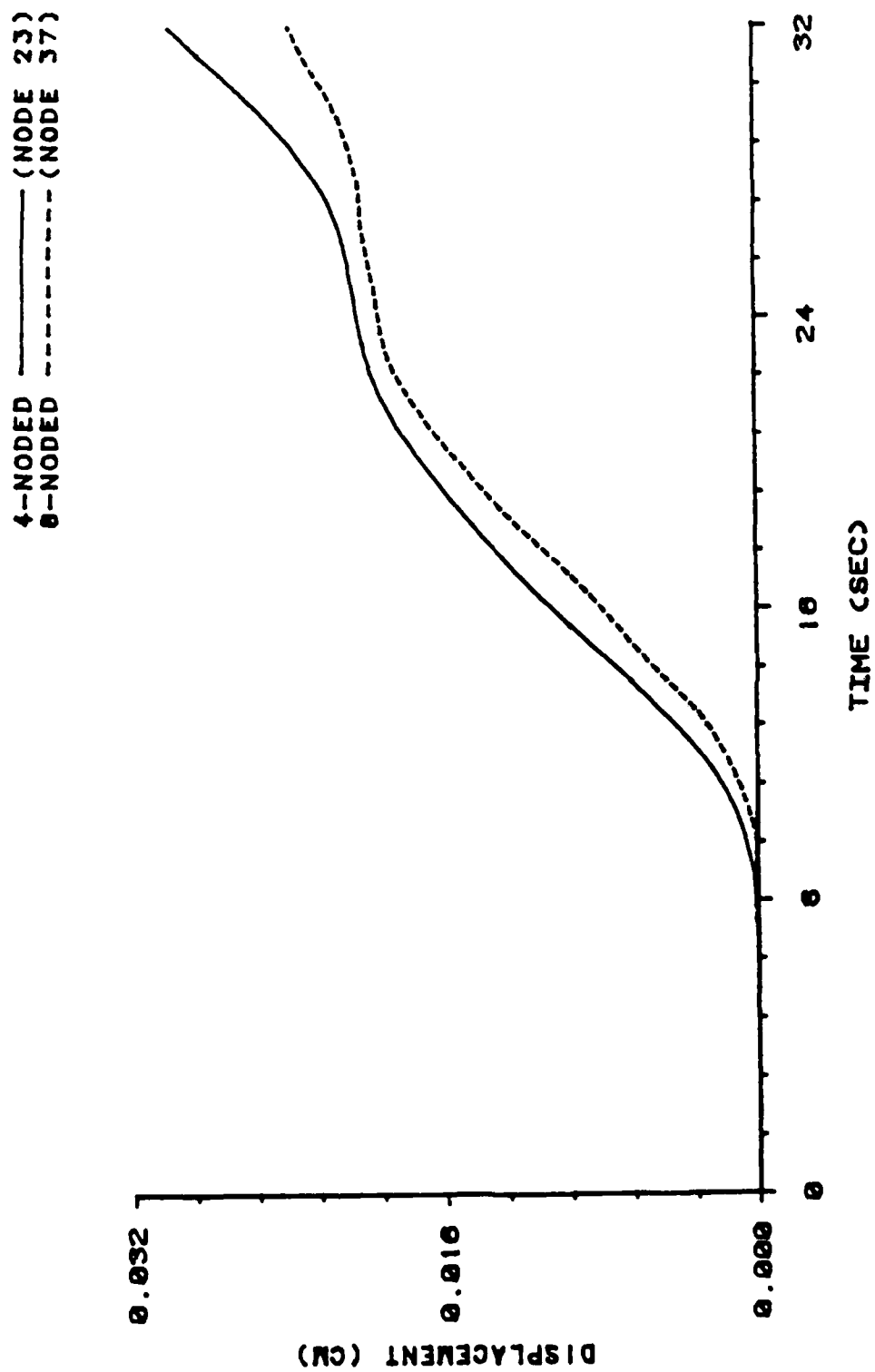
Figure 3.23   Axisymmetric Analysis of the One-Dimensional Wave Propagation Problem: Displacement
vs. Time at Y = 8.0 cm.
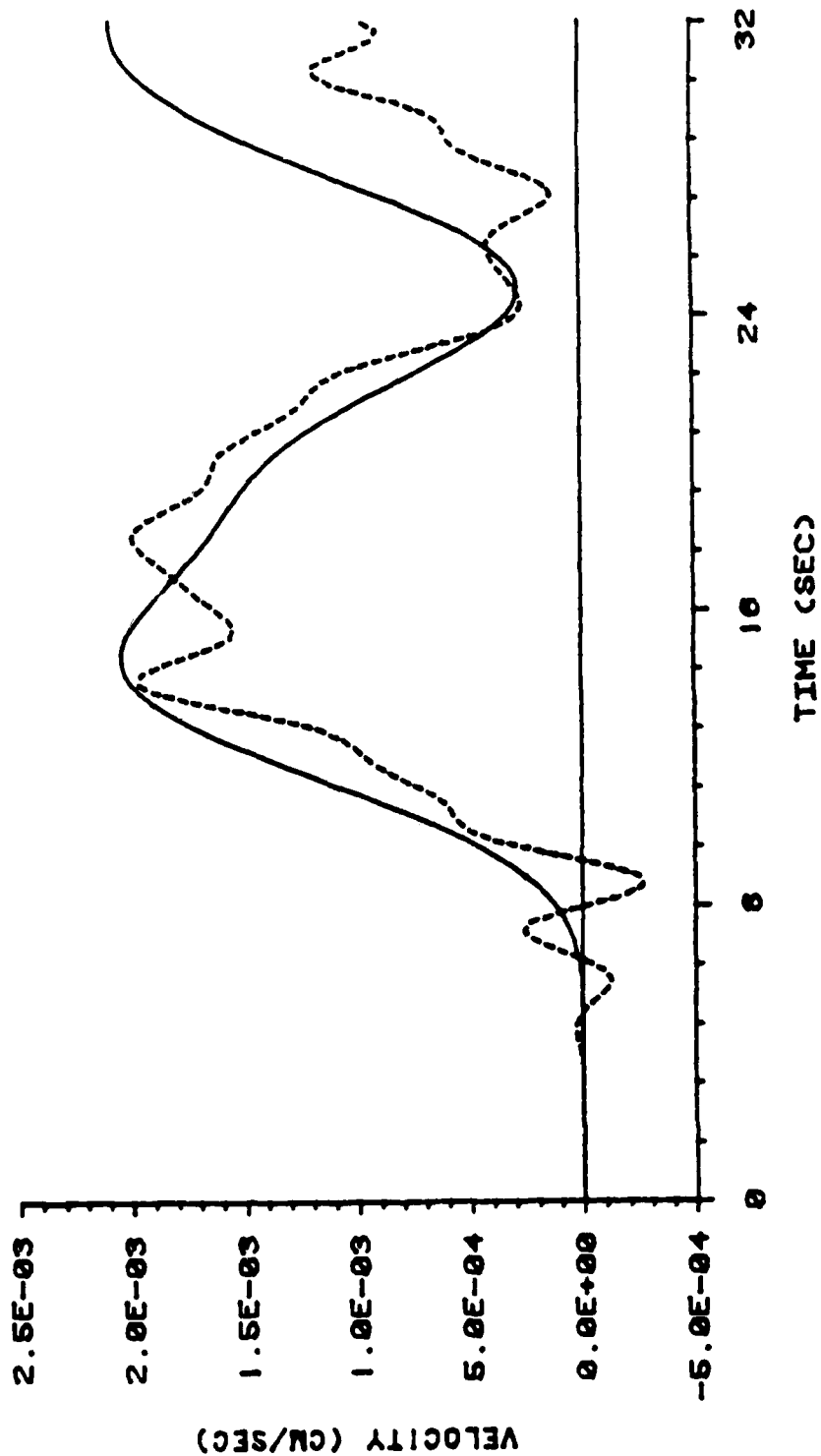
Figure 3.24   Axisymmetric Analysis of the One-Dimensional Wave Propagation Problem: Velocity vs. Time at Y = 8.0 cm.

63
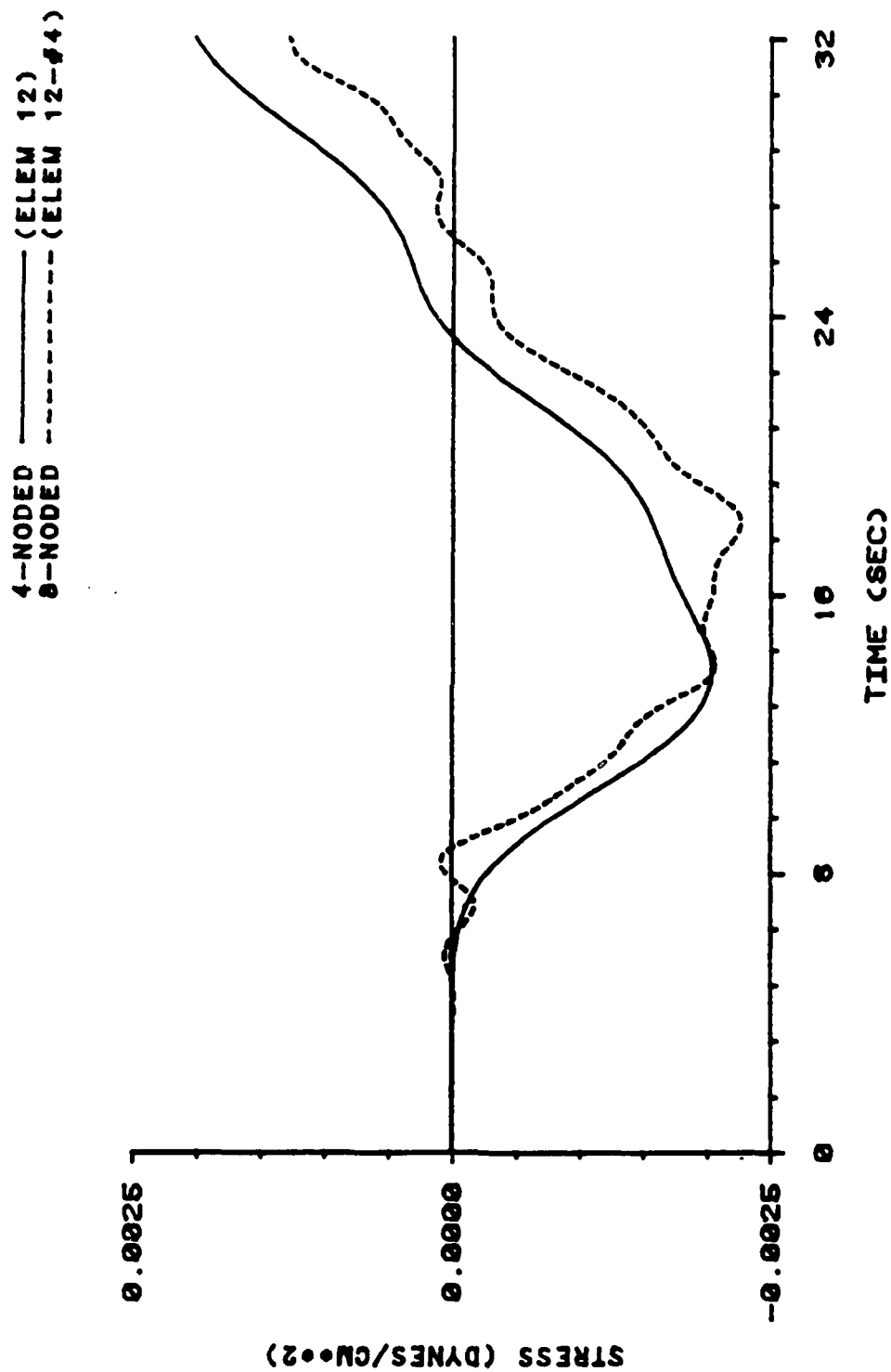
Figure 3.25 Axisymmetric Analysis of the One-Dimensional Wave Propagation Problem: Stress vs. Time at Y = 7.0 cm.

3.5 Summary of Results and Conclusions

Five different problems of various complexities were analyzed using the current 8NQ higher-order element formulation in the SAMSON2 code. The 5NT and 6NT higher-order element formulations were also tested with a cantilever beam solution.

The results from the analyses using the 5NT, 6NT and 8NQ higher-order elements were quite good overall. The 8NQ element results compared exceptionally well with analytical solution values for the dynamic elastic analysis of a one-dimensional wave propagation problem, the static and dynamic elastic analyses of a cantilever beam problem, and the static elastic-perfectly plastic analysis of a fixed-end beam problem. Discrepancies in the 8NQ results were found in the dynamic axisymmetric elastic-plastic analysis of the complex soil-structure interaction problem and the dynamic axisymmetric elastic analysis of a one-dimensional wave propagation problem. The 6NT element results compared very well with values obtained from the analytical solutions for both the static and dynamic elastic analyses of the cantilever beam problem. The 5NT element results compared poorly, in general, to analytical solution values for the cantilever beam analyses. However, some 5NT values did compare well. In particular, the maximum value for the y-displacement obtained for the 5NT from the dynamic analysis of the cantilever beam compared the best (compared to the values from the 6NT and 8NQ analyses) to the value calculated for an analytical solution which neglected shear deformation, axial, and rotary inertia effects. Further results showed that the solutions involving the higher-order

elements were less efficient compared to corresponding 4NQ element solutions.

Some difficulties were encountered prior to and during the execution of the higher-order element analyses. The following is a list of some of these difficulties:

(1) The mesh generation routine in SAMSON2 was not formulated so that the meshes used in the higher-order element solutions could be generated easily. For instance, the 8NQ elements can only be generated perpendicular to the direction in which the nodes were generated due to the fact that these elements have different node increments between corner nodes and midside nodes. Another example, was that the 5NT element mesh used in the cantilever beam analyses could not be generated for reasons similar to those stated for the 8NQ element.

(2) The placement of the midside nodes was critical in order to obtain a solution using the 5NT elements. It was mentioned previously in Section 3.2 that an attempt was made to improve a 5NT solution by changing the locations of the midside nodes. The elemental nodes were input according to Reference 3 for these rearranged nodes, but negative areas were calculated for the elements. This calculation occurred during the nodal mass allocation, and therefore was not affected by the time step size. A solution was never obtained for the mesh containing the reordered nodes.

(3) In the execution phase of each analysis, it was observed that the higher-order element analyses required a smaller time step size as compared to the 4NC element analyses. The time step value used for the cantilever beam analyses was set equal to the maximum value required to obtain a stable solution using the 8NQ as determined by a trial and error procedure. The stable time step for the 4NQ solution was larger even though the 4NQ mesh used in the analyses was significantly finer.

A summary of the conclusions discussed earlier in this chapter is presented here. The higher-order element (5NT, 6NT, and 8NQ) formulation for the calculation of strain appears to be correct for both static and dynamic plane analyses. The 8NQ element formulation for the internal force calculations (stress calculations are part of the internal force calculations) was shown to be functioning properly for static analyses using the biaxial elastic-plastic plane stress material law and for dynamic analyses using the biaxial elastic plane strain and plane stress material laws. Internal force calculations were also executed correctly for the 6NT element in static and dynamic analyses using the biaxial elastic plane stress material law. These calculations were also correct for the 5NT element assuming that the 5NT element cantilever beam solution could have been improved by increasing the number of elements in the mesh. The 8NQ axisymmetric formulation was found to be incorrect for dynamic analyses using the AFWL "engineering" model and the elastic plane strain material laws. Three potential

additional errors were discovered in the SAMSON2 finite element formulation and are as follows:

(1) The energy error formulation is incorrect in its present state as was shown in the analysis of the soil structure-interaction problem.

(2) The slideline calculations for the 8NQ analysis appeared to be quite different when compared to those obtained for the 4NQ analyses.

(3) The AFWL "engineering" model might also be in error for the 8NQ formulation when used for elastic-plastic analyses.

CHAPTER 4

Verification of the SAMSON2 Finite Element Formulation for the

Eight-Node Quadrilateral Isoparametric Continuum Element

The contents of this chapter dealing with the verification of the finite element formulation for the 8NQ isoparametric continuum element are separated into three main sections. The first section provides the necessary background information needed to better understand the capabilities of the SAMSON2 code. This information was also important in the code verification. The second section contains a synopsis of the equations involved in the 8NQ finite element formulation currently in the SAMSON2 code. Each equation presented was compared with information existing in finite element texts, journal articles, and other sources in order to verify the formulation (1, 5, 7, 8, 9, 11-18). Any disagreements obtained from these comparisons are pointed out and the conflicting equations from the reference materials are presented. Solution flow charts and some discussion of the equations are also introduced in this section. The third section in this chapter includes a summary of all of the errors found during the verification of the 8NQ finite element formulation.

4.1 Background Information

The SAMSON2 code is a dynamic nonlinear two-dimensional structu.e-media interaction computer code (1) which uses an explicit central difference finite element solution scheme. Explicit integration is only conditionally stable. Therefore, an accurate solution can only

be obtained by selecting a small time step Δt. An energy balance is performed at the end of each time step to check if the solution is stable (energy error less than 1.0%). A diagonal lumped mass matrix is used in accordance with the explicit integration scheme so that no solution of any simultaneous equations is required in advancing a time step. A stiffness matrix is never computed in an explicit time integration scheme due to the fact that solutions of simultaneous equations are never performed.

The SAMSON2 code was designed specifically for analyses of large displacements, large strain problems involving nonlinear material behavior and structure-media interface (SMI) problems. The stress and strain calculations are performed in the analyses of these nonlinear type problems with the use of the Cauchy stress and velocity strain (rate of deformation) tensors. The evaluation of stresses is performed in a corotational coordinate system which rotates coincident with the rotation of a quadrature point in an element. Therefore, a Jaumann type correction is not needed to maintain objectivity in the solution. The x and y nodal coordinates used in the analyses are the spatial Eulerian coordinates which are consistent with the velocity strain tensor. Gaussian quadrature is used in the numerical integration of the finite element equations for the stress and strain tensors for the 8NQ isoparametric continuum element.

Many other features are present in SAMSON2 that are linked to the general finite element formulation in the code. The following is a list of some of these additional features:

(1) Multiple time step integration is available for problems containing more than one mesh size in order to eliminate unnecessary integration of the coarser meshes.

(2) Dynamic relaxation techniques are employed in the SAMSON2 code in order to reduce the dynamic analyses, with the use of sufficient damping, to a static equilibrium solution.

(3) Mass and stiffness (artificial viscosity) proportional damping are used in the SAMSON2 code.

(4) A single large storage array (Q array) is used to store most of the major variable arrays used in the execution of SAMSON2.

(5) SAMSON2 contains many material models which range from the relatively simple elastic-plastic uniaxial stress material law to the complicated viscoplastic material law.

(6) Slideline interface routines are used in the SAMSON2 code to model relative sliding motion or material separation between two different types of materials such as occurs in SMI problems. These interfaces can also be rigid in order to connect two different type elements.

4.2 8NQ Isoparametric Continuum Element Formulation and Verification

This section contains the documentation of the research which was performed during the verification of the current SAMSON2 finite element formulation for the 8NQ isoparametric continuum element. The following

is a list of the particular items which were investigated in the formulation:

(1) the equations involved in the determination of the total diagonal lumped mass matrix, [M],

(2) the equations involved in the determination of the velocity strains, {d}, Cauchy stresses, {σ}, and internal forces, $\{F_{int}\}$,

(3) the calculations involved in the determination of the nodal forces due to the externally applied loads, $\{F_{ext}\}$,

(4) the mass and stiffness proportional damping $(C_1[M] + C_2[K])$ calculations,

(5) the equations used in calculating the internal strain energy (U) and the external work (W) terms, and

(6) the solution of the equation of motion for the nodal accelerations {ü}, velocities {u̇}, and displacements {u}.

These items were investigated in detail and are discussed in the following subsections.

4.2.1 Element Configuration and Shape Functions
and the Derivatives for the 8NQ

Some important information relevant to many phases of the formulation development for the 8NQ isoparametric continuum element is presented here. The configuration of the 8NQ element for which the formulation was developed is shown in Figure 4.1. The local (ξ,η) coordinate system is shown at the center of the element. This coordinate system is defined such that the values for ξ and η vary

between 1.0 (value on the right and upper element boundaries) and -1.0 (value on the left and lower element boundaries).
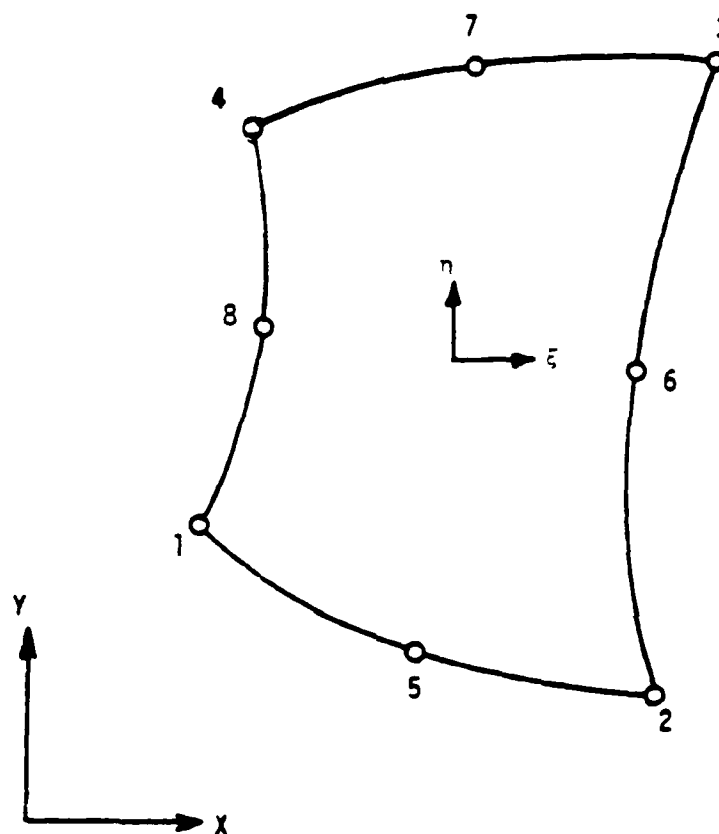
Figure 4.1   8NQ Isoparametric Continuum Element.

The shape (interpolation) functions (N_I) for the 8NQ element are shown in Table 4.1 in terms of the local coordinate system.   These shape functions are used in both the interpolation of the element coordinates (Equation 4.1) and the element displacements (Equation 4.2) for an isoparametric finite element formulation.

$$x = \sum_{I=1}^{8} N_I x_I \qquad y = \sum_{I=1}^{8} N_I y_I \qquad\qquad (4.1)$$

Table 4.1 The Shape Functions and Their Derivatives for the Eight-Node Quadrilateral Element.

Node I	N_I	$\partial N_I/\partial\xi$	$\partial N_I/\partial\eta$
1	$\tfrac{1}{4}(1-\xi)(1-\eta)(-\xi-\eta-1)$	$\tfrac{1}{4}(-2\xi\eta+2\xi+\eta-\eta^2)$	$\tfrac{1}{4}(-\xi^2+\xi-2\xi\eta+2\eta)$
2	$\tfrac{1}{4}(1+\xi)(1-\eta)(\xi-\eta-1)$	$\tfrac{1}{4}(-2\xi\eta+2\xi-\eta+\eta^2)$	$\tfrac{1}{4}(-\xi^2-\xi+2\xi\eta+2\eta)$
3	$\tfrac{1}{4}(1+\xi)(1+\eta)(\xi+\eta-1)$	$\tfrac{1}{4}(2\xi\eta+2\xi+\eta+\eta^2)$	$\tfrac{1}{4}(\xi^2+\xi+2\xi\eta+2\eta)$
4	$\tfrac{1}{4}(1-\xi)(1+\eta)(-\xi+\eta-1)$	$\tfrac{1}{4}(2\xi\eta+2\xi-\eta-\eta^2)$	$\tfrac{1}{4}(\xi^2-\xi-2\xi\eta+2\eta)$
5	$\tfrac{1}{2}(1-\xi^2)(1-\eta)$	$\xi\eta-\xi$	$\tfrac{1}{2}(\xi^2-1)$
6	$\tfrac{1}{2}(1-\eta^2)(1+\xi)$	$\tfrac{1}{2}(1-\eta^2)$	$-\xi\eta-\eta$
7	$\tfrac{1}{2}(1-\xi^2)(1+\eta)$	$-\xi\eta-\xi$	$\tfrac{1}{2}(1-\xi^2)$
8	$\tfrac{1}{2}(1-\eta^2)(1-\xi)$	$\tfrac{1}{2}(\eta^2-1)$	$\xi\eta-\eta$

74

where,

x, y = global (x, y) coordinates for any point in any element,

N_I = shape (interpolation) function corresponding to node I, and

x_I, y_I = global (x, y) coordinates for node I.

$$u_x = \sum_{I=1}^{8} N_I u_{xI} \qquad\qquad u_y = \sum_{I=1}^{8} N_I u_{yI} \qquad (4.2)$$

where,

u_x, u_y = x and y displacements for any point in an element,

N_I = shape (interpolation) function corresponding to node I, and

u_{xI}, u_{yI} = x and y displacements for node I.

The fundamental property associated with these shape functions is that the value for N_I is unity at node I and is zero at all other nodes. The derivatives of these shape functions with respect to the local element coordinates ($\partial N_I / \partial \xi$ and $\partial N_I / \partial \eta$) are also shown in Table 4.1. These derivatives are provided because they are more important than the shape functions in the actual finite element formulation. As a final note to this section, the shape functions and their derivatives from Table 4.1 exist in the SAMSON2 code correctly and were verified through comparisons with References 1 and 12.

4.2.2 Determination of the Total Diagonal Lumped Mass Matrix

This section gives the equations used in SAMSON2 to determine the total diagonal lumped mass matrix, $[M]$, for the 8NQ element. Table 4.2 provides a flow chart of the main subroutines involved in the

calculation of [M] and the operations performed in each subroutine. The mass matrix [M] is developed only once and is assembled prior to any other calculations in the SAMSON2 solution scheme. Therefore, the elemental masses are determined from the initial problem configuration.

Table 4.2   SAMSON2 Flow Chart for the Determination of the Total Diagonal Lumped Mass Matrix [M] for an 8NQ Isoparametric Plane or Axisymmetric Continuum Element.

Subroutine	Operation
1. ASSBLE (called by SMAIN) DO I = 1, # OF ELEMENTS	Assembles the elemental mass matrices into the total diagonal lumped mass matrix [M].
2. VASME	This routine, which is called by ASSBLE, calls the appropriate VnASME routine which is used to compute the mass matrix for an element which contains n nodes.
3. V8ASME	This routine is used to compute the elemental mass matrix for an 8NQ isoparametric plane or axisymmetric continuum element for a particular order of integration (iorder).
4. GAUSS1	This routine provides the Gauss-Legendre abscissae and weight coefficient values based on iorder which are used in V8ASME in order to determine the elemental mass matrices.
CONTINUE	I = I + 1.

The two subroutines of primary importance in this investigation were V8ASME and GAUSS1. The subroutine V8ASME contains all of the formulation used in the calculation of [M]. GAUSS1 provides the necessary Gauss-Legendre abscissae and weight coefficients used in the

numerical integration of [M]. These coefficients are shown in Appendix B with the column labeled ±a containing the abscissae coefficients and the column labeled h containing the weight coefficients. These coefficients exist in the subroutine GAUSS1 to 15 decimal places. However, some of these coefficients were incorrectly typed into the SAMSON2 code. Table 4.3 shows a list of the coefficients that were found to be incorrect.

The first step in the process of determining [M] was to calculate the mass contained in each element (performed in V8ASME). Equations 4.3, 4.4, and 4.5 were used to calculate the area of an element.

$$A = \sum_{i=1}^{iorder} \sum_{j=1}^{iorder} h_i h_j |J| \tag{4.3}$$

$$|J| = \left(\frac{\partial x}{\partial \xi} \times \frac{\partial y}{\partial \eta}\right) - \left(\frac{\partial x}{\partial \eta} \times \frac{\partial y}{\partial \xi}\right) \tag{4.4}$$

$$\frac{\partial x}{\partial \xi} = \sum_{I=1}^{8} \frac{\partial N_I}{\partial \xi} x_I \qquad \frac{\partial x}{\partial \eta} = \sum_{I=1}^{8} \frac{\partial N_I}{\partial \eta} x_I$$

$$\frac{\partial y}{\partial \xi} = \sum_{I=1}^{8} \frac{\partial N_I}{\partial \xi} y_I \qquad \frac{\partial y}{\partial \eta} = \sum_{I=1}^{8} \frac{\partial N_I}{\partial \eta} y_I \tag{4.5}$$

where,

A	=	area of an element,
iorder	=	order of integration selected for the problem analyses,
h_i, h_j	=	Gauss-Legendre weight coefficients,
$\|J\|$	=	determinant of the Jacobian matrix which contains the derivatives of the global (x,y) coordinates with respect to the local (ξ, η) coordinates,

Table 4.3   List of Gauss-Legendre Abscissae and Weight Coefficients Incorrectly Typed into the Subroutine GAUSS1.

Order of Integration n	SAMSON2 Coefficient			Correct Coefficient		
2	-0.57735	02691	8926	-0.57735	02691	89626
4	+0.33998	81043	584856	+0.33998	10435	84856
8	+0.96202	89856	497536	+0.96028	98564	97536
9	+0.83603	11073	2663	+0.83603	11073	26636
9	+0.96816	02395	07656	+0.96816	02395	07626
10	-0.67940	65682	99024	-0.67940	95682	99024

a) Abscissae Coefficients

Order of Integration n	SAMSON2 Coefficient			Correct Coefficient		
3	0.55555	55555	556	0.55555	55555	55556
3	0.88888	88888	888889	0.88888	88888	88889
3	0.55555	55555	556	0.55555	55555	55556
8	0.22238	10345	3374	0.22238	10344	53374
10	0.26926	68193	09996	0.26926	67193	09996
10	0.24908	63625	15982	0.21908	63625	15982

b) Weight Coefficients

$$\frac{\partial x}{\partial \xi}, \frac{\partial x}{\partial \eta}, \frac{\partial y}{\partial \xi}, \frac{\partial y}{\partial \eta} \quad = \quad \text{derivatives of the global } (x,y) \text{ coordinates} \\ \text{with respect to the local } (\xi,\eta) \text{ coordinates,}$$

$$\frac{\partial N_I}{\partial \xi}, \frac{\partial N_I}{\partial \eta} \quad = \quad \text{shape function derivatives from Table 4.1, and}$$

$$x_I, y_I \quad = \quad x \text{ and } y \text{ coordinates for any node } I \text{ in an 8NQ} \\ \text{element.}$$

Equations 4.4 and 4.5 were evaluated using the Gauss-Legendre abscissae coefficients obtained from GAUSS1 for a particular order of integration (iorder). These coefficients were substituted into these equations for ξ and η for all possible combinations of the coefficients. Equation 4.3 requires the use of both the Gauss-Legendre abscissae and weight coefficients in order to numerically integrate the area of an element. These three equations used in the SAMSON2 formulation were verified through comparisons with References 14 and 18. The volume and the corresponding mass of an element were computed upon completion of the area calculation. The volume calculation for a plane element involved multiplying the area by the thickness. The mass of an element was then calculated by multiplying the volume times the mass density as shown in Equation 4.6.

$$M = \rho t \sum_{i=1}^{iorder} \sum_{j=1}^{iorder} h_i h_j \, |J| \tag{4.6}$$

where,

M   =   mass for a plane element,

ρ =   mass density of the element, and

t   =   thickness of the element.

The volume calculation for an axisymmetric element involved multiplying the area by 2π times the distance from the axis of symmetry to the

geometric center of an element ($\bar{r}$). However, the SAMSON2 formulation for determining $\bar{r}$ was found to be incorrect. The correct formulation for the determination of $\bar{r}$ is shown in Equation 4.7.

$$\bar{r} = \frac{x_1 + x_2 + x_3 + x_4}{4.0} \tag{4.7}$$

where,

$\bar{r}$ = distance from the axis of symmetry to the geometric center of an 8NQ element, and

x_1, x_2, x_3, x_4 = x-coordinates for the four corner nodes of an 8NQ element (Figure 4.1).

The SAMSON2 formulation used a value of 3.0 instead of the value 4.0 in the denominator. This error was verified by comparisons to formulae in References 1 and 14 and through comparisons with hand calculated values. In addition to this error, the factor 2π was not used in the calculation of the volume. However the elimination of 2π was justified in that it canceled out in the final solution of the equation of motion. A further note regarding the axisymmetric volume calculation is that the calculation using $\bar{r}$ is only an approximation of the actual value. The mass was computed for an axisymmetric element using Equation 4.8. This equation with the use of the correct $\bar{r}$ value was verified as being correct.

$$M = \rho \bar{r} \sum_{i=1}^{iorder} \sum_{j=1}^{iorder} h_i h_j \left| J \right| \tag{4.8}$$

The second step in the process of determining [M] was the allocation of the calculated element mass to the appropriate nodes. The element mass was allocated to the nodes of an 8NQ according to
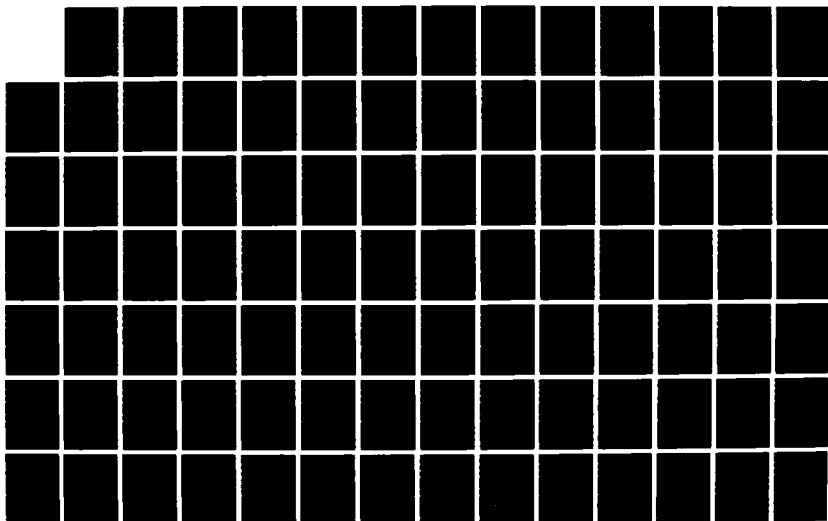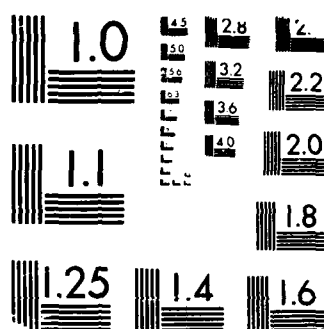
MICROCOPY RESOLUTION TEST CHART

BUREAU STANDARDS 1963 A

Figure 4.2. As illustrated, 20% and 5% of the element mass were allocated to the midside nodes and corner nodes, respectively. This nodal mass distribution used in the SAMSON2 coce could not be verified. However, it was found to be similar to a tributary area approach where the values were 18.75% and 6.25%. It was also found to be similar to an approach which used the scaled diagonal terms of a consistent mass matrix where the values were 22.22% and 2.78%. In reviewing the different references (5, 9, 15), it was determined that no standard lumping scheme for the 8NQ existed. Instead, many schemes were found that provided good results when used in problem solutions involving the 8NQ continuum element.


```
.05          .20          .05



.20                        .20



.05          .20          .05
```
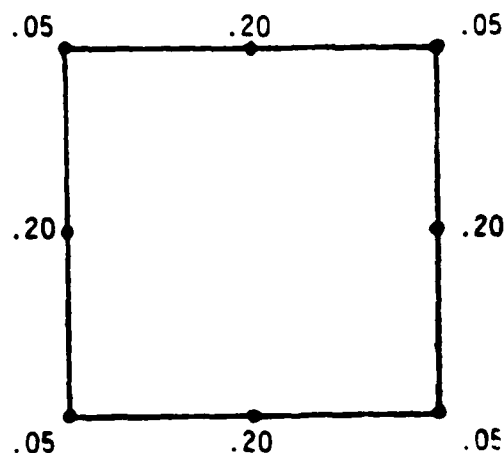
Figure 4.2   Nodal Lumped Masses for an 8NQ Element.

The final step in the process of determining [M] was the storage of these nodal masses. The mass allocated to each node in an element was stored for each nodal degree of freedom in an array called smass. The nodal mass allocations determined in step twc were added to smass for

each element. The diagonal lumped mass matrix [M] was completed when the mass contribution of every element was stored in the smass array. Upon the determination of [M], this mass matrix remained unchanged throughout the entire solution and was only used to solve the equation of motion at the end of each time step.

4.2.3 Determination of the Velocity Strains

This section displays the equations formulated in SAMSON2 that are used to calculate the velocity strain tensor, {d}. The velocity strain tensor measures the current rate of deformation and is used for problems involving geometric nonlinearities (large rigid body rotations and deformations). Table 4.4 shows a flow chart of the pertinent subroutines and their functions that are used in SAMSON2 in order to determine the internal nodal forces $\{F_{int}\}$. The velocity strains {d} are computed in subroutine V8FRCN in step a as shown in Table 4.4.

The general equations for the velocity strains are similar to the strain-displacement relations for small-displacement theory. Equation 4.9 shows the four velocity strain components for an 8NQ axisymmetric continuum element.

$$d_x = \frac{\partial V_x}{\partial x} = \sum_{I=1}^{8} \frac{\partial N_I}{\partial x} V_{xI}$$

$$d_y = \frac{\partial V_y}{\partial y} = \sum_{I=1}^{8} \frac{\partial N_I}{\partial y} V_{yI} \qquad (4.9)$$

$$2d_{xy} = (\frac{\partial V_x}{\partial y} + \frac{\partial V_y}{\partial x}) = \sum_{I=1}^{8} (\frac{\partial N_I}{\partial y} V_{xI} + \frac{\partial N_I}{\partial x} V_{yI})$$

(continued)

Table 4.4   Flow Chart for the Determination of the Internal Nodal
             Forces and Internal Strain Energy for an 8NQ
             Isoparametric Plane or Axisymmetric Continuum Element.

Subroutine	Operation
1. FRCIN (called by SMAIN) DO I = 1, # OF ELEMENTS	Combines the internal nodal forces for each element into a total internal nodal force vector. Combines the internal strain energies for each element into one value for each element type.
2. VFRCIN	Calls the appropriate element routine (VnFRCN) which computes the internal nodal forces for an element with <u>n</u> nodes.
3. V8FRCN	Computes the internal nodal forces for an 8NQ isoparametric plane or axisymmetric continuum element using the following steps: (a) Computes the global components for the velocity strains using subroutines GAUSS1, V8BMAT, V8SHAP, and GMPRD. (b) Computes the corotational strain increments using subroutines VSTRAN and GMPRD. (c) Calls the appropriate stress routines through STRES which compute the total stresses based on the current strain increments and the viscous stresses due to damping (SDAMP). Also, the total strains are updated. (d) Computes the internal nodal forces and the internal strain energy for an 8NQ element using the stress values from (c) and subroutines STPRD and GTPRD.
CONTINUE	I = I + 1.

$$d_z = \frac{V_x}{d} = \frac{\sum\limits_{I=1}^{8} N_I \, V_{xI}}{\sum\limits_{I=1}^{8} N_I \, x_I}$$

where,

d_x, d_y, d_z = three normal velocity strain components in the x, y, and z (r, z, and ⊝) directions,

d_{xy} = shearing velocity strain component,

V_x, V_y = velocity components for any point in an element (these velocities are never calculated),

d = distance from the axis of symmetry to the quadrature point at which the strains were computed,

x_I = current global deformed nodal coordinates for an 8NQ element,

V_{xI}, V_{yI} = velocity components for node I, and

$\frac{\partial N_I}{\partial x}, \frac{\partial N_I}{\partial y}$ = derivatives of the shape functions with respect to the global (x,y) coordinate system.

The velocity strain component in the z-direction, d_z, is equal to zero for analyses of plane continua. The derivatives of the shape functions with respect to the global coordinate system were determined using Equations 4.10 and 4.11.

$$\frac{\partial N_I}{\partial x} = \frac{1}{|J|} \left[\left(\frac{\partial N_I}{\partial \xi} \times \frac{\partial y}{\partial \eta} \right) - \left(\frac{\partial N_I}{\partial \eta} \times \frac{\partial y}{\partial \xi} \right) \right]$$

$$\frac{\partial N_I}{\partial y} = \frac{1}{|J|} \left[\left(\frac{\partial N_I}{\partial \eta} \times \frac{\partial x}{\partial \xi} \right) - \left(\frac{\partial N_I}{\partial \xi} \times \frac{\partial x}{\partial \eta} \right) \right]$$

(4.10)

$$\frac{\partial x}{\partial \xi} = \sum_{I=1}^{8} \frac{\partial N_I}{\partial \xi} x_I \qquad\qquad \frac{\partial x}{\partial \eta} = \sum_{I=1}^{8} \frac{\partial N_I}{\partial \eta} x_I$$

$$\frac{\partial y}{\partial \xi} = \sum_{I=1}^{8} \frac{\partial N_I}{\partial \xi} y_I \qquad\qquad \frac{\partial y}{\partial \eta} = \sum_{I=1}^{8} \frac{\partial N_I}{\partial \eta} y_I$$

$$(4.11)$$

The velocity strain components shown in Ecuation 4.9 were evaluated using a matrix $[\bar{B}]$. This matrix incorporates the expressions from Equations 4.9, 4.10, and 4.11 such that the velocity strain components are obtained through the multiplication of $[\bar{E}]$ times the nodal velocity components (V_{xI} and V_{yI}).

Table 4.5 shows the results obtained when multiplying the $[\bar{B}]$ matrix used in SAMSON2 times the nodal velocities. As shown, the velocity strains are multiplied by a factor equal to $|J|$. The velocity strains were not directly calculated because the $[\bar{B}]$ matrix was developed for use in the determination of the internal nodal forces, so that the $|J|$ term canceled out (see pp. 53-55 in Reference 1). The determination of the $[\bar{B}]$ matrix was performed in the V8BMAT subroutine using values calculated for the shape function derivatives ($\partial N_I/\partial x$, $\partial N_I/\partial y$) in subroutine V8SHAP. The $[\bar{B}]$ matrix was calculated for each quadrature point within an element using the Gauss-Legendre abscissae coefficients obtained from the GAUSS1 routine. Therefore, the velocity strains were also computed for the same quadrature points. The general matrix product routine GMPRD in SAMSON2 was used to multiply the $[\bar{B}]$ matrix by the nodal velocity matrix as shown in Table 4.5.

Table 4.5 Strain-Displacement Matrix $[\tilde{B}]$ Relating the Velocity Strain Components to the Nodal Velocities.

$$\begin{Bmatrix} d_x |J| \\ d_y |J| \\ d_z |J| \\ 2d_{xy} |J| \end{Bmatrix} = \begin{bmatrix} \frac{\partial N_1}{\partial x}^a & 0 & \frac{\partial N_2}{\partial x} & 0 & \frac{\partial N_3}{\partial x} & 0 & \frac{\partial N_4}{\partial x} & 0 & \frac{\partial N_5}{\partial x} & 0 & \frac{\partial N_6}{\partial x} & 0 & \frac{\partial N_7}{\partial x} & 0 & \frac{\partial N_8}{\partial x} & 0 \\[6pt] 0 & \frac{\partial N_1}{\partial y} & 0 & \frac{\partial N_2}{\partial y} & 0 & \frac{\partial N_3}{\partial y} & 0 & \frac{\partial N_4}{\partial y} & 0 & \frac{\partial N_5}{\partial y} & 0 & \frac{\partial N_6}{\partial y} & 0 & \frac{\partial N_7}{\partial y} & 0 & \frac{\partial N_8}{\partial y} \\[6pt] \frac{N_1|J|}{p} & 0 & \frac{N_2|J|}{p} & 0 & \frac{N_3|J|}{p} & 0 & \frac{N_4|J|}{p} & 0 & \frac{N_5|J|}{p} & 0 & \frac{N_6|J|}{p} & 0 & \frac{N_7|J|}{p} & 0 & \frac{N_8|J|}{p} & 0 \\[6pt] \frac{\partial N_1}{\partial y} & \frac{\partial N_1}{\partial x} & \frac{\partial N_2}{\partial y} & \frac{\partial N_2}{\partial x} & \frac{\partial N_3}{\partial y} & \frac{\partial N_3}{\partial x} & \frac{\partial N_4}{\partial y} & \frac{\partial N_4}{\partial x} & \frac{\partial N_5}{\partial y} & \frac{\partial N_5}{\partial x} & \frac{\partial N_6}{\partial y} & \frac{\partial N_6}{\partial x} & \frac{\partial N_7}{\partial y} & \frac{\partial N_7}{\partial x} & \frac{\partial N_8}{\partial y} & \frac{\partial N_8}{\partial x} \end{bmatrix} \{v\}^T$$

where,

$$\{v\}^T = [\ v_{x1}\ v_{y1}\ v_{x2}\ v_{y2} \cdots v_{x7}\ v_{y7}\ v_{x8}\ v_{y8}\ ].$$

[a] The expressions for the shape function derivatives shown in $[\tilde{B}]$ are not equal to those displayed in Equation 4.10. The derivatives used in the $[\tilde{B}]$ matrix do not include the division by $|J|$.

The next step performed in the calculation for the velocity strains was the transformation of these strains from the global (x,y) coordinate system to the corotational reference frame $(\hat{x},\hat{y})$. A corotational reference frame exists at each of the quadrature points and rotates according to the movement of these points. Therefore, in addition to the velocity strain calculations, a rotational velocity (ω) was computed for each quadrature point using Equation 4.12.

$$\omega^{n+\frac{1}{2}} = \frac{1}{2|J|} \left(\frac{\partial V_y^{n+\frac{1}{2}}}{\partial x} - \frac{\partial V_x^{n+\frac{1}{2}}}{\partial y} \right) = \frac{1}{2|J|} \sum_{I=1}^{8} \left(\frac{\partial N_I}{\partial x} V_{yI}^{n+\frac{1}{2}} - \frac{\partial N_I}{\partial y} V_{xI}^{n+\frac{1}{2}} \right) \qquad (4.12)$$

Equation 4.12 was found to be identical to the equation for vorticity used in fluid mechanics (18). The rotational velocity was multiplied by the value for the time step in order to obtain the current rotation increment. The total rotation for the current time step (θ^{n+1}) was then calculated using Equation 4.13 and was then stored in the strs array in the last location assigned to an element quadrature point.

$$\theta^{n+1} = \theta^n + \Delta t \; \omega^{n+\frac{1}{2}} \qquad (4.13)$$

where,

θ^{n+1}, θ^n = total rotations which have occurred at a quadrature point for the current and previous time steps,

Δt = time step used for the explicit integration solution scheme, and

$\omega^{n+\frac{1}{2}}$ = rotational velocity for a quadrature point which occurred during the current time step.

The total rotation, θ^{n+1}, was then used in the transformation matrix, [R], in order to convert the velocity strains from the global (x,y)

coordinate system to the corotational framework $(\hat{x},\hat{y})$. Equations 4.14
and 4.15 show the strain transformation matrix [R] and the multiplica-
tion process which was performed in order to determine the corotational
velocity strains. The [R] matrix was not multiplied by the velocity
strain in the z-direction since d_z is not affected by rotation in the
x,y plane.

$$[R] = \begin{bmatrix} \cos^2\Theta & \sin^2\Theta & \cos\Theta\sin\Theta \\ \sin^2\Theta & \cos^2\Theta & -\cos\Theta\sin\Theta \\ -2\sin\Theta\cos\Theta & 2\sin\Theta\cos\Theta & \cos^2\Theta-\sin^2\Theta \end{bmatrix} \quad (4.14)$$

$$\{\hat{d} \ |J|\} = [R] \ \{d \ |J|\} \quad (4.15)$$

where,

$\{\hat{d} \ |J|\}$ = velocity strains, multiplied by a factor $|J|$, in the $(\hat{x},\hat{y})$ coordinate system,

[R] = velocity strain transformation matrix, and

$\{d \ |J|\}$ = velocity strains, multiplied by a factor $|J|$, in the global (x,y) coordinate system.

The transformation matrix was computed in subroutine VSTRAN in the
SAMSON2 code. A possible error was found in this subroutine VSTRAN.
For values of $|\Theta| < 1.0 \times 10^{-5}$, the value for each of the $\sin\Theta$ terms
was set equal to zero. However, according to small angle theory,
$\sin\Theta \cong \Theta$. This error may be trivial in the overall solution. The
multiplication process illustrated in Equation 4.15 was executed in
subroutine GMPRD.

One last computation was executed for the velocity strains. This
computation involved the multiplication of the corotational velocity
strains by an appropriate factor so as to obtain the incremental strains

for the current time step. This computation is illustrated in Equation 4.16 and was the last one performed prior to the calculation of the stresses, $\{\sigma\}$, and the internal forces, $\{F_{int}\}$.

$$\{\Delta\hat{\epsilon}\} = \frac{\Delta t}{|J|} \{\hat{d} \ |J|\} \tag{4.16}$$

where,

$\{\Delta\hat{\epsilon}\} = $ incremental strains determined for the current time step.

The formulation for the velocity strain calculations was found to be correct when compared to material in References 1, 9, 12, and 16. The only possible error found in the formulation was the use of the approximation of $\sin \theta = 0.0$ for $|\theta| < 1.0 \times 10^{-5}$. Also, the use of the $[\bar{B}]$ matrix for the calculation of the velocity strains was corrected later when a factor of $1/|J|$ was multiplied times the velocity strains.

4.2.4 Evaluation of Stresses and Internal Forces

The stresses calculated in SAMSON2 were evaluated using the Cauchy stress tensor. This tensor was computed in the corotational coordinate system so as to maintain objectivity in the overall solution. The Cauchy stress tensor is energetically conjugate to the velocity strain tensor. Hence, the total internal work can be calculated using these tensors. The Cauchy stress tensor is used for the incremental analysis of geometrically nonlinear problems.

The SAMSON2 code contains eight different constitutive laws which are used to determine the Cauchy stresses based upon the incremental strains already computed. In this study, only the biaxial material laws (subroutines STRES3 and STRES6) and the AFWL engineering" material law

(subroutine STRES9) were investigated. The remainder of the material laws were not investigated because they were considered less important (uniaxial laws) or had been investigated in prior studies. The stress-strain relations are provided in the following subsections for each material law investigated. An example of the derivations that were required in order to determine the biaxial elastic-plastic stress-strain matrices are also provided in Appendix C.

4.2.4.1 Stress Evaluations Using the Biaxial Elastic
Plane Strain Material Law (STRES6)

The formulation for the STRES6 subroutine was developed for isotropic linear elastic materials. STRES6 can be used for plane strain or axisymmetric analyses. All computations were performed in STRES6 under the assumption of totally elastic material behavior. Therefore, no yield condition or plastic flow rule is used.

The stress-strain relations for the biaxial elastic plane strain or axisymmetric material law were expressed in terms of total stresses and total strain as opposed to incremental values due to the assumption of totally elastic behavior. Hence, the current total strains $\{\hat{\epsilon}\}^{n+1}$ were computed prior to any stress calculations by adding the incremental strains $\{\Delta\hat{\epsilon}\}^{n+\frac{1}{2}}$ (Equation 4.16) to the total strains at the end of the previous time step $\{\hat{\epsilon}\}^{n}$ as shown in Equation 4.17.

$$\{\hat{\epsilon}\}^{n+1} = \{\hat{\epsilon}\}^{n} + \Delta t\{\hat{d}\}^{n+\frac{1}{2}} \tag{4.17}$$

The total stresses were then computed using the stress-strain relations shown in Equation 4.18.

$$\hat{\sigma}_x^{n+1} = \frac{E\nu}{(1 + \nu)(1 - 2\nu)}(\hat{\epsilon}_x^{n+1} + \hat{\epsilon}_y^{n+1} + \hat{\epsilon}_z^{n+1}) + \frac{E}{1 + \nu}(\hat{\epsilon}_x^{n+1})$$

$$\hat{\sigma}_y^{n+1} = \frac{E\nu}{(1 + \nu)(1 - 2\nu)}(\hat{\epsilon}_x^{n+1} + \hat{\epsilon}_y^{n+1} + \hat{\epsilon}_z^{n+1}) + \frac{E}{1 + \nu}(\hat{\epsilon}_y^{n+1})$$

$$\hat{\tau}_{xy}^{n+1} = \frac{E}{2(1 + \nu)}\hat{\gamma}_{xy}^{n+1} \tag{4.18}$$

$$\hat{\sigma}_z^{n+1} = \frac{E\nu}{(1 + \nu)(1 - 2\nu)}(\hat{\epsilon}_x^{n+1} + \hat{\epsilon}_y^{n+1} + \hat{\epsilon}_z^{n+1}) + \frac{E}{1 + \nu}(\hat{\epsilon}_z^{n+1})$$

These equations were used for both plane strain and axisymmetric analyses with the strain in the z-direction, $\hat{\epsilon}_z$, being equal to zero for plane strain analyses. The values for $\hat{\epsilon}_z$ and $\hat{\sigma}_z$ were both found to be equal to zero for plane strain analyses using $\nu = 0$ (Poisson's ratio). The current total stresses and total strains for the corotational coordinate system were stored in the appropriate locations within the strs array for each element quadrature point.

The calculations executed in STRES6 using Equations 4.17 and 4.18 were all verified through comparisons to References 1, 7, 12, 14, and 15. Therefore, the biaxial elastic plane strain or axisymmetric material law was found to be correct.

4.2.4.2 Stress Evaluations Using the Biaxial Elastic-Plastic Plane Stress Material Law (STRES3)

The subroutine STRES3 was developed for analyses involving elastic-perfectly plastic or strain hardening materials. The solution scheme for this subroutine is illustrated in Table 4.6 with c^E and c^{EP} referring to the elastic and elastic-plastic stress-strain matrices which will be presented in this section.

Table 4.6   Solution Algorithm for Elastic-Plastic Stress
             Calculations.[a]

Given: STRAIN =   total strains for current time step, $\{\hat{\epsilon}\}^{n+1}$

         EPS   =   total strains for previous time step, $\{\hat{\epsilon}\}^{n}$

         SIG   =   total stresses for previous time step, $\{\hat{\sigma}\}^{n}$

The following procedure is used to calculate the total stresses TAU for the current time step, $\{\hat{\sigma}\}^{n+1}$.

(a) Calculate the strain increment DELEPS, $\{\hat{\Delta\epsilon}\}^{n+\frac{1}{2}}$:

     DELEPS = STRAIN - EPS

(b) Calculate the stress increment DELSIG, $\{\hat{\Delta\sigma}\}^{n+\frac{1}{2}}$, assuming elastic behavior:

     DELSIG = c^E x DELEPS

(c) Calculate TAU:

     TAU = SIG + DELSIG

(d) With TAU as the state of stress, determine the value of the yield function F.

(e) If F(TAU) < 0, elastic behavior assumption correct (loading elastically, neutral loading, or unloading). Hence, TAU is the correct stress value and the calculations for this algorithm are complete (RETURN). If F(TAU) > 0, steps (f), (g), and (h) must be executed.

(f) If the previous state of stress was plastic (as indicated by a flag), set RATIO = 0 and go to step (g). Otherwise, there is a transition from elastic to plastic and RATIO, the portion of DELSIG which is elastic, must be determined. The variable RATIO is determined from the equation

     F {SIG + (RATIO x DELSIG)} = 0

     since at the stress SIG + (RATIO x DELSIG) the yield function F = 0 and yielding is initiated.

(g) Redefine TAU as the stress at start of yield

     TAU = SIG + (RATIO x DELSIG)

     and calculate the elastic-plastic strain increment

     DEPS = (1 - RATIO) x DELEPS

(h) To obtain the final stresses, which include the effect of the complete strain increment DELEPS, the stresses corresponding to the elastic-plastic strain increment DEPS must be added to TAU. Hence, TAU is the current state of stress $\{\hat{\sigma}\}^{n+1}$

     TAU = TAU + (c^{EP} x DEPS)

     and the algorithm calculations are complete (RETURN).

---

[a]This table was obtained from p. 393 in Reference 12.

Incremental stresses, $\{\Delta\hat{\sigma}\}$, were determined in STRES3 based on the previously calculated strain increments (step b in Table 4.6). These stresses were computed at elemental quadrature points as was done for the velocity strains. These incremental stress calculations were performed under the assumption that the strain increments were entirely elastic. For this assumption, the incremental stresses were computed using elastic stress-strain relations. Equations 4.19 and 4.20 show the elastic stress-strain matrix used in the determination of the incremental stresses and the corresponding multiplication process which was executed. The incremental strain in the z-direction, $\hat{\epsilon}_z$, was computed according to Equation 4.21.

$$C^E = \frac{E}{(1 - \nu^2)} \begin{bmatrix} 1 & \nu & 0 \\ \nu & 1 & 0 \\ 0 & 0 & \frac{1-\nu}{2} \end{bmatrix} \tag{4.19}$$

$$\{\Delta\hat{\sigma}\} = C^E \times \{\Delta\hat{\epsilon}\} \tag{4.20}$$

where,

$$\{\Delta\hat{\sigma}\}^T = [\Delta\hat{\sigma}_x \quad \Delta\hat{\sigma}_y \quad \Delta\hat{\tau}_{xy}], \text{ and}$$

$$\{\Delta\hat{\epsilon}\}^T = [\Delta\hat{\epsilon}_x \quad \Delta\hat{\epsilon}_y \quad \Delta\hat{\gamma}_{xy}].$$

$$\Delta\hat{\epsilon}_z = \frac{-\nu}{1 - \nu} (\Delta\hat{\epsilon}_x + \Delta\hat{\epsilon}_y) \tag{4.21}$$

The total stresses for the current time step, $\{\hat{\sigma}\}^{n+1}$, were calculated by updating the total stresses from the previous time step, $\{\hat{\sigma}\}^n$, as shown in Equation 4.22.

$$\{\hat{\sigma}\}^{n+1} = \{\hat{\sigma}\}^n + \{\Delta\hat{\sigma}\} \tag{4.22}$$

These updated total stresses, $\{\hat{\sigma}\}^{n+1}$, were then implemented into the corresponding yield function (F) in order to determine if elastic-plastic behavior had occurred during the time step. The yield function used in STRES3 for the plane stress material law is shown in Equation 4.23.

$$F = (\hat{\sigma}_x^2 + \hat{\sigma}_y^2 - \hat{\sigma}_x \hat{\sigma}_y + 3\hat{\tau}_{xy}^2)^{\frac{1}{2}} \tag{4.23}$$

This function was based on the von Mises yield criterion (11, 12, 15) and was evaluated in subroutine STREQU using values obtained from STRES3. The value for F determined in Equation 4.23 was compared to the yield stress value (σ_{yld}^n) obtained from the previous time step. This yield stress value was initially established such that $\sigma_{yld}^n = \sigma_1$, where σ_1 = the input stress value for the first point (ϵ_1, σ_1) on the monotonically increasing piecewise linear stress-strain curve. This value for σ_{yld}^n remained unchanged for a particular elemental quadrature point until yielding was initiated. The yield stress value was then redetermined such that $\sigma_{yld}^n = F(\hat{\sigma}^n)$, except for the case of elastic-perfectly plastic material behavior, where σ_{yld}^n remains equal to σ_1. The yield value, σ_{yld}^n, was set equal to $F(\hat{\sigma}^n)$ in order to record the previous state of stress or stress history for use in comparison with the current state of stress as determined by Equation 4.23. In comparing F to σ_{yld}^n, if $F \leq \sigma_{yld}^n$, then the assumption of elastic behavior (loading elastically, neutral loading, or unloading) was correct. Therefore, the stresses computed in Equation 4.22 were the

correct total stresses for the current time step (step e in Table 4.6). However, if $F > \sigma_{yld}^n$, then elastic-plastic behavior has occurred and the stresses obtained from Equation 4.22 were incorrect and were recalculated according to the elastic-plastic stress-strain relations in the following paragraphs.

Two additional calculations were necessary for elastic-plastic material behavior. The first calculation was the determination of the plastic modulus (modulus of the next segment on the piecewise linear stress-strain curve) and the next yield point. The plastic modulus (E_T) was determined in subroutine STRMOD using Equation 4.24 and the yield stress value was set equal to σ_I such that $\sigma_I > \sigma_{yld}^n$.

$$E_T = \frac{\sigma_I - \sigma_{I-1}}{\varepsilon_I - \varepsilon_{I-1}} \qquad (4.24)$$

where,

E_T = plastic modulus,

σ_I, ε_I = stress and strain values for the next yield point on the linear stress-strain curve, and

$\sigma_{I-1}, \varepsilon_{I-1}$ = stress and strain values for the current yield point.

However, if the stress-strain point (ε_I, σ_I) did not exist, perfect plasticity was assumed ($E_T = 0$) and the yield stress value remained equal to σ_{I-1}. As a note, the initial von Mises yield surface that was established for the initial yield stress σ_1 was simply expanded for the following yield stresses using an isotropic hardening rule.

The second calculation performed was the evaluation of Equation 4.23 using the stresses from the previous time step. This value $F(\hat{\sigma}_n)$ was then compared with σ^n_{yld} using Equation 4.25.

$$SHIST = \frac{\left| F(\hat{\sigma}^n) - \sigma^n_{yld} \right|}{\sigma^n_{yld}} \qquad (4.25)$$

Equation 4.25 was evaluated in order to determine if the previous state of stress was elastic or plastic. If SHIST $\leq$ 0.001, then the previous state of stress was plastic and the incremental strains calculated in Section 4.2.3 were entirely plastic. Therefore, the incremental stresses calculated using Equation 4.20 were invalid. These incremental stresses were then recalculated using an elastic-plastic stress-strain matrix C^{EP}. However, if SHIST $>$ 0.001, then the previous stress state was elastic and the portion (RATIO) of the incremental stresses, $\{\hat{\Delta\sigma}\}$, which were elastic was determined using Equation 4.26. This equation was obtained based on the expression shown in Equation 4.27.

$$RATIO = \frac{t + \sqrt{t^2 + 4[F(\hat{\Delta\sigma})^2 \times (\sigma^n_{yld}{}^2 - F(\hat{\sigma}^n)^2)]}}{2F(\hat{\Delta\sigma})^2} \qquad (4.26)$$

where,

$$t = -2\hat{\Delta\sigma}_x \hat{\sigma}^n_x - 2\hat{\Delta\sigma}_y \hat{\sigma}^n_y + \hat{\Delta\sigma}_y \hat{\sigma}^n_x + \hat{\Delta\sigma}_x \hat{\sigma}^n_y - 6\hat{\Delta\tau}_{xy} \hat{\tau}^n_{xy}$$

$$F[\hat{\sigma}^n + (RATIO \times \hat{\Delta\sigma})] - \sigma^n_{yld} = 0 \qquad (4.27)$$

Equation 4.26 was verified by comparison with the solution to 4.27. The subroutine STRYIE was used to calculate RATIO. The elastic portion of

the incremental stresses was calculated using RATIO multiplied by the previously calculated incremental stresses. These elastic incremental stresses were then added to the stresses from the previous time step as shown in Equation 4.28.

$$\{\hat{\sigma}\}^n = \{\hat{\sigma}\}^n + \text{RATIO} \times \{\Delta\hat{\sigma}\} \tag{4.28}$$

Equation 4.28 was executed in order to update the old stresses to include the elastic portion of the incremental stresses. These updated stresses were then implemented into the yield function in order to update the stress state to include the elastic stress increments, $\sigma_{yld}^n = F(\hat{\sigma}^n)$. This yield function value was used later in the determination of the elastic-plastic stress-strain matrix C^{EP}. The plastic strain increments ($\Delta\hat{\epsilon}_{xP}$, $\Delta\hat{\epsilon}_{yP}$, and $\Delta\hat{\gamma}_{xyP}$) and the elastic strain increment in the z-direction ($\Delta\hat{\epsilon}_z$) were calculated using RATIO as shown in Equations 4.29 and 4.30.

$$\{\Delta\hat{\epsilon}_p\} = (1 - \text{RATIO}) \{\Delta\hat{\epsilon}\} \tag{4.29}$$

where,

$\{\Delta\hat{\epsilon}_p\}$ = plastic strain increments, and

$\{\Delta\hat{\epsilon}\}$ = incremental strains from Section 4.2.3.

$$\Delta\hat{\epsilon}_z = \text{RATIO} \times \Delta\hat{\epsilon}_z \tag{4.30}$$

The plastic stress increments were calculated using elastic-plastic stress-strain relations developed in accordance with the yield function (F), isotropic hardening and an associated flow rule. These elastic-plastic stress-strain relations are incorporated into the C^{EP} matrix

shown in Table 4.7. This matrix was developed for incremental plasticity analyses using the yield function from Equation 4.23 and an associated flow rule. The derivation of C^{EP} for the plane stress material law was similar to that shown in Appendix C for the biaxial elastic-plastic plane strain or axisymmetric material law. The incremental plastic stresses were determined using Equation 4.31. The incremental strain, both the elastic and plastic portions, in the z-direction, $\Delta\hat{\epsilon}_z$, was calculated using Equation 4.32. However, Equation 4.32 is not correct. The correct formula for determining $\Delta\hat{\epsilon}_z$ is shown in Equation 4.33.

$$\{\Delta\hat{\sigma}_p\} = C^{EP} \times \{\Delta\hat{\epsilon}_p\} \tag{4.31}$$

where,

$\{\Delta\hat{\sigma}_p\}$ = incremental plastic stresses, $\{\Delta\hat{\sigma}_{xP}\ \Delta\hat{\sigma}_{yP}\ \Delta\hat{\tau}_{xyP}\}$,

C^{EP} = elastic-plastic stress-strain matrix shown in Table 4.7, and

$\{\Delta\hat{\epsilon}_p\}$ = plastic strain increments, $\{\Delta\hat{\epsilon}_{xP}\ \Delta\hat{\epsilon}_{yP}\ \Delta\hat{\gamma}_{xyP}\}$ which were either the strains calculated in Section 4.2.3 (previous state of stress plastic) or the strains calculated using Equation 4.29.

$$\Delta\hat{\epsilon}_z = \Delta\hat{\epsilon}_z - \{ \frac{(\frac{\nu}{1-\nu} - \beta\ S_{11}S_{33})}{(\frac{1}{1-\nu} - \beta\ S_{33}^2)}\ \Delta\hat{\epsilon}_x + \frac{(\frac{\nu}{1-\nu} - \beta\ S_{22}S_{33})}{(\frac{1}{1-\nu} - \beta\ S_{33}^2)}\ \Delta\hat{\epsilon}_y +$$

$$\frac{-\beta\ S_{12}S_{33}}{(\frac{1}{1-\nu} - \beta\ S_{33}^2)}\ \Delta\hat{\gamma}_{xy}\ \} (1 - RATIO) \tag{4.32}$$

Table 4.7   Elastic-Plastic Stress-Strain Matrix for the Plane Stress Material Law (STRES3).

$$C^{EP} = \frac{E}{K}
\begin{bmatrix}
S_{22}^2+2\left(\frac{2}{9}\frac{E_T}{E-E_T}\sigma_{yld}^n{}^2+\frac{S_{12}^2}{1+\nu}\right) & -S_{11}S_{22}+2\nu\left(\frac{2}{9}\frac{E_T}{E-E_T}\sigma_{yld}^n{}^2+\frac{S_{12}^2}{1+\nu}\right) & -(S_{11}+\nu S_{22})\frac{S_{12}}{1+\nu} \\[2ex]
\text{symmetric} & S_{11}^2+2\left(\frac{2}{9}\frac{E_T}{E-E_T}\sigma_{yld}^n{}^2+\frac{S_{12}^2}{1+\nu}\right) & -(S_{22}+\nu S_{11})\frac{S_{12}}{1+\nu} \\[2ex]
\text{symmetric} & \text{symmetric} & \frac{S_{11}^2+2\nu S_{11}S_{22}+S_{22}^2}{2(1+\nu)}+\frac{2}{9}\frac{E_T}{E-E_T}\sigma_{yld}^n{}^2(1-\nu)
\end{bmatrix}$$

where,

$K = f(S_{11}^2 + 2\nu S_{11}S_{22} + S_{22}^2) + 2(1 - \nu^2)\left(\frac{2}{9}\frac{E_T}{E-E_T}\sigma_{yld}^n{}^2 + \frac{S_{12}^2}{1+\nu}\right)$,

S_{ij} = deviatoric stresses = $\sigma_{ij} - \dfrac{\hat\sigma_x^n + \hat\sigma_y^n}{3}\,\delta_{ij}$,

such that $\delta_{ij} = 1$ for the normal stresses, and $= 0$ for the shear stresses,

$\sigma_{ij}, \sigma_x, \sigma_y$ = either the stresses from the previous time step ($\hat\sigma^n$) if the previous state of stress was plastic or the updated stresses calculated using Equation 4.28, and

$\sigma_{yld}^n = F(\hat\sigma^n)$, where ($\hat\sigma^n$) is either the stresses from the previous time step for a prior plastic stress state or the updated stresses computed using Equation 4.28.

where,

$$\Delta\hat{\epsilon}_x, \; \Delta\hat{\epsilon}_y, \; \Delta\hat{\gamma}_{xy} = \text{incremental strains calculated in Section 4.2.3,}$$

$$B = \frac{3}{2}\frac{1}{\sigma_{yld}^{n^2}}\left(\frac{1}{1 + \frac{2(1+\nu)E_T}{3(E - E_T)}}\right), \text{ and}$$

$$\Delta\hat{\epsilon}_z = \text{value from Equation 4.21 if RATIO} = 0 \text{ or}$$
$$\text{value from Equation 4.30 } (\Delta\hat{\epsilon}_z) \text{ if RATIO} \neq 0.$$

$$\Delta\hat{\epsilon}_z = \Delta\hat{\epsilon}_z - \left\{ \frac{\left(\frac{\nu}{1-2\nu} - B \, S_{11}S_{33}\right)}{\left(\frac{1-\nu}{1-2\nu} - B \, S_{33}^2\right)} \Delta\hat{\epsilon}_x + \frac{\left(\frac{\nu}{1-2\nu} - B \, S_{22}S_{33}\right)}{\left(\frac{1-\nu}{1-2\nu} - B \, S_{33}^2\right)} \Delta\hat{\epsilon}_y + \right.$$

$$\left. \frac{-B \, S_{12}S_{33}}{\left(\frac{1-\nu}{1-2\nu} - B \, S_{33}^2\right)} \Delta\hat{\gamma}_{xy} \right\} (1 - RATIO) \tag{4.33}$$

The only differences between the two equations exist in the expressions containing Poisson's ratio. Equation 4.32 contains the terms $\frac{\nu}{1-\nu}$ and $\frac{1}{1-\nu}$ while the corresponding terms in Equation 4.33 are $\frac{\nu}{1-2\nu}$ and $\frac{1-\nu}{1-2\nu}$. The terms inside the brackets on the righthand side of Equation 4.33 were obtained by substituting $\Delta\hat{\sigma}_{zP} = 0$ in the elastic-plastic stress-strain relations for the plane strain or axisymmetric material law and solving for $\Delta\hat{\epsilon}_{zP}$.

The total stresses for the current time step $\{\hat{\sigma}\}^{n+1}$ were determined using the plastic increments of stress obtained from the evaluation of Equation 4.31. The total stresses were calculated using Equation 4.34.

$$\{\hat{\sigma}\}^{n+1} = \{\hat{\sigma}\}^n + \{\Delta\hat{\sigma}_p\} \tag{4.34}$$

where,

$\{\hat{\sigma}\}^{n+1}$ =   stresses for the current time step,

$\{\hat{\sigma}\}^{n}$ =   either the stresses from the previous time step if RATIO = 0 or the stresses calculated in Equation 4.28 if RATIO $\neq$ 0, and

$\{\Delta\hat{\sigma}_p\}$ =   plastic increments of stress determined using Equation 4.31.

A value for the yield function (F) was then calculated with these new stresses, $F(\hat{\sigma}^{n+1})$. This value $F(\hat{\sigma}^{n+1})$ was then compared with the value for the next yield point, σ_I, obtained from subroutine STRMOD. This was executed in order to determine if the current state of stress exceeded the failure criterion for the next yield point σ_I. If $F(\hat{\sigma}^{n+1}) \leq \sigma_I$, then the stresses calculated using Equation 4.34 were correct and $\sigma_{yld}^n = F(\hat{\sigma}^{n+1})$. However, if $F(\hat{\sigma}^{n+1}) > \sigma_I$, then $F(\hat{\sigma}^n) = \sigma_{yld}^n$ and $\sigma_{yld}^n = \sigma_I$, and the calculation process was reinitiated beginning with the determination of the next value for the plastic modulus (Equation 4.24) and the next yield point value. One other possibility existed for the case of perfect plasticity. For this case, a reduction factor RED was determined using Equation 4.35 which was then multiplied by the stresses obtained from Equation 4.34 as shown in Equation 4.36. After these two equations were executed, Equation 4.37 was evaluated.

$$\text{RED} = \frac{\sigma_{yld}^n}{F(\hat{\sigma}^{n+1})} \qquad (4.35)$$

where,

RED   =   factor used to reduce the stresses calculated in equation 4.34 so that the failure criterion, $F(\hat{\sigma}^{n+1}) \leq \sigma_{yld}^n$, was met.

$$\{\hat{\sigma}\}^{n+1} = RED \times \{\hat{\sigma}\}^{n+1} \tag{4.36}$$

$$SHIST2 = \frac{\left| F(\hat{\sigma}^{n+1}) - \sigma^n_{yld} \right|}{\sigma^n_{yld}} \tag{4.37}$$

where,

$\{\hat{\sigma}\}^{n+1}$ = stresses obtained from Equation 4.36.

If the value for SHIST2 was less than or equal to 0.001 the stresses calculated using Equation 4.36 were the correct total stresses for the current time step. But, if SHIST2 was greater than 0.001, Equation 4.35, 4.36, and 4.37 were reexecuted until SHIST2 was found to be less than or equal to 0.001.

Upon the determination of the total stresses for the current time step, the total strains were updated to include the incremental strains as shown in Equation 4.38. These new strains and the new stresses were then stored in the appropriate location of the strs array. The value for σ^n_{yld} was also stored in the strs array.

$$\{\hat{\epsilon}\}^{n+1} = \{\hat{\epsilon}\}^n + \{\hat{\Delta\epsilon}\} \tag{4.38}$$

where,

$\{\hat{\Delta\epsilon}\}$ = strains obtained from Section 4.2.3 ($\hat{\Delta\epsilon}_x$, $\hat{\Delta\epsilon}_y$, and $\hat{\Delta\gamma}_{xy}$) and the strain ($\Delta\epsilon_z$) computed in STRES3.

The entire formulation contained in STRES3 for the biaxial elastic-plastic plane stress material law was found to be correct, except for Equation 4.32 which was used to determine the total strain increment in the z-direction ($\hat{\epsilon}_z$). However, it should be mentioned that there should be more information in the SAMSON2 Users Manual (3) with

regard to the types of materials that can be correctly modeled using the STRES3 subroutine. STRES3 should only be used for problems that involve materials which exhibit ductile or semiductile stress-strain material behavior. In fact, the von Mises failure criterion is only good for a yielding mode of failure which is exhibited in ductile or semiductile metals.

4.2.4.3 Stress Evaluations Using the Biaxial Elastic-Plastic Plane Strain or Axisymmetric Material Law (STRES3)

The formulation for the biaxial elastic-plastic plane strain or axisymmetric material law was also contained in subroutine STRES3. Therefore, the identical solution scheme (Table 4.6) was used for the plane strain or axisymmetric material law as was used for the plane strain material law with a few changes in the equations used. In this section, due to this similarity in the solution scheme, only the equations which were different are displayed. The discussion of the solution algorithm will not be presented however.

The first difference between the two material laws was in the elastic stress-strain matrix, c^E. Equations 4.39 and 4.40 show the c^E matrix and the corresponding multiplication process associated with c^E.

$$c^E = \frac{E}{(1+\nu)(1-2\nu)} \begin{bmatrix} 1-\nu & \nu & 0 & \nu \\ \nu & 1-\nu & 0 & \nu \\ 0 & 0 & \frac{1-2\nu}{2} & 0 \\ \nu & \nu & 0 & 1-\nu \end{bmatrix} \qquad (4.39)$$

$$\{\hat{\Delta\sigma}\} = C^E \times \{\hat{\Delta\epsilon}\} \tag{4.40}$$

where,

$$\{\hat{\Delta\sigma}\}^T = [\hat{\Delta\sigma}_x \quad \hat{\Delta\sigma}_y \quad \hat{\Delta\tau}_{xy} \quad \hat{\Delta\sigma}_z], \text{ and}$$

$$\{\hat{\Delta\epsilon}\}^T = [\hat{\Delta\epsilon}_x \quad \hat{\Delta\epsilon}_y \quad \hat{\Delta\gamma}_{xy} \quad \hat{\Delta\epsilon}_z].$$

As illustrated in these two equations, one additional stress term $(\hat{\Delta\sigma}_z)$ and one additional strain term $(\hat{\Delta\epsilon}_z)$ were present. However, the $\hat{\Delta\epsilon}_z$ term equalled zero for plane strain analyses. It should be noted that the Equations 4.21, 4.30, 4.32, and 4.33 that were used to determine the strain increment in the z-direction $(\hat{\Delta\epsilon}_z)$ for the plane stress material law do not apply to the plane strain and axisymmetric material law. The $\hat{\Delta\epsilon}_z$ term for axisymmetric analyses was calculated in subroutine V8FRCN.

The second difference between the two material laws was the yield function that was used. The yield function for the plane strain or axisymmetric material law is shown in Equation 4.41. Three additional terms are present in Equation 4.41 compared to Equation 4.23. These terms are all a function of $\hat{\sigma}_z$ which equalled zero for plane stress.

$$F = (\hat{\sigma}_x^2 + \hat{\sigma}_y^2 + \hat{\sigma}_z^2 - \hat{\sigma}_x\hat{\sigma}_y - \hat{\sigma}_x\hat{\sigma}_z - \hat{\sigma}_y\hat{\sigma}_z + 3\hat{\tau}_{xy}^2)^{\frac{1}{2}} \tag{4.41}$$

The third difference that existed between the two material laws involved the equation for determining RATIO. The value for t in Equation 4.26 needed to be updated in order to include the $\hat{\sigma}_z$ terms. Equation 4.42 shows the formula that was used to determine t for the plane strain or axisymmetric material law.

$$t = -[\Delta\hat{\sigma}_x(2\hat{\sigma}_x^n - \hat{\sigma}_y^n - \hat{\sigma}_z^n) + \Delta\hat{\sigma}_y(2\hat{\sigma}_y^n - \hat{\sigma}_x^n - \hat{\sigma}_z^n) +$$

$$\Delta\hat{\sigma}_z(2\hat{\sigma}_z^n - \hat{\sigma}_x^n - \hat{\sigma}_y^n) + 6\Delta\hat{\tau}_{xy}\,\hat{\tau}_{xy}^n] \qquad (4.42)$$

The value for t determined in Equation 4.42 was substituted into Equation 4.26 in order to determine which portions (RATIO) of the stress and strain increments were elastic.

The final difference between the two material laws existed in the elastic-plastic stress-strain matrix C^{EP}. The derivation involved in the determination of C^{EP} and the final C^{EP} matrix for the plane strain or axisymmetric material law is shown in Appendix C. The incremental stresses and strains corresponding to Equation 4.31 are $\{\Delta\hat{\sigma}_p\}^T = \lceil\Delta\hat{\sigma}_{xp}$ $\Delta\hat{\sigma}_{yp}\ \Delta\hat{\tau}_{xyp}\ \Delta\hat{\sigma}_{zp}\rceil$ and $\{\Delta\hat{\epsilon}_p\}^T = \lceil\Delta\hat{\epsilon}_{xp}\ \Delta\hat{\epsilon}_{yp}\ \Delta\hat{\gamma}_{xyp}\ \Delta\hat{\epsilon}_{zp}\rceil$.

The remainder of the calculations performed in STRES3 were identical for the two material laws. But, there were four stresses and four strains involved in the calculations for the plane strain or axisymmetric material law and only three stresses and three strains for the plane stress material law.

The formulation for the plane strain or axisymmetric material law was found to be correct through comparisons with References 12, 14, and 15. No errors were found in the entire plane strain or axisymmetric formulation.

4.2.4.4 Stress Evaluations Using the Plane Strain or Axisymmetric AFWL "Engineering" Material Law (STRES9)

This section contains a brief discussion on the AFWL "engineering" model. In addition, some of the principal equations that are used in

this model are displayed. The AFWL "engineering" material law was developed primarily for modeling soils. It is defined by a piecewise linear hydrostat (plot of hydrostatic pressure ($[\sigma_x + \sigma_y + \sigma_z]/3$) versus volumetric strain) with corresponding bulk moduli for both loading and unloading/reloading (K_L and K_U) (see Figure 4.3).
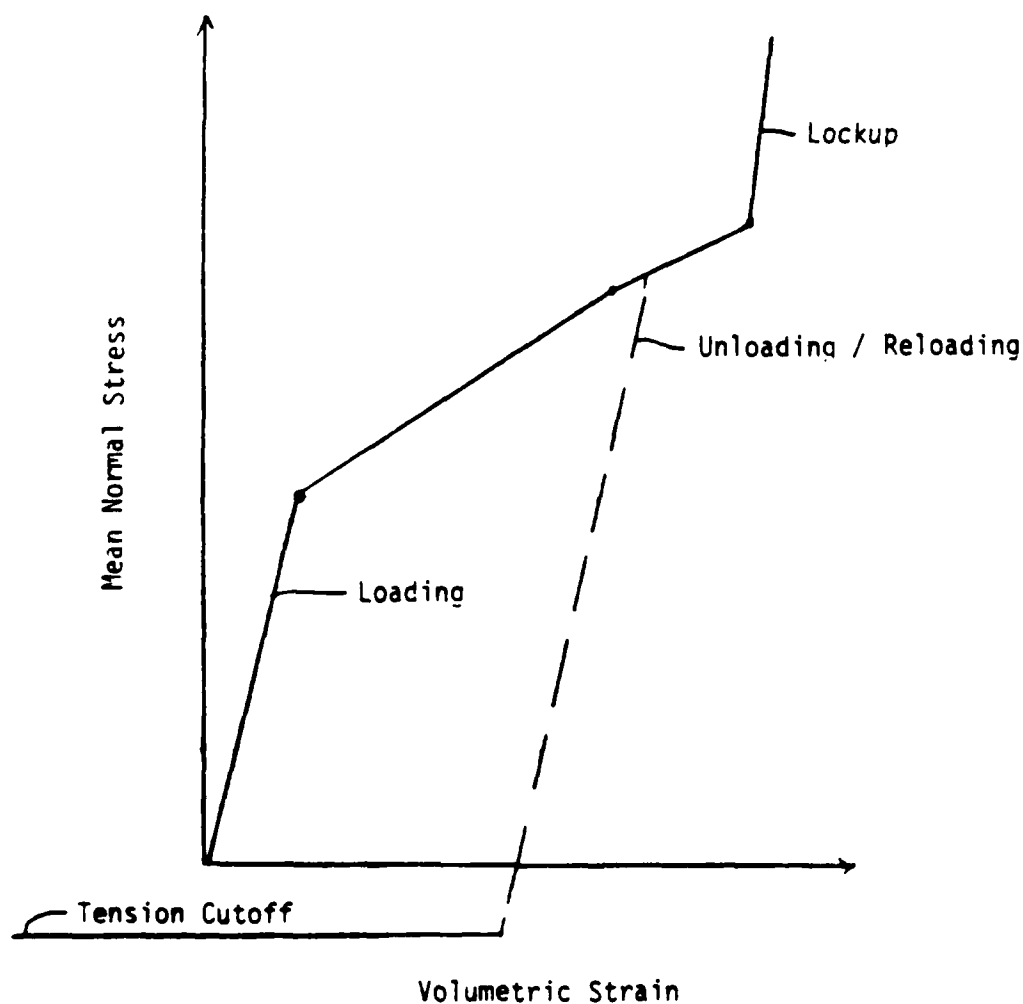
Figure 4.3   An Example of a Piecewise Linear Hydrostat Curve Which is Used to Define the AFWL "Engineering" Material Law.

It is also defined by a yield (failure) surface which plots hydrostatic pressure versus $\sqrt{J_2'}$ (Drucker-Prager yield criterion) where $\sqrt{J_2'}$ equals

the square root of the second invariant of the deviatoric stress tensor. A nonassociated flow rule is employed in the AFWL "engineering" model. It should be mentioned that the AFWL "engineering" model can only be used to model strain hardening materials. Also, the AFWL model was formulated only for plane strain or axisymmetric analyses. Hence, the stresses, $\{\hat{\sigma}\}$, and strains, $\{\hat{\epsilon}\}$, that were used in the calculations are as follows:

$$\{\hat{\sigma}\}^T = [\hat{\sigma}_x \ \hat{\sigma}_y \ \hat{\tau}_{xy} \ \hat{\sigma}_z] \text{ and } \{\hat{\epsilon}\}^T = [\hat{\sigma}_x \ \hat{\sigma}_y \ \hat{\tau}_{xy} \ \hat{\sigma}_z].$$

Some preliminary operations were performed prior to the determination of the stress values at the elemental integration points. The first operation was the determination of the total strains for the current time step, $\{\hat{\epsilon}\}^{n+1}$ (see Equation 4.38). The next operation was the determination of the four history parameters which are described below:

pvolp   =   hydrostatic pressure for the previous time step, P^n,

pevol   =   volumetric strain for the previous time step, ϵ_{vol}^n,

d4   =   minimum volumetric strain which has been computed throughout the solution, and

d6   =   volumetric strain at which the tension cut-off was entered.

The final operation was the calculation of the volumetric strain for the current time step $(\hat{\epsilon}_{vol}^{n+1})$ as shown in Equation 4.43.

$$\hat{\epsilon}_{vol}^{n+1} = \hat{\epsilon}_x^{n+1} + \hat{\epsilon}_y^{n+1} + \hat{\epsilon}_z^{n+1} \tag{4.43}$$

The value which was obtained from Equation 4.43 was compared with the history parameter d4 in order to determine which solution scheme was to be executed. There are two possible solution schemes that are used in STRES9. The first is for a loading case where $\hat{\epsilon}_{vol}^{n+1} \leq d4$ and the second scheme is for an unloading/reloading case $\hat{\epsilon}_{vol}^{n+1} > d4$. These two schemes are discussed separately in the following paragraphs.

If the current value for the volumetric strain was less than or equal to the value for the history parameter d4, then the solution was determined to be in a state of loading. Upon this determination, a bulk modulus ($K = K_L$) value was determined from the hydrostat curve based on the value for $\hat{\epsilon}_{vol}^{n+1}$. Also, the value for d4 was set equal to $\hat{\epsilon}_{vol}^{n+1}$ and a value for ν (Poisson's ratio) was chosen from the input data based on $\hat{\epsilon}_{vol}^{n+1}$. The normal and shear stresses for the current time step ($\hat{\sigma}_i^{n+1}$ and $\hat{\tau}_{xy}^{n+1}$) were then calculated for particular integration points according to Equations 4.44, 4.45 and 4.46.

$$\hat{\sigma}_i^{n+1} = \hat{\sigma}_i^n + 2G \left[\hat{\Delta\epsilon}_i - \frac{(\hat{\epsilon}_{vol}^{n+1} - \hat{\epsilon}_{vol}^n)}{3}\right] + \Delta P \tag{4.44}$$

where,

$$2G = \frac{3K (1 - 2\nu)}{1 + \nu},$$

$\hat{\epsilon}_{vol}^n =$ pevol, and

$\Delta P =$ incremental change in the hydrostatic pressure between the current and previous time steps as was calculated using Equation 4.46.

$$\hat{\tau}_{xy}^{n+1} = \hat{\tau}_{xy}^n + G \hat{\Delta\gamma}_{xy} \tag{4.45}$$

$$\Delta P = K (\epsilon_{vol}^{n+1} - \epsilon_{vol}^n) \tag{4.46}$$

These three equations were found to be correct when compared to information that was obtained from AFWL personnel. However, a possible error was discovered. The stress in the z-direction ($\hat{\sigma}_z$) was set equal to 0.0 for elements having a thickness not equal to 1.0. This appears to be a plane stress correction. The current value for the hydrostatic pressure was calculated using Equation 4.47.

$$P^{n+1} = P^n + \Delta P \tag{4.47}$$

where,

P^n = time history parameter pvolp.

This value for the current hydrostatic pressure was then compared to the limiting mean normal stress value P_{max} (the tension cut-off value). Two possible cases were obtained based on this comparison. The first case was for $P^{n+1} - P_{max} < 0$. This case showed that the loading had occurred outside of the tension cut-off region of the hydrostat curve. For this case ($P^{n+1} - P_{max} < 0$), a value for the failure function (XJ) was computed by substituting the stress values that were calculated using Equations 4.44 and 4.45 into Equation 4.48.

$$XJ = \sqrt{\frac{1}{6} \left[(\hat{\sigma}_x^{n+1} - \hat{\sigma}_y^{n+1})^2 + (\hat{\sigma}_x^{n+1} - \hat{\sigma}_z^{n+1})^2 + (\hat{\sigma}_y^{n+1} - \hat{\sigma}_z^{n+1})^2 + 6(\hat{\tau}_{xy}^{n+1})^2 \right]}$$

$$\tag{4.48}$$

The value XJ was then compared with a value YJ which was obtained from the Drucker-Prager (17) yield (failure) surface (plot of $\sqrt{J_2'}$ versus hydrostatic pressure). The value for YJ was set equal to the value for $\sqrt{J_2'}$ which was obtained from the yield surface corresponding to the value for P^{n+1}. The comparison between YJ and XJ was performed in order to

determine if yielding had occurred. If $XJ \leq YJ$, then the stresses which were previously computed in Equations 4.44 and 4.45 were correct. However, if $XJ > YJ$, then the nonassociated flow rule that was formulated in STRES9 was applied and the stresses were recalculated by substituting the previous stress values from Equations 4.44 and 4.45 into Equation 4.49.

$$\hat{\sigma}_i^{n+1} = P^{n+1} + con1 \, (\hat{\sigma}_i^{n+1} - P^{n+1})$$
$$\hat{\tau}_{xy}^{n+1} = con1 \, \hat{\tau}_{xy}^{n+1}$$

(4.49)

where,

$$con1 = \frac{YJ}{XJ}.$$

The stress values that were obtained from Equation 4.49 were the correct values for the case where yielding had occurred. The second case which was obtained from the comparison between P^{n+1} and P_{max} was for $P^{n+1} - P_{max} \geq 0$. This comparison shows that the current state of stress occurs beyond the tension cut-off region. Therefore, the values for the stresses that were computed in Equations 4.44 and 4.45 exceed the tension cut-off value and must be corrected. These values were changed such that all of the normal stress values ($\hat{\sigma}_x^{n+1}$, $\hat{\sigma}_y^{n+1}$, and $\hat{\sigma}_z^{n+1}$) and the value for P^{n+1} were set equal to the limiting mean normal stress value P_{max}. The shear stress value was set equal to 0.0. The time history parameter d6 was also modified using Equation 4.50.

$$d6 = \epsilon_{vol}^n + (P_{max} - P^n) / K$$

(4.50)

where,

    d6   =   value of the volumetric strain when the solution entered the tension cut-off region.

If the current value for the volumetric strain ϵ_{vol}^{n} was found to be greater than the value for d4, then the solution was determined to be in an unloading/reloading state. The value for the bulk modulus ($K = K_U$) and the value for Poisson's ratio (ν) were determined, as in the loading case, based on the value for $\hat{\epsilon}_{vol}^{n+1}$ as long as pvolp < P_{max}. These values for the bulk modulus and Poisson's ratio were then substituted into Equations 4.44, 4.45 and 4.46, as was done for the loading case, and the remainder of the solution scheme was identical to that for the loading case. However, if pvolp $\geq P_{max}$, then another comparison was required between $\hat{\epsilon}_{vol}^{n+1}$ and d6. If ϵ_{vol}^{n+1} was greater than or equal to d6, then the normal stress values remained equal to P_{max} and the shear stress values equal 0.0. For the other case where $\hat{\epsilon}_{vol}^{n+1}$ < d6, the stresses were recalculated following the same procedure mentioned earlier in this paragraph for the loading/reloading case where pvolp < P_{max}. However, the formulation in subroutine STRES9 was found to be incorrect for this case where pvolp $\geq P_{max}$ and $\hat{\epsilon}_{vol}^{n+1} \leq$ d6 when compared to information which was obtained from personnel at the AFWL. The total increment of volumetric strain cannot be used in order to determine the stresses for a case where reloading has occurred beyond the tension cut-off. The proper formulation requires the determination of a factor F_α which is equal to the percent of the total strain increment which is actually reloading out of the tension cut-off. This factor F_α is computed using Equation 4.51 and needs to be implemented into Equations 4.44, 4.45, and 4.46 in order to calculate the correct values for the stresses.

$$F_\alpha = \frac{\epsilon_{vol}^{n+1} - d6}{\epsilon_{vol}^{n+1} - \epsilon_{vol}^n} \qquad (4.51)$$

Two additional operations were performed after the correct stress values were obtained for either the loading case or the unloading/ reloading case. The first operation which was executed was the storage of the current stress and strain values, which were calculated at particular integration points, in the strs array. The second operation was the storage of the values for the four history parameters in the strs array.

The formulation for the AFWL material model (STRES9) was verified through comparisons with information that was obtained from AFWL personnel and two errors were found. Also, it was found that a segment within the STRES9 subroutine was never used in any analysis. This segment was associated with a plane stress material law and appears to have been eliminated from use in the AFWL model.

4.2.4.5 Evaluation of the Internal Nodal Forces

This section contains the development of the equations used in SAMSON2 for the determination of the internal nodal forces $\{F_{int}\}$. These forces are produced as a result of the stresses and strains which develop within an element (see Table 4.4 on page 83). Therefore, the internal nodal forces $\{F_{int}\}$ are a function of the amount of stress and strain exhibited within an element.

Equation 4.52 is the basic equation used in the determination of the internal nodal forces. However, no stiffness matrix is ever

determined in the execution of SAMSON2 as was mentioned in Section 4.1. Therefore, the terms on the righthand side of Equation 4.52 need to be changed into terms that are consistent with the SAMSON2 formulation.

$$\{F_{int}\} = [K]\{U\} \tag{4.52}$$

where,

$\{F_{int}\}$ = internal nodal force vector,

[K] = structural stiffness matrix, and

{U} = vector containing the nodal displacements.

The stiffness matrix, [K], can be expressed in terms of the strain-displacement and stress-strain matrices ([B] and [C]) that were calculated in the previous sections as given in Equation 4.53.

$$[K] = \int_V [B]^T [C] [B] \, dV \tag{4.53}$$

where,

[K] = elemental stiffness matrix calculated at a particular integration point,

[B] = $[\bar{B}]/|J|$, where $[\bar{B}]$ is the strain-displacement matrix shown in Table 4.5 of Section 4.2.3, and

[C] = stress-strain matrix for a particular material model.

The next step is to substitute this expression for [K] into Equation 4.52 which results in Equation 4.54.

$$\{F_{int}\} = \int_V [B]^T [C] [B] \, dV \{U\} \tag{4.54}$$

But, this equation for {F} can be simplified using the expressions in the following equation:

$$\{\epsilon\} = [B] \{U\}$$

$$\{\sigma\} = [C] \{\epsilon\} \tag{4.55}$$

The equation resulting from the substitution of these two expressions into Equation 4.54 is shown in Equation 4.56. However, Equation 4.56 still needs to be altered in order to incorporate the Gauss-Legendre numerical integration scheme.

$$\{F\} = \int_V [B]^T \{\sigma\} \, dV \tag{4.56}$$

Equations 4.57 and 4.58 are the final expressions that were formulated into the SAMSON2 code in subroutine V8FRCN for the evaluation of the internal nodal forces for plane and axisymmetric analyses, respectively.

$$\{F_{int}\}^{n+1} = t \sum_{i=1}^{n} \sum_{j=1}^{n} h_i \, h_j \, [\tilde{B}(\xi_i, n_j)]^T \, \{\sigma(\xi_i, n_j)\}^{n+1} \tag{4.57}$$

where,

$\{F_{int}\}^{n+1}$ = internal forces applied to the nodes of an 8NQ element for a plane analysis,

$\{F_{int}\}^T$ = $[F_{x1} \, F_{y1} \, F_{x2} \, F_{y2} \, \cdots \, F_{x7} \, F_{y7} \, F_{x8} \, F_{y8}]$, where F_{xI}, F_{yI} = internal nodal forces in the x and y direction for node I,

t = thickness of the element,

n = order of integration selected for the analysis,

h_i, h_j = Gauss-Legendre weight coefficients,

$[\tilde{B}(\xi_i, n_j)]^T$ = transpose of the stress-strain matrix shown in Table 4.5 which was evaluated at a particular elemental quadrature point with the coordinates (ξ_i, n_j) being assigned values corresponding to the Gauss-Legendre abscissae coefficients, and

$\{\sigma(\xi_i, n_j)\}^{n+1}$ = total stresses for the current time step, including the viscous stresses due to damping, which were evaluated at elemental quadrature points using an appropriate material law and were then transformed into the global (x,y) coordinate system.

$$\{F_{int}\}^{n+1} = \sum_{i=1}^{n} \sum_{j=1}^{n} h_i h_j \, r(\xi_i, n_j)[\bar{B}(\xi_i, n_j)]^T \{\sigma(\xi_i, n_j)\}^{n+1} \qquad (4.58)$$

where,

$\{F_{int}\}^{n+1}$ = internal forces applied to the nodes of an 8NQ element for an axisymmetric analysis, and

$r(\xi_i, n_j)$ = distance from the axis of symmetry (y-axis) to a particular quadrature point (ξ_i, n_j) obtained by using Equation 4.1 in Section 4.2.1 and solving only for x.

Equations 4.57 and 4.58 were developed by replacing the integral in Equation 4.56 by the appropriate terms used in the Gauss-Legendre integration scheme. In addition, the expressions in Equations 4.59 and 4.60 were used to simplify Equation 4.56.

$$dV = r^\alpha \, |J| \, d\xi \, dn \qquad (4.59)$$

where,

dV = differential volume used in the integration,

r^α = t for plane analyses ($\alpha = 0$), or
  = $r(\xi_i, n_j)$ for axisymmetric analysis ($\alpha = 1$), and

$d\xi \, dn$ = differential area used in the numerical integration scheme.

$$[\bar{B}]^T = |J| \, [B]^T \qquad (4.60)$$

It should be noted that the total internal nodal forces for a particular node included the contributions from all of the elements to which it was associated.

The stresses that were used in Equations 4.57 and 4.58 were not equal to the stresses that were calculated in the appropriate material law subroutines. The stresses which were calculated using the material laws were first adjusted to include the viscous stresses that were calculated in order to simulate stiffness proportional damping. These adjusted stresses were then rotated from the corotational $(\hat{x},\hat{y})$ coordinate system to the global (x,y) coordinate system by using a suitable transformation matrix. Both of these adjustments to the stress values that were obtained from the material law subroutines are discussed in the following paragraph. One other observation that was made regarding only Equation 4.58 was that the factor 2π was not included. However, this factor is canceled later in obtaining the final solution to the equation of motion.

The stresses $\{\hat{\sigma}\}^{n+1}$ that were calculated previously in the material law subroutines were modified twice prior to their use in Equations 4.57 and 4.58. The first modification was the addition of the viscous stresses $\{\hat{\sigma}\}^{vis}$ which were calculated in SAMSON2 in order to simulate stiffness proportional damping through the use of linear artificial viscosity. The reason for the use of linear artificial viscosity is because a stiffness matrix is never created in the SAMSON2 explicit code. Linear artificial viscosity was formulated such that the viscous stresses $\{\hat{\sigma}\}^{vis}$ damp out the highest frequency of an element by approximately the specified fraction of critical element damping (μ). The corotational viscous normal stresses $\{\hat{\sigma}_{ii}^{vis}\}$ were calculated in SAMSON2 using Equations 4.61, 4.62, and 4.63.

$$\{\hat{\sigma}_{ii}^{vis}\} = \{\hat{P}^{vis}\} + \{\hat{S}_{ii}^{vis}\} \tag{4.61}$$

where,

$\{\hat{P}^{vis}\}$ = hydrostatic viscous normal stresses, and

$\{\hat{S}_{ii}^{vis}\}$ = deviatoric viscous normal stresses.

$$\{\hat{P}^{vis}\} = \frac{2\mu B}{\omega_{max}} \left(\frac{\hat{d}_{11} + \hat{d}_{22} + \hat{d}_{33}}{3}\right) \tag{4.62}$$

where,

μ = specified fraction of critical element damping,

B = bulk modulus computed in the stress routines,

ω_{max} = maximum frequency of the element, and

$\hat{d}_{11}, \hat{d}_{22}, \hat{d}_{33}$ = normal corotational velocity strains in the x, y, and z directions that were calculated in Section 4.2.3.

$$\{\hat{S}_{ii}^{vis}\} = \frac{2\mu G}{\omega_{max}} \left(\hat{d}_{ii} - \frac{\hat{d}_{11} + \hat{d}_{22} + \hat{d}_{33}}{3}\right) \tag{4.62}$$

where,

G = shear modulus for a given material model, and

$\hat{d}_{ii}$ = corotational velocity normal strains, i=1, 2, 3.

The corresponding corotational viscous shear stress $\hat{\tau}_{xy}^{vis}$ was calculated in SAMSON2 using Equation 4.64.

$$\hat{\tau}_{xy}^{vis} = \frac{2\mu G}{\omega_{max}} \frac{\hat{\gamma}_{xy}}{\Delta t} \tag{4.64}$$

The development for Equations 4.61-4.64 and the equations that were used in order to approximate ω_{max} are not shown here, but can be found in

Reference 1. The total corotational stresses for the current time step, including the viscous stresses that were calculated in Equations 4.61-4.64, were calculated in SAMSON2 using the expressions shown in Equation 4.65, where the first terms on the righthand side of the expressions were calculated previously in the corresponding stress routines. These expressions were calculated in subroutine SDAMP and were also verified through comparisons with References 1 and 16.

$$\hat{\sigma}_x^{n+1} = \hat{\sigma}_x^{n+1} + \frac{2\mu B}{\omega_{max}} \frac{(\hat{d}_{11} + \hat{d}_{22} + \hat{d}_{33})}{3} + \frac{2\mu G}{\omega_{max}} \frac{(2\hat{d}_{11} - \hat{d}_{22} - \hat{d}_{33})}{3}$$

$$\hat{\sigma}_y^{n+1} = \hat{\sigma}_y^{n+1} + \frac{2\mu B}{\omega_{max}} \frac{(\hat{d}_{11} + \hat{d}_{22} + \hat{d}_{33})}{3} + \frac{2\mu G}{\omega_{max}} \frac{(2\hat{d}_{22} - \hat{d}_{11} - \hat{d}_{33})}{3}$$

$$\hat{\sigma}_z^{n+1} = \hat{\sigma}_z^{n+1} + \frac{2\mu B}{\omega_{max}} \frac{(\hat{d}_{11} + \hat{d}_{22} + \hat{d}_{33})}{3} + \frac{2\mu G}{\omega_{max}} \frac{(2\hat{d}_{33} - \hat{d}_{11} - \hat{d}_{22})}{3}$$

$$\hat{\tau}_{xy}^{n+1} = \hat{\tau}_{xy}^{n+1} + \frac{2\mu G}{\omega_{max}} \frac{\hat{\gamma}_{xy}}{\Delta t}$$

(4.65)

These modified total stresses were then transformed in the SAMSON2 code from the corotational coordinate system $(\hat{x}, \hat{y})$ to the global coordinate system (x, y) using Equations 4.66 and 4.67.

$$T_\theta = \begin{bmatrix} \cos^2\theta & \sin^2\theta & -\sin\theta\cos\theta \\ \sin^2\theta & \cos^2\theta & \sin\theta\cos\theta \\ 2\sin\theta\cos\theta & -2\sin\theta\cos\theta & \cos^2\theta - \sin^2\theta \end{bmatrix}$$

(4.66)

where,

T_θ = transformation matrix used in SAMSON2 in order to convert the corotational stresses $\{\hat{\sigma}\}$ to stresses in the global coordinate system $\{\sigma\}$, and

θ = current total rotation which has occurred at an element quadrature point as computed by Equation 4.13.

$$\{\sigma\}^{n+1} = [T_\Theta] \{\hat{\sigma}\}^{n+1} \qquad (4.67)$$

where,

$\{\sigma\}^{n+1}$ = global components of the stresses that were computed in Equation 4.65, and

$\{\hat{\sigma}\}^{n+1}$ = stress values that were computed using Equation 4.65.

An error was discovered in the stress transformation matrix, $[T_\Theta]$, when comparisons were made with References 1, 7, and 14. The correct transformation matrix which should be used in the SAMSON2 formulation is shown in Equation 4.68.

$$T_\Theta = [R]^T = \begin{bmatrix} \cos^2\theta & \sin^2\theta & -2\sin\theta\cos\theta \\ \sin^2\theta & \cos^2\theta & 2\sin\theta\cos\theta \\ \sin\theta\cos\theta & -\sin\theta\cos\theta & \cos^2\theta - \sin^2\theta \end{bmatrix} \qquad (4.68)$$

where,

$[R]^T$ = transpose of the strain transformation matrix calculated in Equation 4.14.

It should be mentioned that the incorrect transformation matrix (Equation 4.66) was used in the formulations for the three-node triangular (3NT), 4NQ, 5NT, 6NT, and 8NQ isoparametric continuum finite elements. This error can be corrected by replacing the FORTRAN statement

```
CALL STPRD (temp2,shat,stress)
```

which is formulated in the VnFRCN subroutines (n=3,4,5,6, and 8) with the following FORTRAN statement:

```
CALL GTPRD (temp2,shat,stress,3,3,1).
```

The internal nodal force equations which were formulated into the SAMSON2 code were found to be correct when compared to References 1, 9, 13, and 16. However, one error which was related to the internal force calculation was found. This error was in the formulation for the stress transformation matrix. This is a major error and needs to be corrected in the current versions of SAMSON2 code in order for the program to provide correct results.

4.2.4.6 Evaluation of the Internal Strain Energy

The equations that were formulated in the SAMSON2 code for the determination of the internal strain energy are presented in this section. Strain energy is a function of the Cauchy stresses and the velocity strains within an element. The internal strain energy is calculated correctly for these conjugate measures of strain rate and stress.

The basic relation which is used for determining the internal strain energy is shown in Equation 4.69.

$$U = \frac{1}{2} \int_V \{\epsilon\}^T \{\sigma\} \ dV \tag{4.69}$$

where,

U = total internal strain energy within a system, and

$\{\epsilon\},\{\sigma\}$ = stresses and strains within a system.

However, this equation was altered in order to be consistent with the SAMSON2 formulation. The resulting expressions which were used in the SAMSON2 code for the determination of the total internal strain energy

are shown in Equations 4.70 and 4.71. It should be noted that a 2π term was not included in the determination of the internal strain energy for axisymmetric analyses because it is canceled in the determination of the energy error.

$$U^{n+1} = U^n + \frac{1}{2} \sum_{I=1}^{JE} \{ \sum_{i=1}^{n} \sum_{j=1}^{n} [r^\alpha h_i h_j |J(\xi_i, n_i)| \Delta e] \} \qquad (4.70)$$

where,

U^{n+1}, U^n = total internal strain energies of the system for the current and previous time steps, respectively,

JE = total number of elements in the system, and

Δe = increment of internal strain energy computed for an elemental integration point as shown in Equation 4.71.

$$\Delta e = \sum_{i=1}^{nstres} \{\hat{\Delta\epsilon}(\xi_i, n_j)\}^{n+\frac{1}{2}} \times (\{\hat{\sigma}(\xi_i, n_j)\}^{n+1} + \{\hat{\sigma}(\xi_i, n_j)\}^{n}) \qquad (4.71)$$

where,

nstres = 3 for plane stress analyses, and
= 4 for plane strain or axisymmetric analyses;

$\hat{\Delta\epsilon}(\xi_i, n_j)$ = incremental strains that were computed in Equation 4.16 of Section 4.2.3 for a particular Gaussian quadrature point; and

$\{\hat{\sigma}(\xi_i, n_j)\}^{n+1}$,

$\{\hat{\sigma}(\xi_i, n_j)\}^{n}$ = total stresses that were computed using the appropriate material law routines for the current and previous time steps, respectively.

Equations 4.70 and 4.71 were verified through comparisons with Reference 1. The value for the total internal strain energy, U^{n+1}, was stored in the strs array for use later in the energy error solution.

4.2.5 Determination of the External Nodal Forces

and the Corresponding External Work

The calculations that were involved in the determination of the external nodal forces, $\{F_{ext}\}$, and the external work (W) are discussed in this section. These quantities were calculated in subroutines FREEFD and FREEF2 of the SAMSON2 code. Some of the equations that were used in these calculations are also provided. Formulation errors that were discovered in these two subroutines are also mentioned.

The SAMSON2 code contains the following five different load types (see p. 50 in Reference 3):

    1)   axisymmetric pressure load line

    2)   plane pressure load line

    3)   initial impulse load line

    4)   force line

    5)   displacement history load line

with a load line referring to the consecutive nodes along which the load was applied. The external nodal forces were computed in accordance with the particular load type that was used in the problem solution. Calculations of the external nodal forces were done in approximately the same manner for each of the five load types. These calculations are discussed for each of the load types in the following paragraphs.

Initial nodal velocities were calculated for the initial impulse load line. These initial nodal velocities were calculated prior to the start of the SAMSON2 explicit integration scheme. These initial nodal velocities were calculated in subroutine FREEFD of the SAMSON2 code

using Equation 4.72 for the case in which the initial impulse load was input in terms of the normal and tangential components.

$$V_x = \tfrac{1}{2}(V_t \cos \Theta - V_n \sin \Theta)$$

$$V_y = \tfrac{1}{2}(V_t \sin \Theta + V_n \cos \Theta)$$

(4.72)

where,

V_x, V_y = initial nodal velocities transformed from the input normal and tangential components to the global x and y components,

V_t, V_n = tangential and normal components for the input initial impulse load, and

Θ = angle shown in Figure 4.4.

The sign convention that was used with this impulse load is illustrated in Figure 4.4 with the normal and tangential components (V_n and V_t) shown acting in the positive directions.
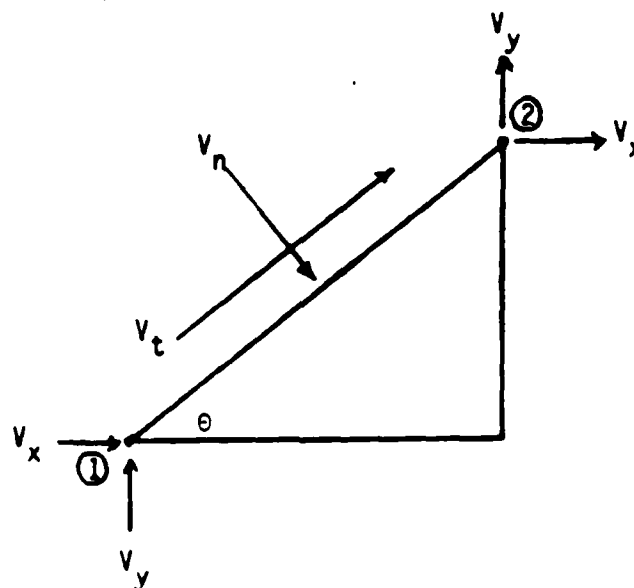
Figure 4.4   Initial Nodal Velocities for an Impulse Load Input in Terms of Normal and Tangential Components.

Equation 4.72 was found to be incorrect. The correct formula for determining the initial nodal velocities (V_x and V_y) is shown in Equation 4.73.

$$V_x = \tfrac{1}{2}(V_t \cos \Theta + V_n \sin \Theta)$$
$$V_y = \tfrac{1}{2}(V_t \sin \Theta - V_n \cos \Theta)$$

(4.73)

In comparing Equation 4.72 to Equation 4.73, the only differences between the two equations are the signs assigned to the normal velocity component terms. For the case in which the impulse load was input in global x- and y-components, the values for V_x and V_y were simply set equal to these input values. The values for V_x and V_y were stored in their respective locations within the velocity (V) array for each segment along the load line. Therefore, all of the nodes, except for the first and last nodes on the load line, had contributions from both of the segments on the load line of which they were a part. Two node factors, factors by which the nodal velocities determined in Equation 4.72 were multiplied (values usually equal 2.0), were used in order to increase the values for the initial velocities for these first and last nodes such that they matched the values for the other nodes on the load line. Upon determination of these initial nodal velocities, no more calculations were executed for the initial impulse load and subroutine FREEFD was never used again.

The calculations that were used in order to determine the external nodal forces (nodal velocities and displacements) for the displacement history load line were similar to those for the impulse load line. However, an input load line history (displacement versus time curve) was

used. Therefore, the first calculation that was performed was the determination of the displacement value for the current time step or the total solution time. This displacement value, u^{n+1}, was calculated in subroutine PRESS. This displacement value was then stored in the locations within the nodal displacement array (x1) corresponding to the specified component (x or y) for the displacement history load line. Nodal velocities were also computed using Equation 4.74 and stored in the appropriate locations within the velocity array (V). No other calculations were performed after the determination of these external forces (nodal velocities and displacement) in the FREEF2 subroutine.

$$V^{n+1} = \frac{u^{n+1} - u^n}{\Delta t} \tag{4.74}$$

where,

V^{n+1} = nodal velocity computed for the current time step Δt, and

u^{n+1}, u^n = displacement values obtained from the load line history data for the current and previous time steps, respectively.

The values for the external nodal forces, $\{F_{ext}\}$, that were computed for the force line load were obtained using the subroutine PRESS in the SAMSON2 code. The values for the external nodal forces were set equal to the force value, P^{n+1}, which was obtained from the force line history data for the current time step using PRESS. These values were then stored in the forcd array in the appropriate locations corresponding to which force component (x or y) of the load line was specified in the input data. Two other parameters were computed for the force line load. These parameters were the total external work, W^{n+1},

and the total linear impulse, WIM^{n+1}, for the current time step. These two parameters were calculated using Equations 4.75 and 4.76.

$$W^{n+1} = W^n + \tfrac{1}{2}\Delta t(P^{n+1} + P^n)\left(\sum_{i=1}^{\text{ndnod}} \dot{u}_i^{n+\frac{1}{2}}\right) \qquad (4.75)$$

where,

W^{n+1}, W^n = total external work computed for a particular force line for the current and previous time steps,

P^{n+1}, P^n = values for the forces for the current and previous time steps that were obtained from the force line history data using PRESS,

ndnod = number of nodes on the force line, and

$\dot{u}_i^{n+\frac{1}{2}}$ = nodal velocity values for the nodes on the load line.

$$\text{WIM}^{n+1} = \text{WIM}^n + \tfrac{1}{2}\Delta t(P^{n+1} + P^n)(\text{ndnod}) \qquad (4.76)$$

where,

$\text{WIM}^{n+1}, \text{WIM}$ = total linear impulse for the externally applied force for the current and previous time steps.

These equations were verified through comparisons with References 1, 5, 9, and 16. The values for W^{n+1}, P^{n+1}, and WIM^{n+1} were all calculated in FREEF2 and were then stored in the strs array.

The calculations for the external nodal forces for the plane and axisymmetric pressure load lines were very similar to those for the force line load. However, the equations that were used in the calculations included the areas over which the pressures were being applied. The expressions that were used in order to determine the external nodal forces for the plane and axisymmetric pressure load lines are shown in Equation 4.77 and 4.78.

$$f_x = \tfrac{1}{2}P^{n+1} \, t(yc2 - yc1)$$

$$f_y = \tfrac{1}{2}P^{n+1} \, t(xc2 - xc1)$$

$$(4.77)$$

where,

f_x, f_y = external nodal force components that were computed for a particular segment along a plane pressure load line,

P^{n+1} = current pressure value that was obtained from the input load line history data using PRESS,

t = thickness of the elements, and

xcI, ycI = current displaced coordinates for node I of the load line.

$$f_x = \tfrac{1}{2}P^{n+1} \, r(yc2 - yc1)$$

$$f_y = \tfrac{1}{2}P^{n+1} \, r(xc2 - xc1)$$

$$(4.78)$$

where,

f_x, f_y = external nodal force components that were computed for a particular segment along an axisymmetric pressure load line, and

$r = \tfrac{1}{2}(xc1+xc2)$ = x-distance from the axis of symmetry to the middle of the load line segment.

Figure 4.5 shows an example segment from a pressure load line with the applied pressure shown acting in the positive direction. The external nodal force components (f_x and f_y) were stored in the appropriate locations within the forcd (external nodal force) array that corresponded to the load line nodes for each segment of the load line. The external work and the linear impulse parameters were also calculated for the pressure load lines.
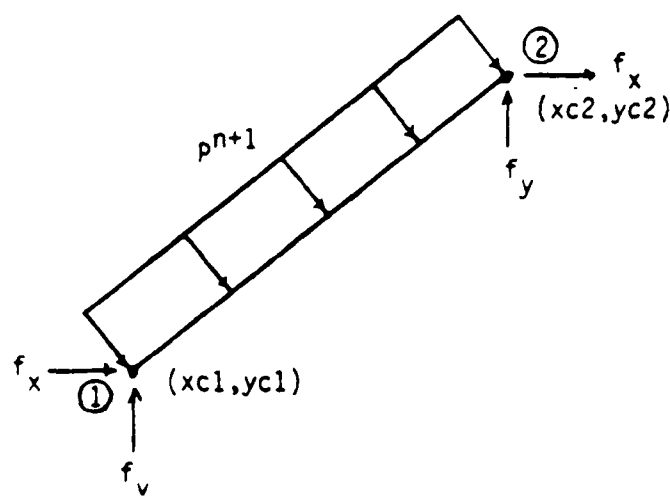
Figure 4.5   Typical Segment Along a Pressure Load Line.

Equations 4.79 and 4.80 are the expressions that were used in subroutine FREEF2 of the SAMSON2 code in order to determine the current total external work for the plane and axisymmetric pressure load lines, respectively.

$$W^{n+1} = W^n + \tfrac{1}{2}(P^{n+1} + P)[(pvol^{n+1} - pvol^n)] \tag{4.79}$$

$$pvol^n = \tfrac{1}{2}r^\alpha \sum_{I=1}^{ndn} [(yc_{I+1} - yc_I)(u_{x_I}^n + u_{xI+1}^n)$$

$$- (xc_{I+1} - xc_I)(u_{yI}^n + u_{yI+1}^n) + (u_{xI}^n)(u_{yI+1}^n) \tag{4.80}$$

$$- (u_{yI}^n)(u_{xI+1}^n)]$$

where,

$pvol^n$ =   parameter calculated for time step n which incorporates the total nodal displacement components and the x- and y-components of the distances between two adjacent nodes on the load line (area units),

xc_I, yc_I =   the originally input x- and y-coordinates for node I,

u_{xI}, u_{yI} = total displacement components for node I in the mesh,

ndn = $ndnod - 1$ = number of nodes on a load line $- 1$, and

r^α = t for plane analyses

= $\frac{1}{2}(xc1 + xc2)$ for axisymmetric analyses.

However, in a preliminary comparison made between these equations and Equation 4.81 (obtained from References 1, 9, and 16), the external work formulation in the SAMSON2 code for the pressure line loads was not verified.

$$W^{n+1} = W^n + \frac{1}{2}\Delta t \{\dot{u}^{n+\frac{1}{2}}\}^T (\{F_{ext}^n\} + \{F_{ext}^{n+1}\}) \tag{4.81}$$

The linear impulse for the external nodal forces was obtained using Equation 4.82. This equation was found to be correct when compared to material in Reference 5.

$$WIM^{n+1} = WIM^n + \frac{1}{2}\Delta t [(\sum_{i=1}^{ndn} f_x^{n+1}) + (\sum_{i=1}^{ndn} f_y^{n+1})]^{\frac{1}{2}} \frac{P^{n+1} + P^n}{P^{n+1}} \tag{4.82}$$

The $pvol^{n+1}$, P^{n+1}, W^{n+1}, and WIM^{n+1} parameters were all stored in the strs array for use in the calculations for the next time step.

The majority of the formulation in subroutines FREEF2 and FREEFD that was used in the determination of the external nodal forces, external work, and the linear impulse was found to be correct. However, two errors in the formulation were found and need to be corrected in order to obtain accurate results for all analyses. These errors were in the determination of the initial nodal velocities for the impulse load and the calculation of the external work for the pressure load lines. One additional note regarding the equations for the axisymmetric

pressure load is that the factor 2π was not included in any of the equations. This elimination of the factor 2π was consistent with previous axisymmetric formulations.

4.2.6 Solution to the Equation of Motion

This section contains a brief discussion regarding the general equation of motion followed by a discussion to the solution of the equation of motion formulated in the SAMSON2 code. The equation of motion is a mathematical expression through which the dynamic displacement values for acceleration, velocity, and displacement are defined. The general expression for the equation of motion is as follows:

$$[M]\{\ddot{u}\} + [C]\{\dot{u}\} + [K]\{u\} = P(t) \tag{4.83}$$

where,

[M]	=	mass matrix for the system,
[C]	=	viscous damping matrix for the system,
[K]	=	system stiffness matrix,
$\{\ddot{u}\},\{\dot{u}\},\{u\}$	=	dynamic displacement values for the acceleration, velocity, and displacement occurring within a system, and
P(t)	=	time varying externally applied load.

Each term in Equation 4.83 corresponds to a type of force with the terms on the lefthand side of the equation being the inertial, damping, and elastic forces, respectively. The solution to the equation of motion provides the values for the accelerations, velocities, and displacements for a particular point in time. And, when the solution to the equation

of motion is obtained for different points in time, the time histories for these three parameters can be obtained.

The equation of motion that was formulated in subroutine SOLVE of the SAMSON2 code for time step n is shown in Equation 4.84.

$$[M]\{\ddot{u}\}^n + [C]\{\dot{u}\}^n + \{F_{int}\}^n = \{F_{ext}\}^n \tag{4.84}$$

where,

$[M]$ = lumped diagonal mass matrix that was determined in Section 4.2.2,

$[C]$ = damping matrix shown in Equation 4.85,

$\{F_{int}\}$ = internal nodal forces that were computed in Section 4.2.4.5, and

$\{F_{ext}\}$ = external nodal forces that were calculated in Section 4.2.5.

This equation required the following two initial conditions: (1) $\{u\}^0 = \{u(0)\}$ and (2) $\{\dot{u}\}^{-\frac{1}{2}} = \{\dot{u}(0)\}$. The accuracy of the solution due to these initial velocity conditions is affected only slightly. The damping matrix that was used in the SAMSON2 formulation is of the form shown in Equation 4.85.

$$[C] = C_1[M] + C_2[K] \tag{4.85}$$

where,

C_1 = mass proportional damping factor, and

C_2 = stiffness proportional damping factor.

The stiffness proportional damping term, $C_2[K]$, was included in the determination of the nodal internal forces through the use of linear

artificial viscosity. The mass proportional damping term was substituted into Equation 4.84 for [C] which resulted in Equation 4.86.

$$[M]\{\ddot{u}\}^n + C_1[M]\{\dot{u}\}^n + \{F_{int}\}^n = \{F_{ext}\}^n \tag{4.86}$$

The mass proportional damping term is only used for dynamic relaxation problems (see Reference 1) in order to simulate static equilibrium through the use of sufficient damping. The value for C_1 is determined with the use of an estimate of the minimum frequency of a system as shown on pp. 128-132 of Reference 3. The values for the nodal accelerations at any time step were obtained from the solution to Equation 4.86. Equation 4.87 shows the expression that was used in SAMSON2 in order to determine the values for the nodal accelerations for time step n, $\{\ddot{u}\}^n$.

$$\{\ddot{u}\}^n = \frac{2}{2 + C_1 \Delta t} \left[[M]^{-1}(\{F_{ext}\}^n - \{F_{int}\}^n) - C_1\{\dot{u}\}^{n-\frac{1}{2}} \right] \tag{4.87}$$

where,

$[M]^{-1}$ = inverse of the diagonal lumped mass matrix, and

$\{\dot{u}\}^{n-\frac{1}{2}}$ = nodal velocities at the half time step.

Equation 4.87 was obtained by substituting the expression shown in Equation 4.88 into Equation 4.86 and rearranging the terms.

$$\{\dot{u}\}^n = \frac{\Delta t}{2} \{\ddot{u}\}^n + \{\dot{u}\}^{n-\frac{1}{2}} \tag{4.88}$$

Equation 4.88 was obtained through the use of central finite difference expressions. The inversion of the diagonal lumped mass matrix, $[M]^{-1}$, in Equation 4.87 is trivial and only involves the inversion of each term

on the diagonal. It should be noted that the acceleration values that are output for a particular analysis involving dynamic relaxation are not equal to the values obtained from Equation 4.87. Instead, the values that are output for the accelerations are obtained from the solution to Equation 4.89. These values are the actual accelerations in a dynamic analysis.

$$\{\ddot{u}\}^n = [M]^{-1}(\{F_{ext}\}^n - \{F_{int}\}^n) \tag{4.89}$$

The values for the nodal displacements and velocities were calculated in SAMSON2 using the central difference expressions shown in Equations 4.90 and 4.91.

$$\{\dot{u}\}^{n+\frac{1}{2}} = \{\dot{u}\}^{n-\frac{1}{2}} + \Delta t\ \{\ddot{u}\}^n \tag{4.90}$$

where,

$\{\dot{u}\}^{n-\frac{1}{2}}$ = nodal velocities for the previous time step, and

$\{\ddot{u}\}^n$ = values for the nodal accelerations that were calculated using Equation 4.87.

$$\{u\}^{n+1} = \{u\}^n + \Delta t\{\dot{u}\}^{n+\frac{1}{2}} \tag{4.91}$$

where,

$\{u\}^{n+1},\{u\}^n$ = nodal displacements for the current and previous time steps.

The values for the accelerations, velocities, and displacements that were calculated using Equations 4.87, 4.89, 4.90, and 4.91 were adjusted in the SOLVE routine to reflect the boundary conditions of the problem. All of the equations in the SOLVE routine were verified through comparison with References 1, 9, and 16. It should be noted that the 2π

factor does cancel out in the equation of motion for axisymmetric analyses.

The values ($\ddot{u}$, $\dot{u}$, and u) that were obtained by solving Equations 4.87, 4.89, 4.90 and 4.91 were stored in the nodal acceleration (a), velocity (v), and displacement (x1) arrays, respectively, for use in the next integration cycle as shown in Table 4.8. This table shows the order for which the calculations that were exhibited in Section 4.2 were performed in the SAMSON2 explicit integration scheme.

4.3 Summary of the SAMSON2 Formulation Errors

The 8NQ higher-order finite element formulation in the SAMSON2 code was investigated and verified. Formulation errors were discovered in SAMSON2 through this investigation and verification process. The following is a list of errors and possible errors that were discovered in the SAMSON2 formulation:

(1) Twelve Gauss-Legendre abscissae and weight coefficients were incorrectly typed into the GAUSS1 subroutine (see Table 4.3).

(2) The equation that was used in subroutine V8ASME in order to determine the mass for an axisymmetric 8NQ isoparametric continuum element is incorrect (see Equation 4.7 and the associated discussion). Also, a possible approximation error exists related to the use of Equation 4.7 in the determination of mass for both the 4NQ and 8NQ elements.

Table 4.8   Flow Chart for the SAMSON2 Explicit Integration Solution
              Scheme.

```
         ┌─────────────────────────────┐
         │ Assemble Diagonal Lumped    │
         │      Mass Matrix [M]        │
         └─────────────────────────────┘
                       │
                       ▼
         ┌─────────────────────────────────────┐
         │ Set Initial Conditions (n=0)        │
         │ {u}⁰ = u(0) and {u̇}ⁿ⁻½ = u̇(0)       │
         └─────────────────────────────────────┘
                       │
                       ▼
    ┌──────────────────────────────────────────────┐
    │ Compute External Forces and External Work    │◄──┐
    │           {F_ext}ⁿ and W                      │   │
    └──────────────────────────────────────────────┘   │
                       │                                │
                       ▼                                │
  ( Loop:  E = 1, Total Number of Elements in Mesh )    │
                       │                                │
                       ▼                                │
         ┌─────────────────────────────┐               │
         │ Compute Velocity Strains, {d}│              │
         └─────────────────────────────┘               │
                       │                                │
                       ▼                                │
         ┌─────────────────────────────┐               │
         │ Compute Cauchy Stresses, {σ̂}│               │
         └─────────────────────────────┘               │
                       │                                │
                       ▼                                │
    ┌──────────────────────────────────────────────┐   │
    │ Compute Internal Forces and Internal Strain  │   │
    │        Energy {F_int}ⁿ, Uⁿ                   │   │
    └──────────────────────────────────────────────┘   │
                       │                                │
                       ▼                                │
    ┌──────────────────────────────────────────────┐   │
    │ Solve Equations 4.87, 4.89, 4.90, and 4.91   │   │
    │ for Nodal Accelerations, Velocities, and     │   │
    │ Displacements {ü}ⁿ, {u̇}ⁿ⁺½, and {u}ⁿ⁺¹       │   │
    └──────────────────────────────────────────────┘   │
                       │                                │
                       ▼                                │
                  ┌─────────┐                           │
                  │ OUTPUT  │                           │
                  └─────────┘                           │
                       │                                │
                       ▼                                │
                ┌───────────┐                           │
                │ n = n + 1 │───────────────────────────┘
                └───────────┘
```

Compute External Forces and External Work $\{F_{ext}\}^n$ and W

Loop: E = 1, Total Number of Elements in Mesh

Compute Velocity Strains, $\{d\}$

Compute Cauchy Stresses, $\{\hat{\sigma}\}$

Compute Internal Forces and Internal Strain Energy $\{F_{int}\}^n$, U^n

Solve Equations 4.87, 4.89, 4.90, and 4.91 for Nodal Accelerations, Velocities, and Displacements $\{\ddot{u}\}^n$, $\{\dot{u}\}^{n+\frac{1}{2}}$, and $\{u\}^{n+1}$

OUTPUT

n = n + 1

(3) A possible error exists in the formulation for the strain transformation matrix (Equation 4.14). The term sin Θ is set equal to zero in subroutine VSTRAN for $|\Theta| < 1.0 \times 10^{-5}$.

(4) An error may result if the biaxial elastic-plastic plane stress and biaxial elastic-plastic plane strain or axisymmetric material laws are used in analyses involving improper materials. The von Mises failure criterion is only valid for ductile or semiductile metals.

(5) The equation in subroutine STRES3 that is used in order to determine the strain increment in the z-direction $(\Delta\hat{\epsilon}_z)$ is incorrect for plane stress analyses where yielding has occurred (see Equations 4.32 and 4.33 and corresponding discussion).

(6) The formulation for the AFWL "engineering" model in subroutine STRES9 (see Section 4.2.4.4) contains the following four errors:

    (a) The out-of-plane stress $(\hat{\sigma}_z)$ is set equal to zero for plane strain analyses which contain elements having a thickness not equal to 1.0.

    (b) The factor F_α which is the portion of the strain which reloads out of the tension cut-off was not included in the STRES9 formulation.

    (c) A possible error exists if the computed value for the volumetric strain $(\hat{\epsilon}_{vol})$ exceeds the last limiting volumetric strain value on the hydrostat curve. This error would occur if the bulk modulus for the last loading segment on the hydrostat curve was not equal to the lockup bulk modulus.

    (d) Another possible error may occur if the value that is calculated for the current hydrostatic pressure (P^{n+1}) exceeds

the value for the hydrostatic pressure which is associated with the last input yield function point. If this condition occurs, then the value for YJ is set equal to the last yield point value $\sqrt{J_2'}$, which may or may not be the correct value.

(7) The transformation matrix which is used in order to transform the stress components from the corotational coordinate system to the global coordinate system is incorrect (see Equations 4.66 and 4.68 and associated discussion). This error exists for all of the plane and axisymmetric continuum elements.

(8) The equations in subroutine FREEFD that are used to calculate the initial nodal velocities for an initial impulse load which has been input in normal and tangential components are incorrect (see Equations 4.72 and corresponding discussion).

(9) The external work equations in subroutine FREEF2 that are used in order to compute the external work due to a plane or axisymmetric pressure load line appear to be incorrect based on a preliminary investigation that was performed (see Equations 4.79, 4.80, and 4.81 and corresponding discussion).

(10) The column labels that are associated with the output from the AFWL "engineering" model are incorrect. The current hydrostatic pressure and the current volumetric strain are labeled sig-yld and rot, respectively.

These errors in the current finite element formulation for the SAMSON2 code need to be corrected and tested.

CHAPTER 5

Effect of the Corrected Formulation on the Finite Element Analyses

This chapter contains a discussion of the changes that occurred in the solutions to the problems from Chapter 3 after the corrections were made to the SAMSON2 finite element formulation based on the results from Chapter 4. The purpose of this chapter was to determine if more consistent and more reliable results could be obtained through the use of the corrected finite element formulation. It should be noted that some of the errors that were discovered in the SAMSON2 finite element formulation were unrelated to the problems from Chapter 3. Hence, the problem solutions were unaffected and the significance of these errors could not be determined.

The majority of the corrections that were made to the SAMSON2 formulation had little or no effect on the results for the problems in Chapter 3. For instance, the corrections for the Gauss-Legendre abscissae and weight coefficients in subroutine GAUSS1 resulted in no change for any of the BNQ element solutions. However, all of these solutions used an order of integration of 2.0. These corrected coefficient values may be significant for problems in which a higher order of integration is specified. The approximation for sin θ that is used in subroutine VSTRAN for $|\theta| < 1.0 \times 10^{-5}$ was changed to sin θ = sin θ for all values of θ. This correction was very insignificant as might be expected. The equation in subroutine STRES3 that is used to calculate the incremental strain in the z-direction ($\Delta\hat{\varepsilon}_z$) was corrected using Equation 4.33. This correction resulted in only a 1% difference

in the values for the total strains $(\hat{\epsilon}_z)$ between the two solutions. No other values (displacements, strains, or stresses) were affected by this correction to the STRES3 routine. The correction to the stress transformation matrix also was insignificant in its effect on the problem solutions. Only slight changes occurred in the solutions due to this modification. The use of the $\bar{r}$ approximation in the determination of the diagonal lumped mass matrix for an axisymmetric continuum was found to have no effect on the results for the axisymmetric problems. However, the equation for determining $\bar{r}$ was in error in the original SAMSON2 formulation. The correct expression for $\bar{r}$ (Equation 4.7) was substituted into the updated formulation which resulted in significant changes in the 8NQ axisymmetric solutions. This corrected $\bar{r}$ expression resulted in very significant changes in the 8NQ element results for both the axisymmetric wave propagation analysis and the axisymmetric analysis of the soil-structure interaction problem. Figures 5.1, 5.2, and 5.3 show the relative improvements in the results for the axisymmetric wave propagation when compared to Figures 3.23, 3.24, and 3.25. As shown, the 8NQ solution which was obtained using the updated formulation no longer lags behind the 4NQ element solution. The corrected $\bar{r}$ formulation also improved the results for the axisymmetric analysis of the soil-structure interaction problem which was obtained using the 8NQ isoparametric element. Table 5.1 when compared to Table 3.6 shows the relative improvement between the two 8NQ solutions. The 8NQ solution which was obtained using the corrected $\bar{r}$ formulation exhibited a much better agreement with the 4NQ solution. A significant improvement in the 8NQ solution to the soil-structure interaction problem for the
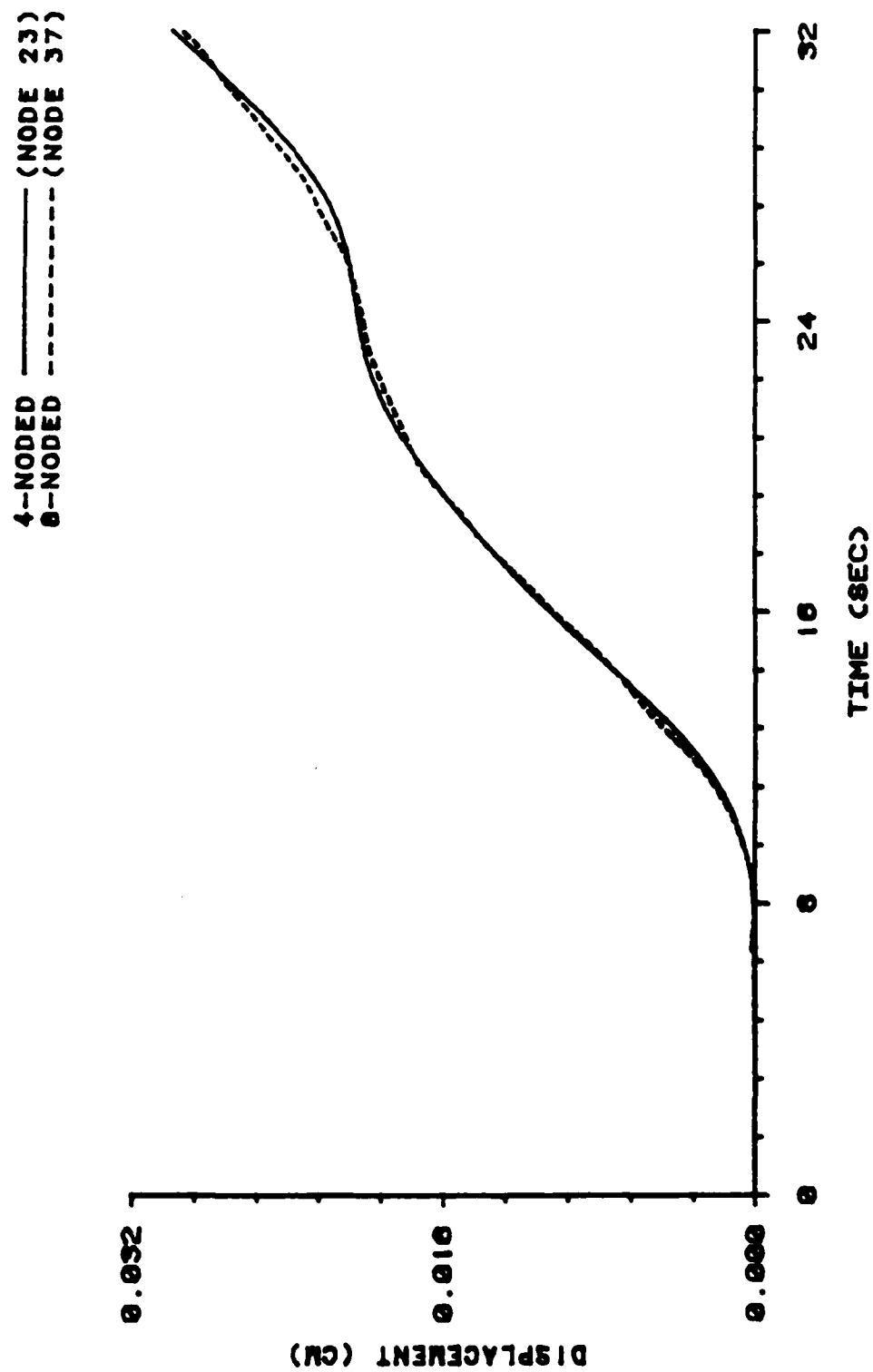
Figure 5.1   Axisymmetric Analysis of the One-Dimensional Wave Propagation Problem: Displacement vs. Time at Y = 8.0 cm.
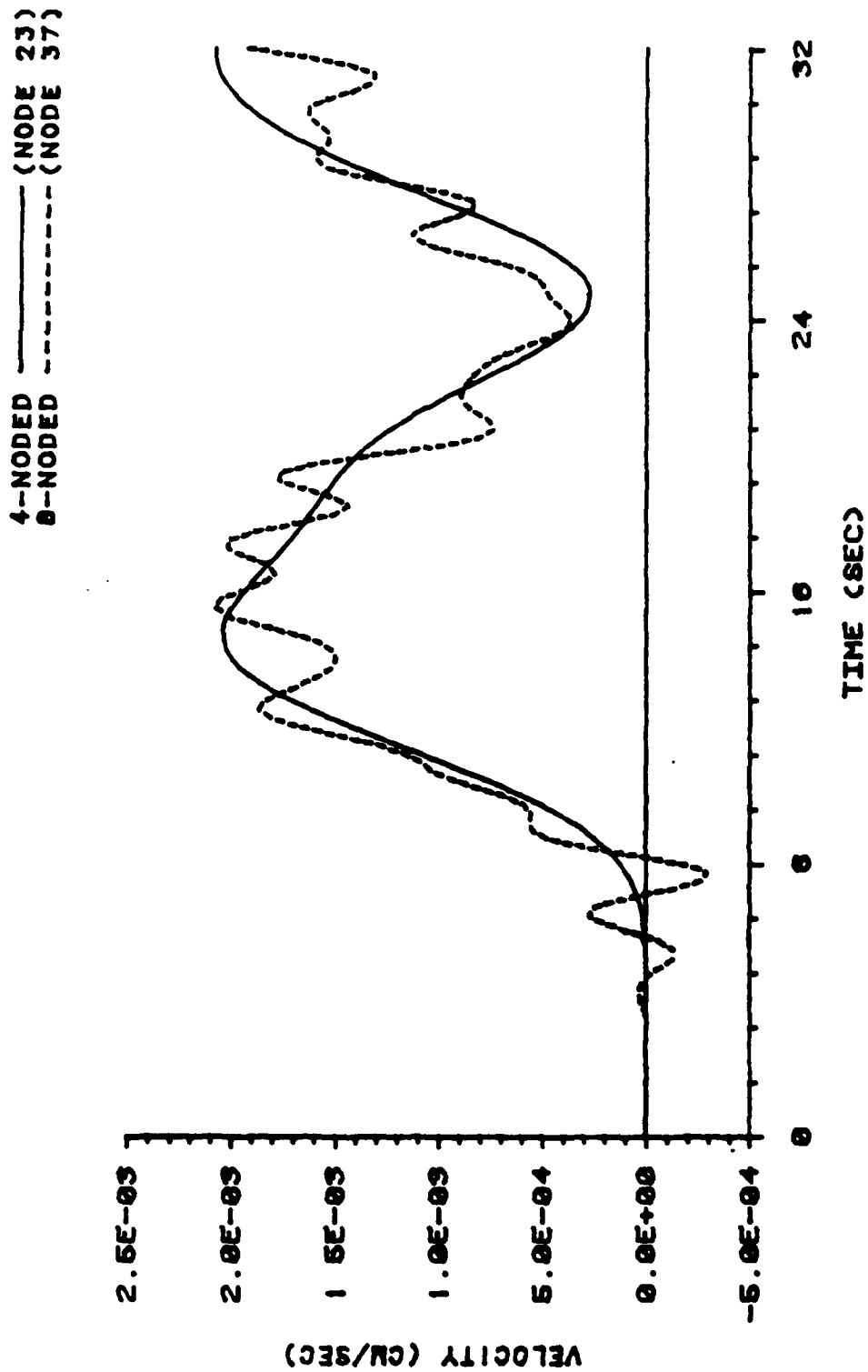
Figure 5.2   Axisymmetric Analysis of the One-Dimensional Wave Propagation Problem: Velocity vs. Time at Y = 8.0 cm.
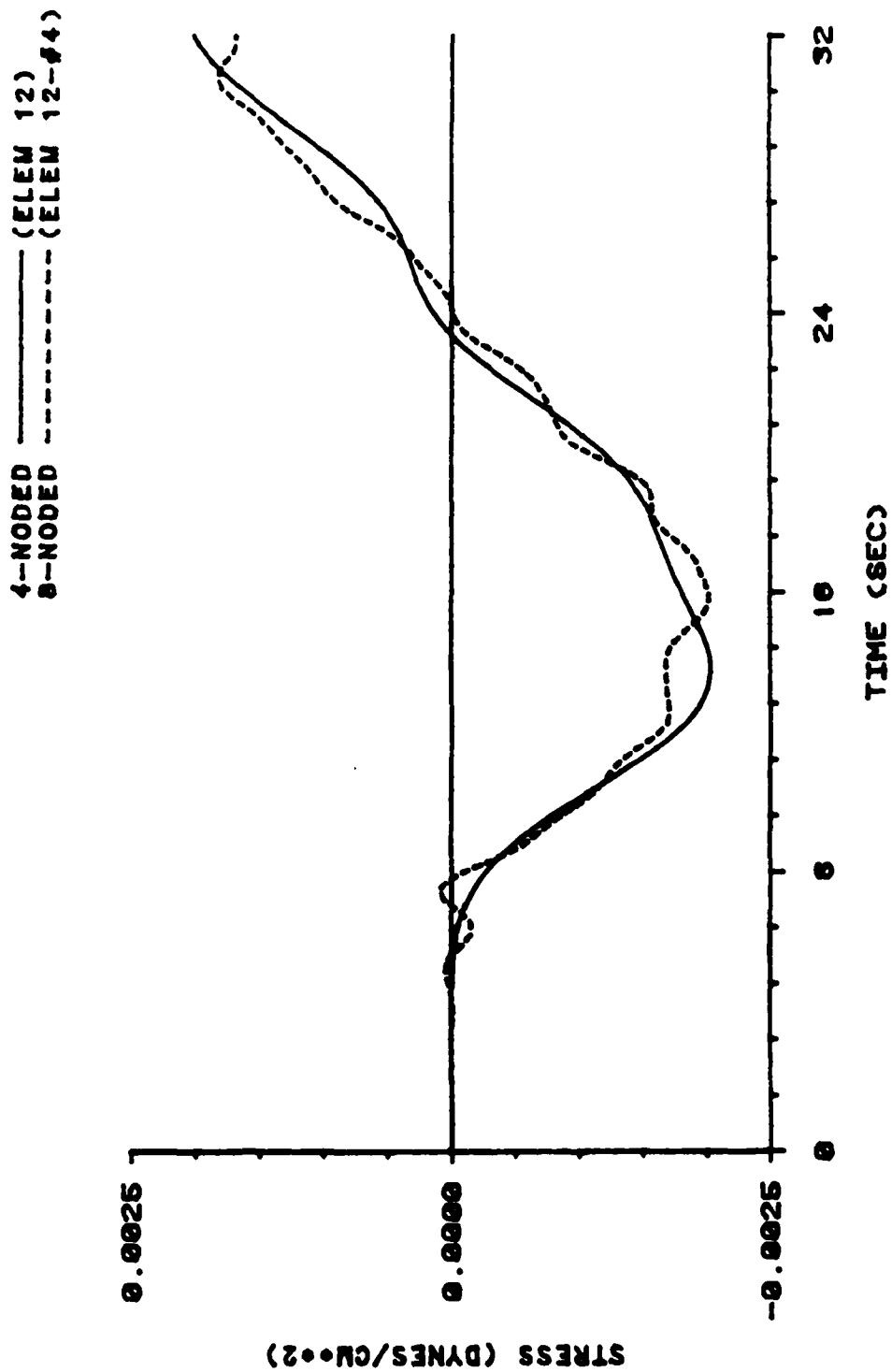
Figure : .3   Axisymmetric Analysis of the One-Dimensional Wave Propagation Problem: Stress vs. Time at Y = 7.0 cm.

Table 5.1   Comparison of Y-Displacement Values Between the 4NQ and 8NQ Solutions for the 8NQ-6 Element Structural Mesh and the 4NQ-12 Element Structural Mesh (1.0 psi Peak Load) (Soil-Structure Interaction Problem) After Mass Formulation Corrected.

Original Node Location		8NQ Y-Displacement	4NQ Y-Displacement	Percent Difference
x-coordinate (in)	y-coordinate (in)	$t=.8 \times 10^{-3}$ sec (in x 10^{-4})	$t=.8 \times 10^{-3}$ sec (in x 10^{-4})	Based on 4NQ Solution
0.0	72.0	-.2231	-.2112	5.6%
3.0	72.0	-.2068	---	---
6.0	72.0	-.1961	-.2009	2.4%
9.0	72.0	-.1882	---	---
12.0	72.0	-.2154	-.1972	9.2%
0.0	66.0	-.2076	-.2073	0.1%
6.0	66.0	-.1894	-.1961	3.4%
12.0	66.0	-.1971	-.1912	3.1%
0.0	60.0	-.1890	-.1996	5.3%
3.0	60.0	-.1869	---	---
6.0	60.0	-.1916	-.1878	2.0%
9.0	60.0	-.1941	---	---
12.0	60.0	-.1827	-.1831	0.2%
0.0	54.0	-.1886	-.1949	3.2%
6.0	54.0	-.1882	-.1785	5.4%
12.0	54.0	-.1777	-.1710	3.9%
0.0	48.0	-.1731	-.1898	8.8%
3.0	48.0	-.1795	---	---
6.0	48.0	-.1792	-.1711	4.7%
9.0	48.0	-.1751	---	---
12.0	48.0	-.1745	-.1612	8.3%
0.0	42.0	-.1584	-.1788	11.4%
6.0	42.0	-.1685	-.1639	2.8%
12.0	42.0	-.1724	-.1563	10.3%

applied blast load was also observed. The remainder of the errors, listed in Chapter 4 and not discussed in this section, were not related to the problem solutions in Chapter 3.

In conclusion, the majority of the SAMSON2 formulation errors that were presented in Chapter 4 were insignificant in their effect on the problem solutions. However, the corrected $\bar{r}$ formulation rendered a significant improvement in the 8NQ axisymmetric analyses. On the basis of this result, the corrected SAMSON2 formulation does provide more consistent and more reliable results.

CHAPTER 6

Conclusions and Recommendations

The primary conclusion, based on the results that were presented in the previous chapters, is that the current finite element formulation for the eight-node quadrilateral isoparametric continuum element provides consistent and reliable results for problems which involve plane analyses. However, some minor errors exist in the general SAMSON2 finite element formulation that need to be corrected. Also, the 8NQ axisymmetric continuum formulation contains a significant error in the axisymmetric mass formulation that needs to be corrected in the current formulation in order for accurate results to be obtained. Hence, the errors that were discovered in the SAMSON2 formulation (see Chapter 4) must be corrected in order for consistent and reliable results to be obtained for both 8NQ axisymmetric analyses and general continuum finite element analyses.

Some further conclusions that were drawn based on the results from the previous chapters are as follows:

(1) The higher-order element (5NT, 6NT, and 8NQ) solution schemes are less efficient than the 4NQ solution scheme. This conclusion is based on the fact that much longer execution times were required for the higher-order element solutions.

(2) The finite element formulation for the 6NT isoparametric continuum element works properly for elastic plane analyses of flexure problems. This conclusion is based on the good correlation in

results that was obtained in the cantilever beam analyses between the SAMSON2 and the corresponding analytical solutions.

(3) The 5NT isoparametric continuum element should only be used as a transition element for which it was designed. This conclusion is based on the 5NT results for the cantilever beam problem.

(4) Smaller time step values are necessary for solutions which involve higher-order elements as opposed to the values that are required for 4NQ element solutions.

(5) The higher-order element (6NT and 8NQ) solutions were more accurate in some cases compared to corresponding 4NQ solutions and were obtained using fewer nodes and elements.

Recommendations for future work are presented below. These recommendations are based upon both the work that has already been performed and the results that were obtained during this study.

(1) The 8NQ element needs to be used with the corrected formulation in a soil-structure interaction (SSI) problem for which test data are available in order to determine whether the 8NQ element solution is accurate for an SSI problem.

(2) Additional problems need to be analyzed using the 8NQ higher-order element in order to test the performance of the SAMSON2 8NQ finite element formulation more thoroughly.

(3) The 5NT and 6NT continuum elements need to be investigated more extensively through the solutions to more problems and the formulation verifications.

(4) Problems need to be analyzed using discretizations which contain both the higher-order and the 4NQ elements. Results for these

problems could be used to determine whether transitions can be made between the different elements with accurate results still being obtained.

(5) The corrected finite element formulation needs to be further tested since some of the errors were unrelated to the problem analyses that were performed in this investigation. For instance, the corrections in the AFWL "engineering" model need to be further tested.

(6) A further investigation and verification needs to be undertaken regarding the equations that are used in the SAMSON2 code in order to compute the external work for plane and axisymmetric pressure loadings.

(7) If the 8NQ finite element formulation produces inaccurate results in future problem analyses, then the following two items should be performed:

    (a) development of alternative schemes for determining the nodal masses, and

    (b) investigation of the addresses and indexes that are used in the 8NQ finite element formulation in order to store and recall information from the various parameter arrays.

REFERENCES

1. Belytschko, T. and Robinson, R. R., SAMSON2: A Nonlinear Two-Dimensional Structure-Media Interaction Computer Code, AFWL-TR-81-109, Air Force Weapons Laboratory, Kirtland Air Force Base, New Mexico, January 1982.

2. Schreyer, H. L., Personal communication with regard to the higher-order finite element formulation in the SAMSON2 code.

3. Schreyer, H. L., et al., SAMSON2, A Nonlinear Two-Dimensional Structure-Media Interaction Computer Code: User's Manual (Update), AFWL-TN-82-18, Air Force Weapons Laboratory, Kirtland Air Force Base, New Mexico, June 1984.

4. Seemann, D. R., Personal communication with regard to the higher-order finite element formulation in the SAMSON2 code.

5. Clough, R. W. and Penzien, J., Dynamics of Structures, McGraw-Hill, New York, 1975.

6. Berglund, J. W. and Rudeen, D. K., STEALTH and SAMSON2 Verification Calculations, NTE-TN-83-20, Air Force Weapons Laboratory, Kirtland Air Force Base, New Mexico.

7. Higdon, A., et al., Mechanics of Materials, 4th ed., John Wiley & Sons, New York, 1985.

8. Paz, M., Structural Dynamics: Theory and Computation, 2nd ed., Van Nostrand Reinhold Company, New York, 1985.

9. Belytschko, T. and Hughes, T. J. R., eds., Computational Methods for Transient Analysis, Elsevier Science Publishers B.V., Amsterdam, 1983.

10. Fenves, S. J., et al., eds., Numerical and Computer Methods in Structural Mechanics, Academic Press, New York, 1973.

11. Boresi, A. P., et al., Advanced Mechanics of Materials, 3rd ed., John Wiley & Sons, New York, 1978.

12. Bathe, K. J., Finite Element Procedures in Engineering Analysis, Prentice-Hall, Englewood Cliffs, New Jersey, 1982.

13. Gallagher, R. H., Finite Element Analysis: Fundamentals, Prentice-Hall, Englewood Cliffs, New Jersey, 1975.

14. Weaver, W. and Johnston, P. R., Finite Elements for Structural Analysis, Prentice-Hall, Englewood Cliffs, New Jersey, 1984.

15. Zienkiewicz, O. C., The Finite Element Method, 3rd ed., McGraw-Hill, New York, 1979.

16. Belytschko, T., Chiapetta, R. L., and Bartel, H. D., "Efficient Large Scale Non-Linear Transient Analysis by Finite Elements." *International Journal for Numerical Methods in Engineering,* Vol. 10, pp. 579-596. 1976.

17. Drucker, D. C. and Prager, W., "Soil Mechanics and Plastic Analysis or Limit Design." *Quarterly of Applied Mechanics*, Vol. 10, No. 2, pp. 157-165, 1952.

18. Kreyszig, E., *Advanced Engineering Mathematics*, 5th ed., John Wiley & Sons, New York, 1983.

APPENDIX A

Examples of SAMSON2 Input for the Finite Element Analyses

```
ELASTIC CONT. 16 QUAD ELTS WITH DISPLACEMENT/FREE RT END
   27   16    1    6  130              0.25    1    0
         3                                      1
       980.                CM DYNE DYNE
    1    6    4     ELASTIC PLANE STRESS
        0.0         1.0
        1.0         1.0        0.0         0.0
    1
    9              16.0
   10                          2.0
   18              16.0        2.0
   19               0.0        4.0
   27              16.0        4.0
    1    1    2   11   10                        1
    8    8    9   18   17                        1
    9   10   11   20   19                        1
   16   17   18   27   26                        1
     121
    1021
    1921
     901
    1801
    2701
      1          8         3         2
     1104X-DISPL NODE= 1
     3104X-DISPL NODE= 3
     5104X-DISPL NODE= 5
     7104X-DISPL NODE= 7
    14104X-DISPL NODE=14
     3114X-VEL NODE=3
     5114X-VEL NODE=5
     7114X-VEL NODE=7
     2 54STRESS AT 2
     4 54STRESS AT 4
     6 54STRESS AT 6
        25        3
        50        3
    2    1    5    3
    1    3    5    7   14
    2    4    6
    1    3    2         1    9   10
        0.          0.         2.    8.0E-5       4.    2.93E-3      6.    6.17E-3
        8.          .01       10.    1.383E-2    12.    1.707E-2    14.    1.924E-2
       16.          .02       35.    .02
    1   19
```

Figure A.1   One-Dimensional Wave Propagation Problem: Input for the
             4NQ Element Discretization.

```
ELASTIC CONT. 16 8-NODED QUAD ELTS WITH DISPLACEMENT/FREE RT END
   69   16    1   10  130              0.25    1    0
         3                                      1
      980.              CM DYNE DYNE
    1    6    4       ELASTIC PLANE STRESS
       2.0         1.0
       1.0         1.0            0.0          0.0
    1
    5                            4.0
    6            1.0
    8            1.0            4.0
    9            2.0
   13            2.0            4.0
   14            3.0
   16            3.0            4.0
   17            4.0
   21            4.0            4.0
   22            5.0
   24            5.0            4.0
   25            6.0
   29            6.0            4.0
   30            7.0
   32            7.0            4.0
   33            8.0
   37            8.0            4.0
   38            9.0
   40            9.0            4.0
   41           10.0
   45           10.0            4.0
   46           11.0
   48           11.0            4.0
   49           12.0
   53           12.0            4.0
   54           13.0
   56           13.0            4.0
   57           14.0
   61           14.0            4.0
   62           15.0
   64           15.0            4.0
   65           16.0
   69           16.0            4.0
    1    1    9   11    3    6   10    7    2    1    8
    8   57   65   67   59   62   66   63   58    1    8
    9    3   11   13    5    7   12    8    4    1    8
   16   59   67   69   61   63   68   64   60    1    8
      121                   1
     -521                   1
```

Figure A.2   One-Dimensional Wave Propagation Problem: Input for the
              8NQ Element Discretization.

```
  6501                    1
 -6901                    1
     1          8        12          2
   1104X-DISPL NODE= 1
  17104X-DISPL NODE=17
  33104X-DISPL NODE=33
  49104X-DISPL NODE=49
  35104X-DISPL NODE=35
  17114X-VEL NODE=17
  33114X-VEL NODE=33
  49114X-VEL NODE=49
   2 54STRESS EL2 #1
  2144STRESS EL2 #2

  2234STRESS EL2 #3
  2324STRESS EL2 #4
   4 54STRESS EL4 #1
  4144STRESS EL4 #2
  4234STRESS EL4 #3
  4324STRESS EL4 #4
   6 54STRESS EL6 #1
  6144STRESS EL6 #2
  6234STRESS EL6 #3
  6324STRESS EL6 #4
     25          3
     50          3
  2   1    5     3
  1   17   33    49    35
  2   4    6
  1   5    2          1   1   10
          0.         0.       2.     8.0E-5      4.    2.93E-3      6.    6.17E-3
          8.        .01      10.    1.383E-2    12.    1.707E-2    14.    1.924E-2
         16.        .02      35.       .02                                 .
  1   5
```

Figure A.2   One-Dimensional Wave Propagation Problem: Input for the
                8NQ Element Discretization (Continued).

```
STATIC ANAL. OF A CANT. BEAM USING 64 4NQ ELEMS. 6/20/85 BY S. MILLER
     85   64    1    5 4000              3.4E-5   1    0                1000.
           2    0    0              0                1
         32.2              FT
     1    3    4         4-NODE PLANE CONTINUUM ELEMENTS
         0.01         2.0
         16.0  4176.0E6           0.0      0.00       0.0
     1              0.0         0.0
    17             16.0         0.0
    18              0.0         1.0
    34             16.0         1.0
    35              0.0         2.0
    51             16.0         2.0
    52              0.0         3.0
    68             16.0         3.0
    69              0.0         4.0
    85             16.0         4.0
     1    1    2   19   18                          1
    16   16   17   34   33                          1
    17   18   19   36   35                          1
    32   33   34   51   50                          1
    33   35   36   53   52                          1
    48   50   51   68   67                          1
    49   52   53   70   69                          1
    64   67   68   85   84                          1
       111
      1811
      3511
      5211
      6911
         1         1              2
     51200
      1 50
      8 50
  5000 5000
     1   17   -1              1    3
       0.0              3.1E-3    100.0       1.0      100.0
    69
```

Figure A.3   Cantilever Beam Problem: Input for the 4NQ Element
              Discretization.

```
STATIC ANAL. OF A CANT. BEAM USING 32 5NT ELEMS. 6/20/85 BY S. MILLER
    61    32     1    5 4000           3.4E-5    1    0              100C.
           2                                     1
         32.2              FT
    1     3     4        5-NODED TRIANGULAR CONTINUUM ELEMENTS
         2.0         2.0
        16.0  4176.0E6          0.0        0.0        0.0
     1            0.0        0.0
     9           16.0        0.0
    10            0.0        1.0
    26           16.0        1.0
    27            0.0        2.0
    35           16.0        2.0
    36            0.0        3.0
    52           16.0        3.0
    53            0.0        4.0
    61           16.0        4.0
     1    1     2    27    11    10                        1
     2    2     3    29    14    13                        1
     3    3     4    29    15    14                        1
     4    4     5    31    18    17                        1
     5    5     6    31    19    18                        1
     6    6     7    33    22    21                        1
     7    7     8    33    23    22                        1
     8    8     9    35    26    25                        1
     9   28    27     2    11    12                        1
    10   29    28     2    12    13                        1
    11   30    29     4    15    16                        1
    12   31    30     4    16    17                        1
    13   32    31     6    19    20                        1
    14   33    32     6    20    21                        1
    15   34    33     8    23    24                        1
    16   35    34     8    24    25                        1
    17   27    28    54    38    37                        1
    18   28    29    54    39    38                        1
    19   29    30    56    42    41                        1
    20   30    31    56    43    42                        1
    21   31    32    58    46    45                        1
    22   32    33    58    47    46                        1
    23   33    34    60    50    49                        1
    24   34    35    60    51    50                        1
    25   54    53    27    36    37                        1
    26   55    54    29    39    40                        1
    27   56    55    29    40    41                        1
    28   57    56    31    43    44                        1
    29   58    57    31    44    45                        1
    30   59    58    33    47    48                        1
```

Figure A.4   Cantilever Beam Problem: Input for the 5NT Element
             Discretization.

```
31    60    59    33    48    49                    1
32    61    60    35    51    52                    1
      111
      1011
      2711
      3611
      5311
         1          1          2
      35200
      1250
      4150
5000 5000    0     0
   1    9   -1               1    3
      0.0              3.1E-3    100.0       1.0       100.0
     53
```

Figure A.4   Cantilever Beam Problem: Input for the 5NT Element
              Discretization (Continued).

```
STATIC ANAL. OF A CANT. BEAM USING 32 6NT ELEMS. 6/20/85 BY S. MILLER
  85    32    1    5 4000           3.4E-5    1    0              1000.
        2                                     1
      32.2              FT
   1    3    4    6-NODED TRIANGULAR CONTINUUM ELEMENTS
      2.0        2.0
     16.0  4176.0E6        0.0        0.0        0.0
   1            0.0        0.0
  17           16.0        0.0
  18            0.0        1.0
  34           16.0        1.0
  35            0.0        2.0
  51           16.0        2.0
  52            0.0        3.0
  68           16.0        3.0
  69            0.0        4.0
  85           16.0        4.0
   1    1    3   35    2   19   18              1    4
   4   13   15   47   14   31   30              1    4
   5    3    5   39    4   22   21              1    4
   8   15   17   51   16   34   33              1    4
   9    3   37   35   20   36   19              1    4
  12   15   49   47   32   48   31              1    4
  13    3   39   37   21   38   20              1    4
  16   15   51   49   33   50   32              1    4
  17   35   37   71   36   54   53              1    4
  20   47   49   83   48   66   65              1    4
  21   37   39   71   38   55   54              1    4
  24   49   51   83   50   67   66              1·   4
  25   35   71   69   53   70   52              1    4
  28   47   83   81   65   82   64              1    4
  29   39   73   71   56   72   55              1    4
  32   51   85   83   68   84   67              1    4
     111              17
   -6911              17
       1         1         2
     51200
     1250
     6150
 5000 5000
   1   17   -1              1    3
                        3.1E-3    100.0       1.0       100.0
  69
```

Figure A.5   Cantilever Beam Problem: Input for the 6NT Element
              Discretization.

```
STATIC ANAL. OF A CANT. BEAM USING 16 8NQ ELEMS. 6/26/85 BY S. MILLER
  69    16     1    5 4000              3.4E-5     1    0               1000.
          2     0    0                             1
        32.2                FT
   1     3     4        8-NODE PLANE CONTINUUM ELEMENTS
          2.0          2.0
         16.0   4176.0E6         0.00          0.00
   1
  17             16.0
  18                        1.0
  26             16.0        1.0
  27                         2.0
  43             16.0        2.0
  44                         3.0
  52             16.0        3.0
  53                         4.0
  69             16.0        4.0
   1     1     3    29    27     2    19    28    18     1
   2     3     5    31    29     4    20    30    19     1
   3     5     7    33    31     6    21    32    20     1
   4     7     9    35    33     8    22    34    21     1
   5     9    11    37    35    10    23    36    22     1
   6    11    13    39    37    12    24    38    23     1
   7    13    15    41    39    14    25    40    24     1
   8    15    17    43    41    16    26    42    25     1
   9    27    29    55    53    28    45    54    44     1
  10    29    31    57    55    30    46    56    45     1
  11    31    33    59    57    32    47    58    46     1
  12    33    35    61    59    34    48    60    47     1
  13    35    37    63    61    36    49    62    48     1
  14    37    39    65    63    38    50    64    49     1
  15    39    41    67    65    40    51    66    50     1
  16    41    43    69    67    42    52    68    51     1
     111
    1811
    2711
    4411
    5311
          1              1              2
    43200
     1 50
     4250
 5000 5000
    1    17    -1              1     3
       0.0         0.0     3.1E-3       100.0         1.0      100.
   53
```

Figure A.6   Cantilever Beam Problem: Input for the 8NQ Element
              Discretization.

```
SOIL-STRUCTURE INTERACTION ANAL. USING 4NQ AXIS. CONT.ELEMS. 7/25/85
   300   252    2   31 1600          0.5E-6    2    1
            3                                  1


     1    9    14      YUMA SOIL PARAMETERS
          0.05
  0.173E-3    0.158E7       0.38      0.01       5.0       1.0       2.0
  0.2644E5   -0.122        0.38
  0.4429E5   -0.156        0.38
  0.1553E6   -0.192        0.38
  0.3442E6   -0.212        0.38
  0.2199E7   -0.999        0.38
  0.2199E7     0.0         0.38
  0.7249E2     0.0        0.65E6     -0.1E7
     2    9    14      FIBER REINF. CONC. PARAMETERS
          0.05
  0.2516E-3   0.42E7       0.24      0.01       4.0       1.0       3.0
  0.1125E7  -0.6E-2        0.24
  0.1940E6  -0.32E-1       0.24
   .1380E6  -0.5E-1        0.24
   .2700E7  -0.999         0.24
  0.1125E7   0.625E3       0.24
    0.4E3    0.2E3        0.81E4    -0.47E4  0.2916E5  -0.268E5
      1       0.0          0.0
      7       0.0         36.0
      8       6.0          0.0
     14       6.0         36.0
     15      12.0          0.0
     27      12.0         72.0
     28      18.0          0.0
     40      18.0         72.0
     41      24.0          0.0
     53      24.0         72.0
     54      30.0          0.0
     66      30.0         72.0
     67      36.0          0.0
     79      36.0         72.0
     80      42.0          0.0
     92      42.0         72.0
     93   -  48.0          0.0
    105      48.0         72.0
    106      54.0          0.0
    118      54.0         72.0
    119      60.0          0.0
    131      60.0         72.0
    132      66.0          0.0
    144      66.0         72.0
```

Figure A.7   Soil-Structure Interaction Problem: Input for the Finer
              4NQ Element Discretization.

145			72.0	0.0		
157			72.0	72.0		
158			78.0	0.0		
170			78.0	72.0		
171			84.0	0.0		
183			84.0	72.0		
184			90.0	0.0		
196			90.0	72.0		
197			96.0	0.0		
209			96.0	72.0		
210			102.0	0.0		
222			102.0	72.0		
223			108.0	0.0		
235			108.0	72.0		
236			0.0	36.0		
248			0.0	72.0		
249			3.0	36.0		
261			3.0	72.0		
262			6.0	36.0		
274			6.0	72.0		
275			9.0	36.0		
287			9.0	72.0		
288			12.0	36.0		
300			12.0	72.0		
1	1	8	9	2		1
6	6	13	14	7		1
7	8	15	16	9		1
12	13	20	21	14		1
13	15	28	29	16		1
24	26	39	40	27		1
25	28	41	42	29		1
36	39	52	53	40		1
37	41	54	55	42		1
48	52	65	66	53		1
49	54	67	68	55		1
60	65	78	79	66		1
61	67	80	81	68		1
72	78	91	92	79		1
73	80	93	94	81		1
84	91-	104	105	92		1
85	93	106	107	94		1
96	104	117	118	105		1
97	106	119	120	107		1
108	117	130	131	118		1
109	119	132	133	120		1
120	130	143	144	131		1
121	132	145	146	133		1

Figure A.7   Soil-Structure Interaction Problem: Input for the Finer
4NQ Element Discretization (Continued).

```
132  143  156  157  144                              1
133  145  158  159  146                              1
144  156  169  170  157                              1
145  158  171  172  159                              1
156  169  182  183  170                              1
157  171  184  185  172                              1
168  182  195  196  183                              1
169  184  197  198  185                              1
180  195  208  209  196                              1
181  197  210  211  198                              1
192  208  221  222  209                              1
193  210  223  224  211                              1
204  221  234  235  222                              1
205  236  249  250  237                              2
216  247  260  261  248                              2
217  249  262  263  250                              2
228  260  273  274  261                              2
229  262  275  276  263                              2
240  273  286  287  274                              2
241  275  288  289  276                              2
252  286  299  300  287                              2
      101
    -1501                    7
     2801
   -21001                   13
    22311
    22410
   -23510                    1
         20        16        13         1
     248204DIS248
     248224ACC248
     261204DIS261
     261224ACC261
     274204DIS274
     274224ACC274
     287204DIS287
     287224ACC287
     300204DIS300
     300224ACC300
     105204DIS105
     105224ACC105
     118204DIS118
     118224ACC118
     131204DIS131
     131224ACC131
     215 64STR 215
     216 64STR 216
```

Figure A.7   Soil-Structure Interaction Problem: Input for the Finer
              4NQ Element Discretization (Continued).

```
227 64STR 227
228 64STR 228
239 64STR 239
240 64STR 240
251 64STR 251
252 64STR 252
 95 64STR  95
 96 64STR  96
107 64STR 107
108 64STR 108
253 54ENERGY ERROR
    1600           3
1601    40   24   56
 248  261  274  287  300  246  259  272  285  298  244  257  270  283  296
 105  118  131  103  116  129  101  114  127
 215  216  227  228  239  240  251  252  213  214  225  226  237  238  249
 250  211  212  223  224  235  236  247  248  209  210  221  222  233  234
 245  246   95   96  107  108   93   94  105  106   91   92  103  104   89
  90  101  102   87   88   99  100   85   86   97   98
   1    5   -2    0    0   13    9
      0.0         0.0      0.2E-3      0.5E5      0.4E-3      0.25E5   0.12E-2      0.15E5
    0.3E-2       7000.      0.6E-2     3000. 0.1020E-1      2200. 0.2020E-1      1000.
  0.402E-1       500.
 248
   2   17   -2    0    0   13    9
      0.0         0.0      0.2E-3      0.5E5      0.4E-3      0.25E5   0.12E-2      0.15E5
    0.3E-2       7000.      0.6E-2     3000. 0.1020E-1      2200. 0.2020E-1      1000.
  0.402E-1       500.
  27
   1    9   17    0    0
      0  0.3E-6       0.2                       0.58       72.5     0.17
   7   14   21   22   23   24   25   26   27  300  299  298  297  296  295  294
 293  292  291  290  289  288  275  262  249  236
```

Figure A.7   Soil-Structure Interaction Problem: Input for the Finer
               4NQ Element Discretization (Continued).

SOIL-STRUCTURE INTERACTION ANAL. USING 8NQ AXIS. CONT.ELEMS. 7/25/85

```
237    63    2   31 1600          0.5E-6    2    1
        3    0    0                         1

  1   9   14      YUMA SOIL PARAMETERS
       2.0
0.173E-3     0.158E7      0.38       0.01       5.0        1.0        2.0
0.2644E5     -0.122       0.38
0.4429E5     -0.156       0.38
0.1553E6     -0.192       0.38
0.3442E6     -0.212       0.38
0.2199E7     -0.999       0.38
0.2199E7      0.0         0.38
0.7249E2      0.0         0.65E6      -0.1E7
  2   9   14      FIBER REINF. CONC. PARAMETERS
       2.0
0.2516E-3     0.42E7      0.24        0.01       4.0        1.0        3.0
0.1125E7     -0.6E-2      0.24
0.1940E6    -0.32E-1      0.24
 .1380E6     -0.5E-1      0.24
 .2700E7     -0.999       0.24
0.1125E7     0.625E3      0.24
   0.4E3      0.2E3       0.81E4      -0.47E4    0.2916E5   -0.268E5
   1          0.0         0.0
  19        108.0         0.0
  20          0.0         6.0
  29        108.0         6.0
  30          0.0        12.0
  48        108.0        12.0
  49          0.0        18.0
  58        108.0        18.0
  59          0.0        24.0
  77        108.0        24.0
  78          0.0        30.0
  87        108.0        30.0
  88          0.0        36.0
 106        108.0        36.0
 107         12.0        42.0
 115        108.0        42.0
 116         12.0        48.0
 132        108.0        48.0
 133         12.0        54.0
 141        108.0        54.0
 142         12.0        60.0
 158        108.0        60.0
 159         12.0        66.0
 167        108.0        66.0
```

Figure A.8   Soil-Structure Interaction Problem: Input for the Finest
              8NQ Element Discretization.

168			12.0	72.0					
184			108.0	72.0					
185			0.0	36.0					
189			12.0	36.0					
190			0.0	39.0					
192			12.0	39.0					
193			0.0	42.0					
197			12.0	42.0					
198			0.0	45.0					
200			12.0	45.0					
201			0.0	48.0					
205			12.0	48.0					
206			0.0	51.0					
208			12.0	51.0					
209			0.0	54.0					
213			12.0	54.0					
214				57.0					
216			12.0	57.0					
217				60.0					
221			12.0	60.0					
222				63.0					
224			12.0	63.0					
225				66.0					
229			12.0	66.0					
230				69.0					
232			12.0	69.0					
233				72.0					
237			12.0	72.0					
1	1	3	32	30	2	21	31	20	1	29
3	59	61	90	88	60	79	89	78	1	29
4	3	5	34	32	4	22	33	21	1	29
6	61	63	92	90	62	80	91	79	1	29
7	90	92	118	116	91	108	117	107	1	26
9	142	144	170	168	143	160	169	159	1	26
10	5	7	36	34	6	23	35	22	1	29
12	63	65	94	92	64	81	93	80	1	29
13	92	94	120	118	93	109	119	108	1	26
15	144	146	172	170	145	161	171	160	1	26
16	7	9	38	36	8	24	37	23	1	29
18	65	67	96	94	66	82	95	81	1	29
19	94	96	122	120	95	110	121	109	1	26
21	146	148	174	172	147	162	173	161	1	26
22	9	11	40	38	10	25	39	24	1	29
24	67	69	98	96	68	83	97	82	1	29
25	96	98	124	122	97	111	123	110	1	26
27	148	150	176	174	149	163	175	162	1	26
28	11	13	42	40	12	26	41	25	1	29

Figure A.8   Soil-Structure Interaction Problem: Input for the Finest
8NQ Element Discretization (Continued).

```
30    69    71   100    98    70    84    99    83    1    29
31    98   100   126   124    99   112   125   111    1    26
33   150   152   178   176   151   164   177   163    1    26
34    13    15    44    42    14    27    43    26    1    29
36    71    73   102   100    72    85   101    84    1    29
37   100   102   128   126   101   113   127   112    1    26
39   152   154   180   178   153   165   179   164    1    26
40    15    17    46    44    16    28    45    27    1    29
42    73    75   104   102    74    86   103    85    1    29
43   102   104   130   128   103   114   129   113    1    26
45   154   156   182   180   155   166   181   165    1    26
46    17    19    48    46    18    29    47    28    1    29
48    75    77   106   104    76    87   105    86    1    29
49   104   106   132   130   105   115   131   114    1    26
51   156   158   184   182   157   167   183   166    1    26
52   185   187   195   193   186   191   194   190    2     8
57   225   227   235   233   226   231   234   230    2     8
58   187   189   197   195   188   192   196   191    2     8
63   227   229   237   235   228   232   236   231    2     8
   101
 -1801                    1
  1911
  2910
  4810
  5810
  7710
  8710
 10610
 11510
 13210
 14110
 15810
 16710
 18410
      20          16          13           1
 233204DIS233
 233224ACC233
 234204DIS234
 234224AGC234
 235204DIS235
 235224ACC235
 236204DIS236
 236224ACC236
 237204DIS237
 237224ACC237
 174204DIS174
 174224ACC174
```

Figure A.8   Soil-Structure Interaction Problem: Input for the Finest 8NQ Element Discretization (Continued).

```
175204DIS175
175224ACC175
176204DIS176
176224ACC176
 57 64STR 57#1
 57194STR 57#2
 57324STR 57#3
 57454STR 57#4
 63 64STR 63#1
 63194STR 63#2
 63324STR 63#3
 63454STR 63#4
 27 64STR 27#1
 27194STR 27#2
 27324STR 27#3
 27454STR 27#4
 64 54 ENERGY ERROR
    1600        3
1601   40   24   14
 233  234  235  236  237  225  226  227  228  229  217  218  219  220  221
 174  175  176  148  149  150  122  123  124
  57   63   56   62   55   61   54   60   27   26   25   24   23   22
  1    5   -2              1    9
     0.0         0.0      0.2E-3      0.5E5      0.4E-3      0.25E5      0.12E-2      0.15E5
    0.3E-2       7000.    0.6E-2      3000. 0.1020E-1      2200. 0.2020E-1      1000.
 0.402E-1        500.
 233
  2   17   -2              1    9
     0.0         0.0      0.2E-3      0.5E5      0.4E-3      0.25E5      0.12E-2      0.15E5
    0.3E-2       7000.    0.6E-2      3000. 0.1020E-1      2200. 0.2020E-1      1000.
 0.402E-1        500.
 168
  1    9   17
     0  0.3E-6      0.2                      0.58      72.5      0.17
  88   89   90  107  116  133  142  159  168  237  232  229  224  221  216  213
 208  205  200  197  192  189  188  187  186  185
```

Figure A.8   Soil-Structure Interaction Problem: Input for the Finest
            8NQ Element Discretization (Continued).

```
ELAST.-PERFECTLY PLAST. ANAL.OF A FIXED-ENDED BEAM WITH A CONC.LD (4NQ ELEMS.)
   85   64    1   10 2000          3.4E-5   1    0              2000.
            3    0    0          0              1
        32.2                FT
   1    3    4        4-NODE PLANE CONTINUUM ELEMENTS
        0.01          2.0
        16.0  4176.0E6          0.0     0.01       1.0
    0.1E-2  0.4176E7
    1               0.0      0.0
   17              16.0      0.0
   18               0.0      1.0
   34              16.0      1.0
   35               0.0      2.0
   51              16.0      2.0
   52               0.0      3.0
   68              16.0      3.0
   69               0.0      4.0
   85              16.0      4.0
    1    1    2   19   18                        1
   16   16   17   34   33                        1
   17   18   19   36   35                        1
   32   33   34   51   50                        1
   33   35   36   53   52                        1
   48   50   51   68   67                        1
   49   52   53   70   69                        1
   64   67   68   85   84                        1
      111
      1711
      1811
      3411
      3511
      5111
      5211
      6811
      6911
      8511
        10          5      24          2
     9204Y-DISPL NODE  9
    2630 4Y-DISPL NODE 26
    4320 4Y-DISPL NODE 43
    6020 4Y-DISPL NODE 60
    7720 4Y-DISPL NODE 77
     1 54STR  1
    17 54STR 17
    33 54STR 33
    49 54STR 49
     2 54STR  2
    18 54STR 18
    34 54STR 34
    50 54STR 50
     3 54STR  3
    19 54STR 19
    35 54STR 35
```

Figure A.9   Fixed-Ended Beam Problem: Input for the 4NQ Discretiza-
tion.

```
51 54STR 51
 6 54STR  6
22 54STR 22
38 54STR 38
54 54STR 54
 7 54STR  7
23 54STR 23
39 54STR 39
55 54STR 55
 8 54STR  8
24 54STR 24
40 54STR 40
56 54STR 56
  1000        3
  2000        3

 1   5   1        2  17   5
   0.0              1.7E-2 -2.7648E6    3.4E-2 -2.7648E6    5.1E-2 -4.1472E6
   1.0 -4.1472E6
 9
```

Figure A.9   Fixed-Ended Beam Problem: Input for the 4NQ Discretiza-
              tion (Continued).

```
ELAST.-PERFECTLY PLAST. ANAL.OF A FIXED-ENDED BEAM WITH A CONC.LD.(8NQ ELEMS.)
  69    16     1    10 2000          3.4E-5    1    0              2000.0
          3     0     0                          1
     32.2            FT
  1     3     4        8-NODE PLANE CONTINUUM ELEMENTS
     2.0          2.0
    16.0  4176.0E6       0.00      0.01       1.0
  0.1E-2  0.4176E7
   1
  17          16.0
  18                    1.0
  26          16.0      1.0
  27                    2.0
  43          16.0      2.0
  44                    3.0
  52          16.0      3.0
  53                    4.0
  69          16.0      4.0
   1    1     3    29    27     2    19    28    18     1
   2    3     5    31    29     4    20    30    19     1
   3    5     7    33    31     6    21    32    20     1
   4    7     9    35    33     8    22    34    21     1
   5    9    11    37    35    10    23    36    22     1
   6   11    13    39    37    12    24    38    23     1
   7   13    15    41    39    14    25    40    24     1
   8   15    17    43    41    16    26    42    25     1
   9   27    29    55    53    28    45    54    44     1
  10   29    31    57    55    30    46    56    45     1
  11   31    33    59    57    32    47    58    46     1
  12   33    35    61    59    34    48    60    47     1
  13   35    37    63    61    36    49    62    48     1
  14   37    39    65    63    38    50    64    49     1
  15   39    41    67    65    40    51    66    50     1
  16   41    43    69    67    42    52    68    51     1
     111
    1811
    2711
    4411
    5311
    1711
    2611
    4311
    5211
    6911
        10          5          24          2
    9204Y-DISPL NODE   9
   22206Y-DISPL NODE  22
   35204Y-DISPL NODE  35
   48204Y-DISPL NODE  48
   61204Y-DISPL NODE  61
    1 54STR 101
   11 54STR 102
    9 54STR 901
```

Figure A.10   Fixed-Ended Beam Problem: Input for the 8NQ Discretiza-
tion.

```
 9154STR 9#2
 1254STR 1#3
 1354STR 1#4
 9254STR 9#3
 9354STR 9#4
 2 54STR 2#1
 2154STR 2#2
10 54STR10#1
10154STR10#2
 3254STR 3#3
 3354STR 3#4
11254STR11#3
11354STR11#4
 4 54STR 4#1
 4154STR 4#2
12 54STR12#1
12154STR12#2
 4254STR 4#3
 4354STR 4#4
12254STR12#3
12354STR12#4
 1000        3
 2000        3

1   5   1         2   13   5
                  1.7E-2 -2.7648E6    3.4E-2 -2.7648E6    5.1E-2 -4.1472E6
    1.0 -4.1472E6
 9
```

Figure A.10   Fixed-Ended Beam Problem: Input for the 8NQ Discretiza-
               tion Continued).

AXIS. ANAL. OF ONE-DIMENSIONAL WAVE PROPAGATION WITH DISPL./FREE END(4NQ ELEMS)

```
  27    16     1     6   130              0.25    1    0
         3                                         1
       980.                  CM DYNE DYNE
   1     6    14       ELASTIC PLANE STRESS
         0.0
         1.0          1.0        0.0        0.0
   1                  0.0        0.0
   9                  0.0       16.0
  10                  2.0        0.0
  18                  2.0       16.0
  19                  4.0        0.0
  27                  4.0       16.0
   1     1    10    11     2                         1
   8     8    17    18     9                         1
   9    10    19    20    11                         1
  16    17    26    27    18                         1
      112
     1012
     1912
      910
     1810
     2710
         1           19         6          3
     1204Y-DISPL NODE= 1
     3204Y-DISPL NODE= 3
     5204Y-DISPL NODE= 5
     7204Y-DISPL NODE= 7
    12204Y-DISPL NODE=12
    14204Y-DISPL NODE=14
    16204Y-DISPL NODE=16
    21204Y-DISPL NODE=21
    23204Y-DISPL NODE=23
    25204Y-DISPL NODE=25
     3214Y-VEL  NODE= 3
     5214Y-VEL  NODE= 5
     7214Y-VEL  NODE= 7
    12214Y-VEL  NODE=12
    14214Y-VEL  NODE=14
    16214Y-VEL  NODE=16
    21214Y-VEL  NODE=21
    23214Y-VEL  NODE=23
    25214Y-VEL  NODE=25
     2 64STRESS ELEM  2
     4 64STRESS ELEM  4
     6 64STRESS ELEM  6
    10 64STRESS ELEM 10
    12 64STRESS ELEM 12
    14 64STRESS ELEM 14
        25           3
        50           3
       130           3
  150     1    10     6
```

Figure A.11   Axisymmetric Wave Propagation Problem: Input for the 4NQ
                Discretization.

```
1    3    5    7    12   14   16   21   23   25
2    4    6    10   12   14
1    3    2              2    9    10
     0.        0.        2.   8.0E-5         4.   2.93E-3        6.   6.17E-3
     8.        .01       10.  1.383E-2       12.  1.707E-2       14.  1.924E-2
     16.       .02       35.       .02
1    19
```

Figure A.11   Axisymmetric Wave Propagation Problem: Input for the 4NQ
Discretization (Continued).

```
AXIS. ANAL. OF ONE-DIMENSIONAL WAVE PROPAGATION WITH DISPL./FREE END(8NQ ELEMS)
    69   16    1   10  130              0.25    1    0
         3                                      1
        980.                   CM DYNE DYNE
     1    6   14       ELASTIC PLANE STRESS
         2.0
         1.0          1.0          0.0          0.0
     1                0.0          0.0
     5                4.0          0.0
     6                0.0          1.0
     8                4.0          1.0
     9                0.0          2.0
    13                4.0          2.0
    14                0.0          3.0
    16                4.0          3.0
    17                0.0          4.0
    21                4.0          4.0
    22                0.0          5.0
    24                4.0          5.0
    25                0.0          6.0
    29                4.0          6.0
    30                0.0          7.0
    32                4.0          7.0
    33                0.0          8.0
    37                4.0          8.0
    38                0.0          9.0
    40                4.0          9.0
    41                0.0         10.0
    45                4.0         10.0
    46                0.0         11.0
    48                4.0         11.0
    49                0.0         12.0
    53                4.0         12.0
    54                0.0         13.0
    56                4.0         13.0
    57                0.0         14.0
    61                4.0         14.0
    62                0.0         15.0
    64                4.0         15.0
    65                0.0         16.0
    69                4.0         16.0
     1    1    3   11    9    2    7   10    6    1    8
     8   57   59   67   65   58   63   66   62    1    8
     9    3    5   13   11    4    8   12    7    1    8
    16   59   61   69   67   60   64   68   63    1    8
       112              1
      -512              1
      6510              1
     -6910              1
         1             19          24           3
       1204Y-DISPL NODE= 1
      17204Y-DISPL NODE=17
      33204Y-DISPL NODE=33
```

Figure A.12   Axisymmetric Wave Propagation Problem: Input for the 8NQ
               Discretization.

```
49204Y-DISPL NODE=49
19204Y-DISPL NODE=19
35204Y-DISPL NODE=35
51204Y-DISPL NODE=51
21204Y-DISPL NODE=21
37204Y-DISPL NODE=37
53204Y-DISPL NODE=53
17214Y-VEL NODE=17
33214Y-VEL NODE=33
49214Y-VEL NODE=49
19214Y-VEL NODE=19
35214Y-VEL NODE=35
51214Y-VEL NODE=51
21214Y-VEL NODE=21
37214Y-VEL NODE=37
53214Y-VEL NODE=53
 2 64STRESS EL2 #1
 2154STRESS EL2 #2
 2244STRESS EL2 #3
 2334STRESS EL2 #4
 4 64STRESS EL4 #1
 4154STRESS EL4 #2
 4244STRESS EL4 #3
 4334STRESS EL4 #4
 6 64STRESS EL6 #1
 6154STRESS EL6 #2
 6244STRESS EL6 #3
 6334STRESS EL6 #4
10 64STRESS EL10#1
10154STRESS EL10#2
10244STRESS EL10#3
10334STRESS EL10#4
12 64STRESS EL12#1
12154STRESS EL12#2
12244STRESS EL12#3
12334STRESS EL12#4
14 64STRESS EL14#1
14154STRESS EL14#2
14244STRESS EL14#3
14334STRESS EL14#4
         25        3
         50        3
        130        3
150    1  _10      6
  1    17   33     49    19   35    51    21    37    53
  2     4    6     10    12   14
  1     5    2            2    1    10
        0.        0.      2.   8.0E-5      4.  2.93E-3      6.  6.17E-3
        8.       .01     10.  1.383E-2    12.  1.707E-2    14.  1.924E-2
       16.       .02     35.     .02
  1     5
```

Figure A.12   Axisymmetric Wave Propagation Problem: Input for the 8NQ
                Discretizati n (Continued).

APPENDIX B

Gauss-Legendre Abscissae and Weight Coefficients

Table B.1 shows the Gauss-Legendre abscissae and weight coefficients ($\pm a$ and h) which are used in the Gaussian quadrature method of numerical integration. These coefficients for Gaussian quadrature are used in the SAMSON2 code in order to determine the lumped mass matrix $[M]$, the internal nodal force vector $\{F_{int}\}$, the internal strain energy of the system U, and the external work of the system W for the 8NQ higher-order isoparametric continuum element. References 12, 14, and 15 contain additional information about Gaussian quadrature and they also contain a discussion on the practical applications of Gaussian quadrature for the isoparametric element formulation.

-

Table B.1   Gauss-Legendre Abscissae and Weight Coefficients for a Particular Order of Integration n(n=1,10).[a]

±a				h		
			n = 1			
0				2.00000	00000	00000
			n = 2			
0.57735	02691	89626		1.00000	00000	00000
			n = 3			
0.77459	66692	41483		0.55555	55555	55556
0.00000	00000	00000		0.88888	88888	88889
			n = 4			
0.86113	63115	94053		0.34785	48451	37454
0.33998	10435	84856		0.65214	51548	62546
			n = 5			
0.90617	98459	38664		0.23692	68850	56189
0.53846	93101	05683		0.47862	86704	99366
0.00000	00000	00000		0.56888	88888	88889
			n = 6			
0.93246	95142	03152		0.17132	44923	79170
0.66120	93864	66265		0.36076	15730	48139
0.23861	91860	83197		0.46791	39345	72691
			n = 7			
0.94910	79123	42759		0.12948	49661	68870
0.74153	11855	99394		0.27970	53914	89277
0.40584	51513	77397		0.38183	00505	05119
0.00000	00000	00000		0.41795	91836	73469
			n = 8			
0.96028	98564	97536		0.10122	85362	90376
0.79666	64774	13627		0.22238	10344	53374
0.52553	24099	16329		0.31370	66458	77887
0.18343	46424	95650		0.36268	37833	78362
			n = 9			
0.96816	02395	07626		0.08127	43883	61574
0.83603	11073	26636		0.18064	81606	94857
0.61337	14327	00590		0.26061	06964	02935
0.32425	34234	03809		0.31234	70770	40003
0.00000	00000	00000		0.33023	93550	01260
			n = 10			
0.97390	65285	17172		0.06667	13443	08688
0.86506	33666	88985		0.14945	13491	50581
0.67940	95682	99024		0.21908	63625	15982
0.43339	53941	29247		0.26926	67193	09996
0.14887	43389	81631		0.29552	42247	14753

[a]The values for these coefficients were obtained from page 198 of Reference 15.

MICROCOPY RESOLUTION TEST CHART

1.0

1.1

1.25   1.4   1.6

1.8

2.0

2.2

2.8

3.2

3.6

4.0
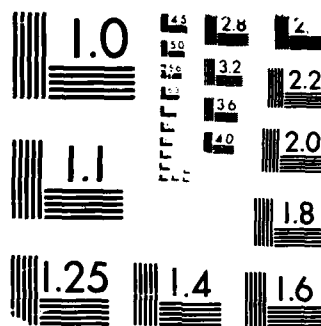
APPENDIX C

Development of the Elastic-Plastic Stress-Strain Matrix

for the Plane Strain or Axisymmetric Material Law

The general equation that is used in order to determine the elastic-plastic stress-strain matrix (C^{EP}) for biaxial analysis is shown in Equation C.1 (see pp. 388-389 of Reference 14).

$$C^{EP} = C^E - \frac{C^E\{q\}(C^E\{q\})^T}{\{p\}^T\{q\} + \{q\}^T C^E\{q\}} \qquad (C.1)$$

where,

C^E = elastic stress-strain matrix,

$\{q\}^T$ = $[q_{11}\ q_{22}\ 2q_{12}\ q_{33}]$

$\{p\}^T$ = $[p_{11}\ p_{22}\ p_{12}\ p_{33}]$

This equation was formulated under the assumptions of isothermal conditions, isotropic hardening and an associated flow rule. The values for $\{q\}$ and $\{p\}$ are determined using the expressions shown in Equation C.2.

$$q_{ij} = \frac{\partial F}{\partial \sigma_{ij}} \qquad\qquad p_{ij} = \frac{\partial F}{\partial \epsilon_{ij}^p} \qquad (C.2)$$

where,

F = yield function that specifies the state of multiaxial stress which corresponds to the start of plastic flow.

σ_{ij} = normal and shearing stress components, and

ϵ_{ij}^p = plastic strain increments.

The C^{EP} matrix for the biaxial elastic-plastic plane strain or axisymmetric material law was developed by substituting the expressions shown in Equation C.3 into Equations C.1 and C.2.

$$F = \frac{1}{2} S_{ij} S_{ij} - \frac{1}{3} \sigma_{yld}^{n}{}^{2}$$

$$q_{ij} = S_{ij} \qquad p_{ij} = H \sigma_{ij}$$

(C.3)

where,

S_{ij} = deviatoric stresses,

$$= \sigma_{ij} - \frac{\sigma_x + \sigma_y + \sigma_z}{3} \delta_{ij};$$

where δ_{ij} = 1 for the normal stresses and = 0 for the shear stresses, and

$$H = \frac{2}{3} \left(\frac{E\, E_T}{(E-E_T)} \right)$$

The development of C^{EP} was performed in three tasks. The first task was the multiplication of C^E (Equation 4.39 in Section 4.2.4.2) by $\{q\}$. The results of this multiplication are shown in Equation C.4.

$$C^E\{\underline{q}\} = \frac{E(1-\nu)}{(1+\nu)(1-2\nu)} \begin{Bmatrix} S_{11} + \frac{\nu}{1-\nu}(S_{22} + S_{33}) \\ S_{22} + \frac{\nu}{1-\nu}(S_{11} + S_{33}) \\ \frac{1-2\nu}{1-\nu} S_{12} \\ S_{33} + \frac{\nu}{1-\nu}(S_{11} + S_{22}) \end{Bmatrix}$$

(C.4)

The next task was the multiplication of $\{p\}^T$ by $\{q\}$ with the result shown in Equation C.5.

$$\{p\}^T \{q\} = \frac{2}{3} \left(\frac{E\ E_T}{E-E_T}\right) \sigma_{yld}^{n\ 2} \tag{C.5}$$

where,

$$\sigma_{yld}^{n\ 2} = \frac{2}{3} \cdot (\sigma_x^2 + \sigma_y^2 + \sigma_z^2 - \sigma_x \sigma_y - \sigma_x \sigma_z - \sigma_y \sigma_z) + 2\tau_{xy}^2.$$

The final task involved the substitution of the results shown in Equations C.4 and C.5 into Equation C.1. This task resulted in the C^{EP} matrix shown in Table C.1. This matrix was used in subroutine STRES3 according to the discussion in Sections 4.2.4.2 and 4.2.4.3.

Table C.1[a]   Elastic-Plastic Stress-Strain Matrix for the Plane Strain or Axisymmetric Material Law (STRES3).

$$C^{EP} = \frac{E}{1+\nu} \begin{bmatrix} \frac{1-\nu}{1-2\nu} - \beta S_{11}^2 & \frac{\nu}{1-2\nu} - \beta S_{11} S_{22} & -\beta S_{11} S_{12} & \frac{\nu}{1-2\nu} - \beta S_{11} S_{33} \\ & \frac{1-\nu}{1-2\nu} - \beta S_{22}^2 & -\beta S_{22} S_{12} & \frac{\nu}{1-2\nu} - \beta S_{22} S_{33} \\ & & \frac{1}{2} - \beta S_{12}^2 & -\beta S_{33} S_{12} \\ & \text{symmetric} & & \frac{1-\nu}{1-2\nu} - \beta S_{33}^2 \end{bmatrix}$$

where,

$$\beta = \frac{3}{2} \frac{1}{\sigma_{yld}^n} \; {}^2 \left(\frac{1}{1 + \frac{2}{3} \frac{E}{E-E_T} (1+\nu)} \right) , \text{ and}$$

S_{ij} = deviatoric stresses = $\sigma_{ij} - \frac{\sigma_{mm}}{3} \delta_{ij}$; $\sigma_{mm} = \sigma_x + \sigma_y + \sigma_z$ and

δ_{ij} = 1 for normal stresses, = 0 for shear stresses.

[a]This matrix was obtained from p. 390 in Bathe (12).

END

DATE
FILMED

8-88

DTIC